Functions of the conserved ribosome-bound protein Lso2 in translation and physiology

By

Yinuo J Wang

B.A. Biochemistry
Columbia University, 2012

Submitted to the Graduate Program in Microbiology in Partial Fulfillment of the Requirements for the Degree of

Doctor of Philosophy

at the

Massachusetts Institute of Technology

June 2017

Signature of Author: Signature redacted
Yinuo J Wang
Graduate Program in Microbiology
May 24th, 2017

Certified by: Signature redacted
Dr. Wendy V. Gilbert
Associate Professor of Biology
Thesis Adviser

Accepted by: Signature redacted
Dr. Kristala Prather
Associate Professor of Chemical Engineering
Co-chair, Microbiology Graduate Program Committee

Functions of the conserved ribosome-bound protein Lso2 in translation and physiology

By

Yinuo J Wang

Submitted to the Graduate Program in Microbiology on May 24th, 2017 in Partial Fulfillment of the Requirements for the Degree of Doctor of Philosophy in Biology

Abstract

The ribosome is a highly conserved macromolecular machine that carries out translation, the synthesis of proteins from mRNAs, in all domains of life. The core ribosome interacts with dozens of general translation factors that ensure accurate and efficient progression through the translation cycle. Their detailed characterization has significantly advanced our understanding of protein synthesis. However, a growing number of ribosome-associated proteins have also been discovered whose functions are less well understood. In Chapter 1, I will overview the translation cycle and describe how it is affected by nutrient availability, with a focus on functions of starvation-induced proteins that directly bind the ribosome. I will also discuss discovery approaches for expanding the study of ribosome-associated proteins.

In Chapter 2, I will present the discovery and characterization of Lso2 as a conserved ribosome-bound protein required for translational recovery in budding yeast. Using quantitative mass spectrometry, we found this protein to be ribosome-associated during glucose-starved and replete growth, with moderate enrichment on translating ribosomes during starvation. *Saccharomyces cerevisiae* lacking Lso2 accumulate monoribosomes that are not translating normally following a shift from stationary phase to rich medium. To understand the basis of this phenotype, we used genome-wide RNA crosslinking and sequencing to determine that Lso2 binds near the A site of the ribosome tRNA channel, in a region that overlaps with the GTPase activating center, and that Lso2 also interacts with a broad spectrum of tRNAs. Consistently, Lso2 binding in the tRNA channel stabilizes ribosomal subunit association *in vitro*. These data, together with evidence that the accumulated ribosomes in *lso2* nulls are devoid of obvious barriers to initiation, lead to a model in which Lso2 promotes productive elongation. Finally, I show that the ribosome binding activity of Lso2 is conserved in its human ortholog, suggesting a broad importance of its molecular function.

In Chapter 3, I will elaborate on the model of a function for Lso2 in elongation, propose alternative models to rationalize its effects on translation, and describe experiments for testing them. I will also describe the implications of this protein for our understanding of translation in different physiological states.

Thesis adviser: Professor Wendy V. Gilbert
Title: Associate Professor of Biology

Acknowledgements

First and foremost I thank my adviser, Professor Wendy Gilbert, for making every part of this project possible. Wendy is profoundly invested in how her students read, write, think, and speak. It was a privilege to work with a mentor who cares so much about the entire intellect. I know the training I received with her will serve me in every turn of my future careers.

The members and alumni of the Gilbert lab are also inseparable from this project: Dr. Josh Arribere, Dr. Kristen Bartoli, Tristan Bell, Dr. Thomas Carlile, Paritosh Gangaramani, Dr. Jiří Koubek, Dr. Nicole Martinez, Gina Mawla, Dr. Rachel Niederer, Maria Rojas-Duran, Cassandra Schaening, Dr. Mary K Thompson, Dr. Pavan Vaidyanathan, Dr. Boris Zinshteyn, Amanda Su, and George Zakusilo. Pavan launched this project with a heroic proteomic screen. Boris, Cassandra, and Mary K supplied me with foundational code. Boris was also indispensable to the biochemistry that illuminated a path forward. Jiří and Rachel joined at the eleventh hour to re-invigorate my perspective on translation. Jiří also provided advice and encouragement while I wrote this thesis. Maria kept the lab running with energy and grace. I thank the young mentees who challenged me to be more giving: Ryan Kohn, Kalki Kukreja, and Laura Cardona. I am also grateful to our administrators, Sally MacGillivray and Tau Zaman, for their investment. My warmest thanks goes to my baymate and close friend, Kristen, who weathered with me each triumph, defeat, and daily vicissitude. Kristen is a scientist blessed with perception and humanity. I cannot imagine this experience without her.

I thank Professors Alan Grossman, Allan Jacobson, and Gene-Wei Li for serving on my thesis defense committee: Allan, for bringing his expertise in translation and his critical insights to my project; Alan and Gene, for being true mentors. From my interview dinner to the career options at the end of my PhD, I found Alan's empathy and clarifying wisdom at each milepost. Gene and his lab, in letting me attend their weekly meetings, enriched my education more than I imagined possible. By example they taught me creativity, courage, and quantitative rigor. I thank Dr. Aaron DeLoughery, Dr. Lydia Herzel, Grace Johnson, Jean-Benoît Lalanne, Darren Parker, Ariel Schieler, James Taggart, Dr. Yingwu Xu, and collaborator Dr. Monica Guo. I also thank Jean and Darren for their friendship. Jean is not only a wildly gifted scientist, but a citizen who inspires those around him to work harder, to think more deeply, and to act more conscientiously. He is a role model in and outside of the lab. From Darren, whom I counted on never to give me less than his real opinion, I learned the value of a friend for all seasons.

I thank the Microbiology Program and its faculty committee over the years: Professors Kris Prather, Martin Polz, Alan Grossman, Michael Laub, and others who make its communal spirit possible, including our administrator Bonnielee. I am also grateful to my classmates. Jennifer Nguyen is my close friend whose resilience takes the steeliest form, which is irrepressible sunniness. To her I owe three indelible days in Paris.

I thank two mentors outside of MIT, Dr. Saúl Nava and Dr. Alice Rushforth, who built careers in science outreach of the highest caliber. Saúl and Alice are an inspiration for using science to empower the public; they never talked down to the madding crowd.

I thank other friends who broadened my horizons: Tristan Bell, Mr. John Burbella, Kathleen Davis, Kim Davis, Fatima Hussein, Dr. Meera Sahni, Dr. Eugene Serebryany, Caroline St. Angelo, Ana Cristina Vargas, and Maria Zakhalyavko.

I will be indebted always to Mr. Michael St. Angelo and Mrs. May St. Angelo, who took me under their wing sixteen years ago, and who continue to welcome me back as family.

I thank my grandparents, who helped raise me and who live by their example of ageless ethics.

Finally, I thank my parents, who are my friends, councilors, benefactors, confidants, aides-de-camp, sages, cheerleaders, and givers of pastoral care in every waking hour. To me you will always be the real pioneers.

Table of Contents

Chapter I:

Introduction

Overview

The translation cycle is complex and highly regulated in response to cellular conditions. Accurate and efficient translation requires the interaction of the core ribosome with dozens of initiation, elongation, and termination factors. Translation also affects all aspects of cellular physiology by virtue of its energy demands and its final output, the proteome. These broader connections to physiology have been illustrated by a number of ribosome-associated proteins beyond the core translation factors. This introductory chapter will provide context for understanding the function of Lso2, the novel ribosome-associated protein whose discovery and characterization is presented in Chapter 2. Here I will first overview the translation cycle, as well as ribosome-associated systems for terminating unproductive translation. Next, I will discuss how starvation affects translation at the molecular level in eukaryotes and in prokaryotes, where a greater number of stress-specific ribosome-bound proteins have been characterized. Finally, I will broaden the discussion to approaches that have identified direct ribosome-binding proteins as mediators of gene expression during starvation and beyond.

Overview of the translation cycle

In eukaryotes, more than a dozen initiation factors recruit an mRNA to a ribosome (Figure 1-1). The substrate mRNA is bound by eIF4F, comprising eIF4E, which recognizes the m^7G cap on the 5′ end of an mRNA (O'Leary et al., 2013); the weakly associated eIF4A (Mitchell et al., 2010), a helicase that unwinds secondary structure in the mRNA transcript leader; and eIF4G, a large scaffolding protein with binding domains for eIF4E and eIF4A (Hershey et al., 1999; Hilbert et al., 2011; Schütz et al., 2008). Prior to interaction with the transcript, the 40S small subunit must be pre-loaded with methionyl initiator transfer RNA (Met-$tRNA_i$), which is in a ternary complex with eIF2•GTP; eIF5, a GTPase activating protein that

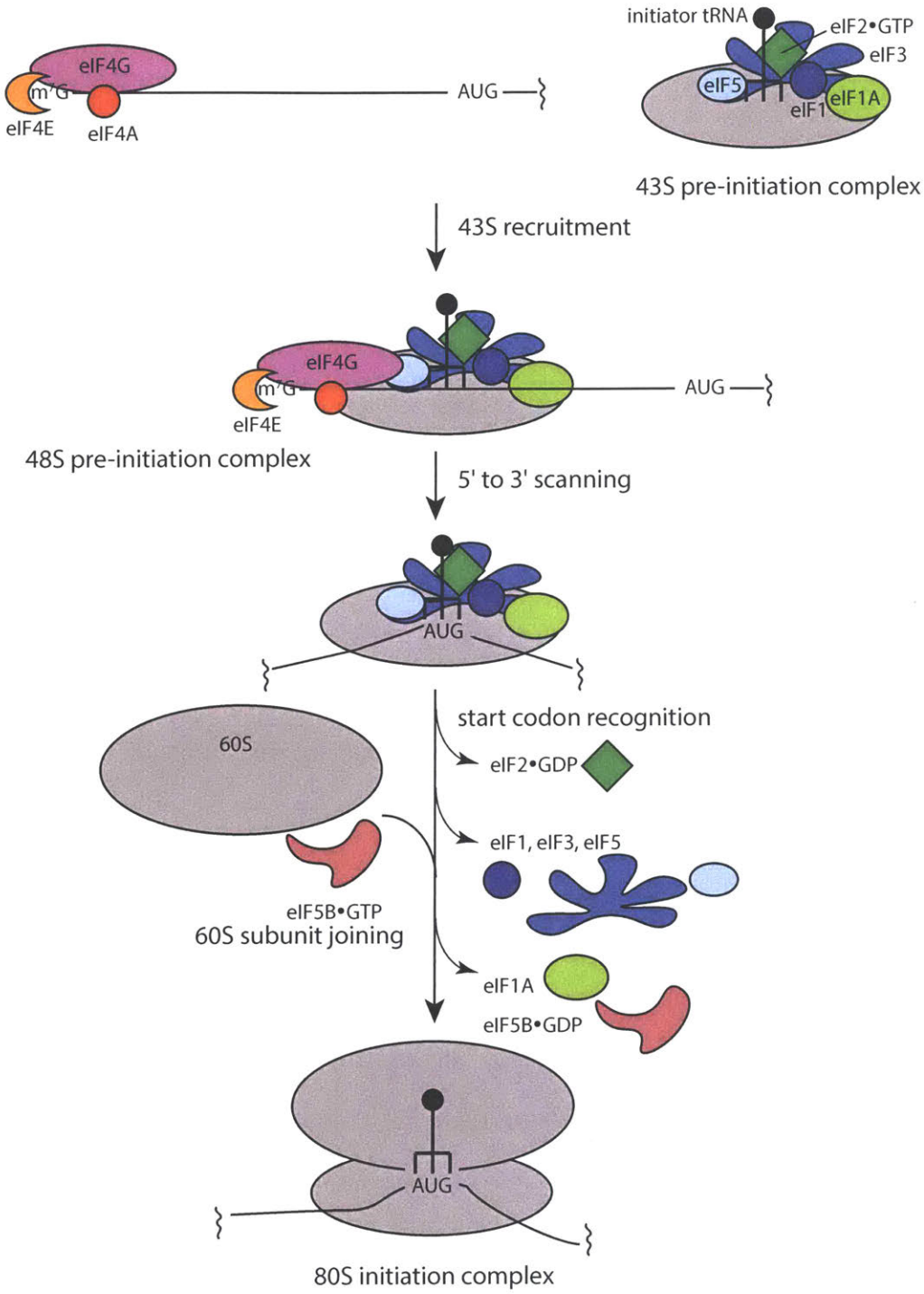

Figure 1-1: Summary of eukaryotic translation initiation. The eIF4F complex comprising eIF4E, eIF4G, and the weakly associated eIF4A binds to the 5′ capped end of an mRNA. The 40S subunit is loaded with initiator tRNA in a ternary complex with eIF2•GTP, and also with eIFs 1, 1A, 5, and 3. Following ribosome recruitment to the eIF4F complex, the molecular bridge of which is unknown in yeast, scanning proceeds from the 5′ cap to the first start codon that stably triplet pairs with initiator tRNA. Start codon recognition triggers eIF2•GTP hydrolysis and release of all eIFs except eIF1A and possibly eIF3.

eIF1A helps to recruit eIF5B•GTP, which catalyzes 60S subunit joining. eIF5B•GTP hydrolysis stimulates eIF5B•GDP and the remaining eIFs to dissociate. The 80S initiation complex with Met-tRNA$_i$ in the P site is ready for the first round of elongation.

promotes eIF2•GTP hydrolysis upon start codon recognition (Das et al., 2001; Huang et al., 1997); eIF1, which promotes the open scanning conformation of the ribosome (Hussain et al., 2014; Martin-Marcos et al., 2014); eIF1A, which promotes scanning until recognition of the start codon, whereupon structural changes in the eIF1A N-terminus prevent the ribosome from further scanning (Hussain et al., 2014; Llácer et al., 2015); and eIF3, a large scaffolding protein (6 subunits in yeast and 13 subunits in mammals) with direct interactions to eIFs 1, 1A, 2, 5, and later with mRNA (Asano et al., 2000; Aylett et al., 2015; Valasek, 2002). The 40S subunit and these factors together comprise the 43S pre-initiation complex (PIC). In higher eukaryotes, the 43S PIC is recruited to eIF4F-bound mRNA by a domain of eIF4G that interacts directly with eIF3 (Villa et al., 2013). However, yeast eIF4G lacks the eIF3 interaction domain, and the molecular bridge in ribosome recruitment remains unclear. There is preliminary evidence that yeast eIF4G instead associates with eIF5 (Yamamoto et al., 2000; He et al., 2003). The 43S then scans from 5′ to 3′ along the mRNA. Triplet pairing of the start codon with initiator tRNA leads to eIF2•GTP hydrolysis and dissociation of all but eIF1A and potentially eIF3 (Hussain et al., 2014; Mohammad et al., 2017). The subunit interface is accordingly cleared for 60S subunit joining. eIF1A helps to recruit the GTPase eIF5B•GTP, which catalyzes subunit joining (Acker et al., 2006; Pestova et al., 2000). Following GTP hydrolysis of eIF5B•GTP, eIF5B•GDP and the remaining initiation factors dissociate. The resulting 80S initiation complex contains Met-tRNA$_i$ based-paired with the start codon in the peptidyl (P) site and empty exit (E) and aminoacyl (A) sites. By contrast, initiation in prokaryotes involves direct annealing between the Shine-Dalgarno sequence of the substrate mRNA and the anti-Shine-Dalgarno region of the 16S rRNA, with only three initiation factors required for subsequent start codon recognition and subunit joining (Duval et al., 2015). This difference between eukaryotes and prokaryotes in their

factor requirements for initiation also leads to substantial differences in their mechanisms of translational regulation, as discussed in "The effects of nutrient availability on translation."

Elongation as opposed to initiation is highly conserved between eukaryotes and prokaryotes (Figure 1-2). Most of our mechanistic understanding comes from structural and biochemical experiments on bacterial elongation factors (reviewed in Voorhees and Ramakrishnan, 2013); however, crystal and cryo-EM structures have since confirmed their high degree of conservation in eukaryotes and archaea (Becker et al., 2011; Kobayashi et al., 2010; Soe et al., 2007). Aminoacyl-tRNA in a ternary complex with eEF1A•GTP (eukaryotic Elongation Factor 1A), whose bacterial homolog is EF-Tu (Elongation Factor Thermounstable), arrives at the A site and samples the codon with its anticodon loop. The tRNA is initially in a distorted conformation (A/T state) as it simultaneously interacts with eEF1A and reaches into the decoding center of the small subunit (Schmeing et al., 2009; Shao et al., 2016). Triplet pairing leads to additional stabilizing interactions between the codon:anticodon duplex and highly conserved regions of the small subunit that favor cognate tRNA selection (Selmer, 2006; Shao et al., 2016). Correct pairing also stimulates eEF1A to hydrolyze GTP to GDP, lowering eEF1A affinity for tRNA and causing it to dissociate. The acceptor end of the tRNA subsequently rotates, or "accommodates," into the peptidyl transferase center (PTC) of the large subunit (Blanchard et al., 2004; Stark et al., 2002; Voorhees et al., 2010). Together, selection prior to and kinetic proofreading following GTP hydrolysis increase the fidelity of translation by several orders of magnitude. In a study of reconstituted bacterial translation, near-cognate tRNAs dissociated 100 times as quickly during initial selection, while they were also an order of magnitude less stable following EF-Tu dissociation (Gromadski and Rodnina, 2004). Both passive dissociation of non-cognate tRNA from the A site, in addition to a lack of stabilizing interactions necessary to swing through the accommodation corridor, contribute to fidelity during kinetic proofreading (Shao et al., 2016; Voorhees and Ramakrishnan, 2013; Whitford et al., 2010). Following accommodation, the PTC rapidly catalyzes transfer of the nascent chain from

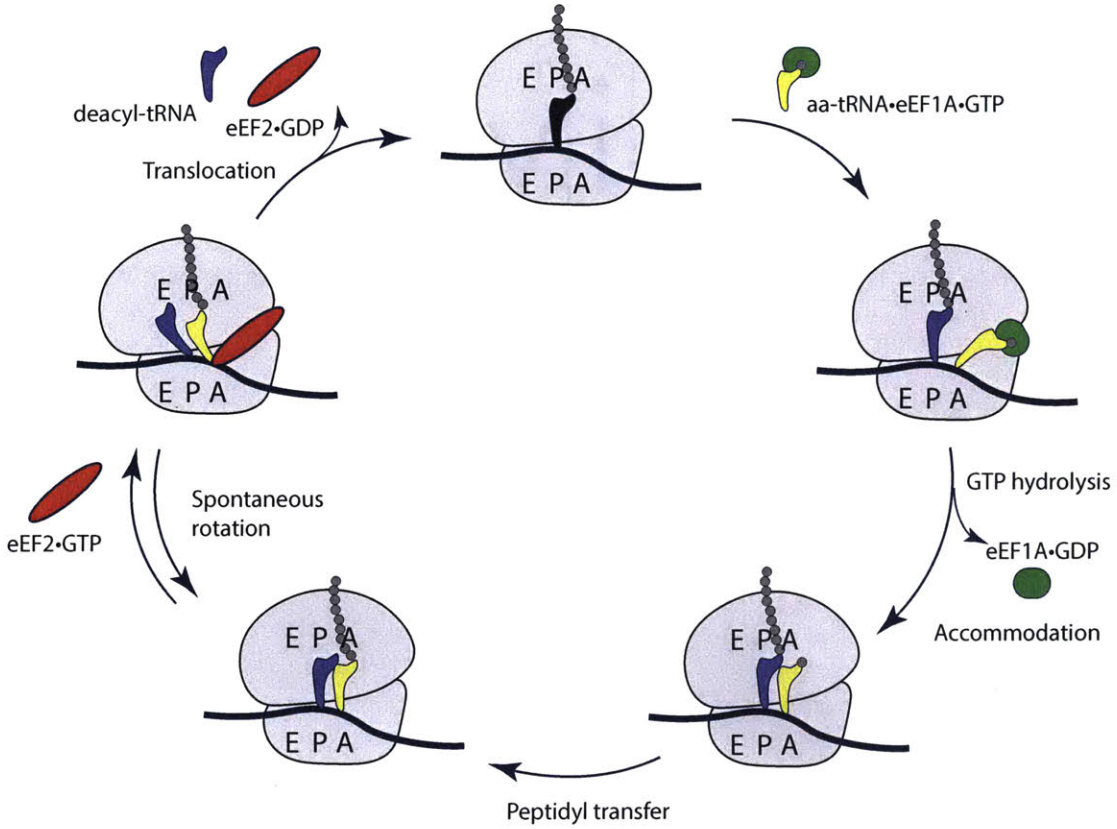

Figure 1-2: Overview of translation elongation. (Top, proceeding clockwise) tRNA arrives in a ternary complex with eEF1A•GTP and samples the A site codon. Correct triplet pairing stimulates eEF1A•GTP hydrolysis, leading to dissociation of eEF1A•GDP. The acceptor end of the tRNA then accommodates into the A site of the large subunit. The peptidyl transferase center catalyzes peptidyl transfer from the P site tRNA to the amino group of the A site aminoacyl-tRNA. The subunits rotate to position the tRNAs in the hybrid state (E/P and P/A, respectively). eEF2•GTP binds to the rotated state and "traps" the ribosome in its back-rotation of the small subunit. Following GTP hydrolysis, eEF2•GDP dissociates from the ribosome. The net effect of translocation is to move the mRNA and tRNAs relative to the small subunit, thus advancing the ribosome by 3 nucleotides and realigning the tRNAs within the decoding center. Deacylated tRNA in the E site dissociates.

the P site tRNA to the amino group of the A site aminoacyl-tRNA. The subunits then spontaneously rotate in the plane of the subunit interface to position the tRNAs in the hybrid state: The deacylated acceptor end of the small subunit P site tRNA shifts into the large subunit E site, and the peptidyl end of the small subunit A site tRNA shifts into the large subunit P site (Aitken and Puglisi, 2010; Cornish et al., 2008; Rodnina and Wintermeyer, 2009). The translocation factor eEF2 (eukaryotic Elongation Factor 2), whose bacterial homolog is EF-G (Elongation Factor G), binds to this rotated conformation and is thought to act as a pawl in a

Brownian ratchet, trapping the ribosome in its spontaneous back-rotation of the small subunit (Ermolenko and Noller, 2011; Liu et al., 2014). GTP hydrolysis, rather than acting as a power stroke, stimulates eEF2•GDP release from the ribosome that is restored to its classic state (Ermolenko and Noller, 2011; Ling and Ermolenko, 2016). The net effect is to move the small subunit relative to the mRNA and tRNAs, such that the tRNAs are re-aligned with the E and P sites in the large subunit. The deacylated tRNA in the E site leaves the ribosome while the peptidyl tRNA occupies the P site and the A site is again vacant.

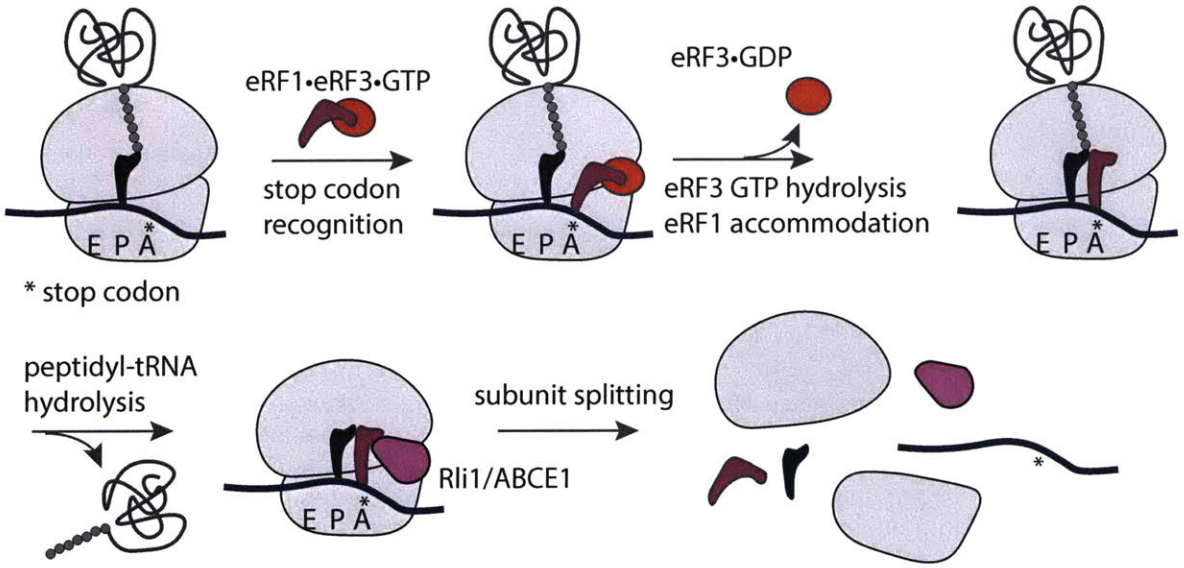

Figure 1-3: Overview of eukaryotic translation termination. A stop codon (UGA, UAA, or UAG) in the A site is decoded by the NIKS loop of eRF1, which is delivered to the ribosome in a ternary complex with eRF3•GTP. Following eRF3•GTP hydrolysis and dissociation of eRF3•GDP, eRF1 is accommodated into the 60S PTC. Its GGQ motif catalyzes peptidyl-tRNA hydrolysis, releasing the newly synthesized protein from the exit tunnel. The ATPase Rli1 (conserved in humans as ABCE1) splits the ribosomal complex to recycle subunits, tRNA, mRNA, and eRF1.

Canonical termination is triggered by the arrival of a stop codon in the A site (Figure 1-3). In eukaryotes, eRF1 recognizes all three stop codons (UGA, UAA, and UAG) through its conserved NIKS loop (Brown et al., 2015; Song et al., 2000). eRF1 arrives at the A site in a ternary complex with eRF3•GTP, a GTPase related to eEF1A/EF-Tu, and eRF3•GTP hydrolysis positions the conserved GGQ motif of eRF1 to hydrolyze the nascent chain from the P site

tRNA. Following termination, the ribosome remains engaged with mRNA, P site tRNA, and eRF1 until dissociation by the ATPase Rli1 (Preis et al., 2014; Young et al., 2015). In bacteria, the evolutionarily unrelated but functionally convergent RF1 and RF2 recognize UAG and UAA vs UGA and UAA, respectively, and hydrolyze peptidyl-tRNA (Laurberg et al., 2008; Weixlbaumer et al., 2008). RF3•GTP, a GTPase related to EF-G, then binds to the ribosome to stimulate RF1/RF2 release (Koutmou et al., 2014; Zhou et al., 2012). The prokaryote-specific Ribosome Recycling Factor (RRF) splits the ribosomal subunits, with IF3 re-binding the small subunit to keep it accessible for a new round of initiation (Dever and Green, 2012). It is interesting to note that eukaryotic release factors function analogously to the pre-translocation steps of elongation, in that eRF3•GTP delivers eRF1 to the A site of the non-rotated ribosome and eRF1 accommodates into the PTC following GTP hydrolysis and eRF3•GDP dissociation. By contrast, prokaryotic termination is more similar (but not identical) to translocation: RF3 is thought to initially bind the non-rotated conformation, but GTP hydrolysis is associated with a subsequent rotation of the small subunit that frees RF1/RF2 (Jin et al., 2011; Koutmou et al., 2014; Zhou et al., 2012).

In addition to canonical termination, which both liberates the newly synthesized protein and recycles the translation machinery, ribosome stalls during elongation must be resolved to avoid sequestering ribosomes and tRNA. A number of inhibitory features can cause ribosomes to stall internally, including rare codons, a stable stem-loop, or a polyproline tract (Doma and Parker, 2006; Letzring et al., 2013; Schuller et al., 2017). A ribosome may also reach the 3' end of a message without encountering a stop codon to trigger the proper sequence of termination events, leaving the A site empty of mRNA (Graille and Séraphin, 2012; Guydosh and Green, 2014; Shoemaker and Green, 2012). In eukaryotes and prokaryotes, the best-characterized quality control systems are evolutionarily unrelated but share functional parallels in resolving the same molecular issues. The key ribosome-associated quality control proteins in yeast are Dom34 (conserved in humans as Pelota) and Hbs1, which are respectively homologous to the

termination factors eRF1 and eRF3 (Becker et al., 2011; Chen et al., 2010). Biochemical experiments demonstrated that Dom34•Hbs1 splits ribosomal subunits programmed with stalling messages *in vitro* and that this activity was comparable over a range of A and P site codon identities (Shoemaker et al., 2010). This suggested that Dom34•Hbs1 might act broadly on stalled ribosomes *in vivo*. Structurally, Dom34 extends deep into the 40S decoding center of an A site lacking a tRNA, while the GTPase Hbs1 contacts the mRNA entry channel (Fig 1-2) (Becker et al., 2011; Chen et al., 2010). Recognition of the empty A site stimulates GTP hydrolysis by Hbs1, which is required for subunit splitting (Shoemaker et al., 2010). *In vivo*, recruitment of Dom34•Hbs1 triggers a cascade that further degrades the associated translation ligands. The mRNA is cleaved immediately 5′ of the stalled ribosome by an unknown Dom34-recruited endonuclease (Doma and Parker, 2006; Tsuboi et al., 2012), then digested by the exonuclease Ski7 (van Hoof et al., 2002; Letzring et al., 2013). Following splitting of ribosomal subunits on the downstream fragment, the mRNA is degraded by exonucleases. Peptidyl-tRNA in the 60S P site is targeted by the Ribosome Quality Control complex (RQC), which tags the nascent chain with ubiquitin and extracts peptidyl-tRNA for degradation (Brandman and Hegde, 2016; Brandman et al., 2012). Additionally, ribosomes that stall on mRNAs due to engineered mutations in their PTCs - which presumably block the very first round of elongation - are themselves degraded in a Dom34-dependent manner, in a pathway called non-functional rRNA decay (NRD) (Cole et al., 2009; LaRiviere et al., 2006). Through these quality control mechanisms, the cell clears each entity - ribosome, mRNA, and/or truncated protein - that could be toxic in a future round of translation or as a constituent of the proteome.

In bacteria, the *trans*-translation system resolves elongation stalls and targets nascent peptides in a consolidated pathway. When the ribosome reaches the end of a message without encountering a stop codon, tmRNA (transfer-messenger RNA), which is charged with alanine and delivered to the ribosome by EF-Tu, enters the empty A site (Barends et al., 2001). Its partner SmpB (Small protein B) binds in the 30S decoding center with a C-terminal tail that

structurally mimics mRNA, thus discriminating between normal versus non-stop ribosomal complexes (Neubauer et al., 2012). Following accommodation of tmRNA into the PTC, the abortive nascent chain is transferred from the P site tRNA to the charged tmRNA. EF-G catalyzes a round of elongation to free the previously stalled peptidyl tRNA as well as the truncated mRNA (Ivanova et al., 2005; Miller et al., 2011), which becomes a target for exonucleases. Translation is then templated from the mRNA-mimicking region of tmRNA to append a degradative tag to the nascent peptide (Flynn et al., 2001; Keiler et al., 1996). Although this mode of rescue would appear to recognize only non-stop stalls, no-go substrates have been reported as well, whose structural basis remains unclear (Buskirk and Green, 2017; Janssen et al., 2013). In the absence of tmRNA, the back-up rescue systems ArfA and ArfB dissociate ribosomes through mechanisms more similar to canonical termination. ArfA binds in the empty A site to recruit the bona fide release factor RF2, which hydrolyzes peptidyl-tRNA (Huter et al., 2017; Ma et al., 2017). ArfB structurally mimics a release factor in its anticodon loop-like C-terminal domain and its GGQ motif, which catalyzes peptidyl-tRNA hydrolysis (Starosta et al., 2014). Thus, the redundancy in bacterial ribosome-associated quality control, and the conservation of Dom34•Hbs1 in eukaryotes from yeast to humans, attest to the importance of clearing translational stalls.

The effects of nutrient availability on translation

Unicellular microbes cycle between "feast and famine" in their natural environments, with global translation programs that respond on rapid time scales to these fluctuations. Because translation is limiting for growth (Warner, 1999), sustaining the maximal translation rate during nutrient-rich conditions is essential to competitive fitness. At the same time, continued translation in the absence of sufficient nutrients wastes cellular resources and could dysregulate the cell cycle (Polymenis and Schmidt, 1997). Here I describe the best-characterized systems in eukaryotes and prokaryotes for remodeling their protein synthesis programs during starvation.

Their regulatory strategies differ significantly, with prokaryotes relying more heavily on proteins that directly bind the ribosome to affect various stages of translation.

In eukaryotes, where the interplay of more than a dozen proteins dictates initiation, reducing the functional levels of initiation factors is a conserved strategy for globally attenuating protein synthesis. One of two primary targets is eIF4E, the cap-binding protein within the eIF4F assembly. The master regulator of growth TOR (Target Of Rapamycin) directly phosphorylates eIF4E Binding Proteins (4E-BPs) during rapid growth to keep them inactive (Sonenberg and Hinnebusch, 2009). During amino acid starvation and a range of other "slow growth" conditions (Gasch et al., 2000), the 4E-BPs are dephosphorylated, thus activating them to sequester eIF4E from the scaffolding partner eIF4G. Functional eIF4E depletion is selective in inhibiting translation of growth-promoting mRNAs, such as those of ribosomal proteins, and enhancing translation of the more limited cadre of stress response genes (Thoreen, 2017; Thoreen et al., 2012). The other primary initiation target is the ternary complex of initiator tRNA•eIF2•GTP via the General control (Gcn) pathway. Ribosome-free and uncharged tRNA activates the kinase Gcn2 (Dong et al., 2000), which phosphorylates Ser51 in eIF2α to competitively inhibit the guanine nucleotide exchange factor eIF2B. The effect is to reduce eIF2•GTP available for forming the ternary complex (Kimball et al., 1998; Krishnamoorthy et al., 2001). A reduction in initiator tRNA•eIF2•GTP leads to gene-specific consequences for translational control that have been exhaustively studied using *GCN4*. Its complex transcript leader contains a series of upstream ORFs (uORFs) that, when translated in nutrient-rich conditions, repress translation from the genic ORF, whereas nutrient limitation favors ribosome bypassing of uORFs and initiation at the genic ORF (reviewed in Hinnebusch, 2005). Moreover, the same pathway is conserved in mammals, in which the homolog of *GCN4* is *ATF4* (Activating Transcription Factor 4), the activator of the integrated stress response. The Gcn response thus globally reduces initiation while permitting finer expression control over starvation-adaptive messages.

In contrast to eukaryotes, translational control in prokaryotes mainly targets the accessibility of Shine-Dalgarno sequences in mRNAs or the ribosome itself (Duval et al., 2015). The best-characterized initiation inhibitors are the ribosome hibernation factors, which bind to ribosomes at sites that sterically occlude initiation factors. These include protein Y, HPF (Hibernation Promoting Factor), and RMF (Ribosome Modulation Factor) (Agafonov et al., 1999; Basu and Yap, 2016; Polikanov et al., 2012; Vila-Sanjurjo et al., 2004). The resulting complexes are stabilized in translationally inactive conformations that also prevent catabolic nucleases from cleaving rRNA at the subunit interface (Basturea et al., 2011). Mirroring their rapid induction during stress, a nutrient upshift causes hibernation factors to dissociate from ribosomes within minutes (Aiso et al., 2005).

Other proteins monitor and further inhibit elongation during starvation. The ATP Binding Cassette protein EttA binds in the E site with contacts to the P site tRNA acceptor arm, and its putative function is to block methionyl transfer from the P to the A site tRNA during the first round of elongation. Importantly, this activity is only significant at high concentrations of ADP, leading to the model that EttA is regulated by the cell's energy status (Boël et al., 2014; Chen et al., 2014) Another well-characterized elongation "sensor" is RelA, the enzymatic initiator of the stringent response that globally reprograms gene expression and metabolism during starvation (Goldman and Jakubowski, 1990; Hauryliuk et al., 2015). As the ratio of charged to uncharged tRNA drops, uncharged tRNA increasingly competes with the cognate ternary complex for binding in the 30S A site. Moderate limitation decreases the rate of protein synthesis without activating RelA, because of the high dissociation rate of free tRNA (without EF-Tu) from the ribosome. At a 5- to 10-fold excess, however, uncharged tRNA begins to interact with RelA at the A site (Goldman and Jakubowski, 1990). This enzyme, whose biochemical activity is to synthesize (p)ppGpp from GTP and ATP, is autoinhibited when ribosome-free. By contrast, ribosome-bound RelA interacts with the deacylated acceptor end of the A site tRNA in a manner sterically incompatible with aminoacylation (Brown et al., 2016). Following (p)ppGpp synthesis,

RelA dissociates and is free to interact with another ribosome, thereby monitoring translational status across the cell (Wendrich et al., 2002). The (p)ppGpp alarmone produced by RelA binds directly to RNA Polymerase in *E. coli*, inhibiting transcription at rDNA and ribosomal protein gene loci to reduce new ribosome production. Conversely, transcription of amino acid biosynthesis genes is induced to support translation of a more limited subset of genes (Hauryliuk et al., 2015). ppGpp also binds stably to EF-Tu and is thought to increase the accuracy of tRNA selection in a milieu of increased competition by noncognate tRNAs for A site binding. By interacting with ribosomal complexes containing aminoacyl-tRNA in the A site and slowing peptide bond formation, EF-Tu•ppGpp prolongs kinetic proofreading to bias dissociation of non-cognate versus cognate tRNA (Dix and Thompson, 1986; Pingoud et al., 1983). Thus, the stringent response comprises multiple mechanisms to remodel the translatome and to increase the fidelity of translation during starvation.

To stimulate premature termination, the toxin RelE cleaves mRNAs in the A site of translating ribosomes (Hwang and Buskirk, 2017; Pedersen et al., 2003). Absence of mRNA in the A site then recruits the tmRNA system (or ArfA/B) to dismantle the stalled ribosome and to degrade its associated ligands. In summary, bacteria deploy a variety of strategies to modulate each stage of the translation cycle during starvation.

Discovery of eukaryotic ribosome-associated proteins that modulate gene expression

In contrast to the ribosome-associated quality control systems, there are fewer known proteins in eukaryotes that directly target the ribosome. Nevertheless, those characterized underscore the idea of translational control by proteins beyond the core initiation, elongation, and termination machinery. Here I will provide a molecularly well-studied example from humans. I will then overview proteomics as a discovery tool for identification of novel ribosome-bound proteins with potentially significant functions.

The Fragile X Mental Retardation Protein (FMRP), which is highly expressed in neurons and whose loss causes Fragile X Syndrome, exerts gene-specific translational control by inhibiting elongation. FMRP was first found to interact with mRNA in polysomes (Corbin et al., 1997). It was later recognized to interact with ribosomes in a manner sensitive to the chain terminator puromycin (Stefani et al., 2004), raising the possibility that it specifically affects elongation. A breakthrough came with the application of genome-wide RNA crosslinking and immunoprecipitation to capture the full spectrum of FMRP mRNA interactions in endogenous mouse brain (Darnell et al., 2011), from which the authors were able to identify genes in synaptic transmission and regulation of small GTPase signaling as its most enriched targets. Importantly, *in vitro* translation extracts demonstrated that FMRP selectively blocks elongation of its targets, but not of its non-targets. Surprisingly, these *in vivo* targets lacked the G-quadruplex and pseudoknot structures identified earlier by *in vitro* selection (Darnell et al., 2001, 2005). Moreover, a comparison of these targets with those of three other FRMP genome-wide association assays (Ascano et al., 2012; Brown et al., 2001; Miyashiro et al., 2003) also identified only a small percentage of overlap, and enrichment solely of the degenerate GACR motif (Suhl et al., 2014). The full set of FMRP's mRNA specificity determinants therefore remains unknown. A full structure of a translating ribosome bound to FMRP would also begin to clarify how it interacts with an elongating complex, and what advantage this mode of gene regulation could confer to neuronal cells.

FMRP and most of the ribosome-associated proteins discussed in this chapter were first identified in genetic studies. Only later were they serendipitously found to intersect with translation. Proteomics is now a targeted strategy to interrogate the composition of ribosomal complexes (Chaker-Margot et al., 2015; Fleischer et al., 2006; Nissan et al., 2002). The historic antecedent of this approach was two-dimensional gel electrophoresis, which revealed the bacterial ribosome hibernation factors from gradient fractions of stationary phase bacteria (Agafonov et al., 1999; Ueta et al., 2010; Wada et al., 2000). More recently, researchers

isolated ribosomal complexes from rapidly growing *S. cerevisiae* and identified their interactors using mass spectrometry (Fleischer et al., 2006). Following validation of the highest confidence hits by western blotting of gradient fractions, they screened for translation phenotypes among these Translation Machinery-Associated (TMA) proteins. Three affected fidelity and bulk protein synthesis by unknown mechanisms. Since then, Listerin was independently characterized as a conserved ubiquitin ligase associated with the RQC (Brandman et al., 2012). Tma108 (108 kDa) was also characterized as a chaperone specific to a subset of ATP- and zinc-binding domain proteins. However, the full functional scope of these novel proteins, and the eukaryotic ribosome composition under other growth conditions, is only beginning to be explored.

Thesis overview

In the following chapter I describe the discovery and functional characterization of the conserved ribosome-bound protein Lso2. The motivation was to determine whether changes in the composition of ribosomes affect gene expression during glucose starvation in yeast, for which canonical targeting of initiation factors fails to explain the dramatic translational reprogramming (Ashe et al., 2000; Vaidyanathan et al., 2014). Using quantitative proteomics, we identified Lso2 as being constitutively ribosome-associated, with moderately increased polysome association in glucose withdrawal. Lso2 was previously uncharacterized due to its length being shorter than 100 amino acids, which led to its exclusion from the first yeast genome annotation. We validated that the entire cellular pool of Lso2 co-sediments with ribosomes in both glucose-replete and -starved conditions, where it is enriched in the 80S monosome fractions. Although Lso2 has little effect on bulk translation in glucose-starved or replete growth, I subsequently found that *lso2* nulls (*lso2*Δ) are defective in resuming translation during nutrient upshift from stationary phase. More specifically, *lso2*Δ accumulates monosomes that are not translating normally. To understand the basis of this phenotype, we sought to identify its ribosome binding site and other potential RNA targets. We used genome-wide

crosslinking and immunoprecipitation to determine that Lso2 crosslinks specifically to a region of the 25S rRNA that overlaps with the GTPase activating center, about 30 Å from the A site in the tRNA channel. This binding site was corroborated with a biochemical assay demonstrating that Lso2 stabilizes ribosomal subunit association *in vitro*, which is a known function of the similarly sized bacterial ribosome hibernation factors that bind in the tRNA channel. Importantly, Lso2 also crosslinked to a broad suite of tRNAs, which is consistent with its ribosome binding site. Given that the entire pool of Lso2 is ribosome-bound, these interactions with tRNA most likely occur on translating ribosomes. Furthermore, because ribosomes in *lso2Δ* recovering from stationary phase are devoid of gross abnormalities that could prevent them from initiating, I conjecture that the monosome accumulation is a defect downstream of abortive elongation. Finally, I show that the human ortholog of Lso2, CCDC124, is partially ribosome-associated in HeLa cells and that its ribosome binding activity is conserved. This suggests that the molecular function of Lso2 in translation is broadly important. In Chapter 3, I will justify my preferred model of Lso2 promoting productive elongation, present alternative models for its functions in other stages of translation, and describe approaches for refining our understanding of its translational complex and its molecular impacts on the translation cycle.

References

Acker, M.G., Shin, B.-S., Dever, T.E., and Lorsch, J.R. (2006). Interaction between Eukaryotic Initiation Factors 1A and 5B Is Required for Efficient Ribosomal Subunit Joining. J. Biol. Chem. *281*, 8469–8475.

Agafonov, D.E., Kolb, V.A., Nazimov, I.V., and Spirin, A.S. (1999). A protein residing at the subunit interface of the bacterial ribosome. Proc. Natl. Acad. Sci. U. S. A. *96*, 12345–12349.

Aiso, T., Yoshida, H., Wada, A., and Ohki, R. (2005). Modulation of mRNA Stability Participates in Stationary-Phase-Specific Expression of Ribosome Modulation Factor. J. Bacteriol. *187*, 1951–1958.

Aitken, C.E., and Puglisi, J.D. (2010). Following the intersubunit conformation of the ribosome during translation in real time. Nat. Struct. Mol. Biol. *17*, 793–800.

Asano, K., Clayton, J., Shalev, A., and Hinnebusch, A.G. (2000). A multifactor complex of eukaryotic initiation factors, eIF1, eIF2, eIF3, eIF5, and initiator tRNA(Met) is an important translation initiation intermediate in vivo. Genes Dev. *14*, 2534–2546.

Ascano, M., Mukherjee, N., Bandaru, P., Miller, J.B., Nusbaum, J.D., Corcoran, D.L., Langlois, C., Munschauer, M., Dewell, S., Hafner, M., et al. (2012). FMRP targets distinct mRNA sequence elements to regulate protein expression. Nature *492*, 382–386.

Ashe, M.P., De Long, S.K., and Sachs, A.B. (2000). Glucose depletion rapidly inhibits translation initiation in yeast. Mol. Biol. Cell *11*, 833–848.

Aylett, C.H.S., Boehringer, D., Erzberger, J.P., Schaefer, T., and Ban, N. (2015). Structure of a Yeast 40S–eIF1–eIF1A–eIF3–eIF3j initiation complex. Nat. Struct. Mol. Biol. *22*, 269–271.

Barends, S., Karzai, A.W., Sauer, R.T., Wower, J., and Kraal, B. (2001). Simultaneous and functional binding of SmpB and EF-Tu·GTP to the alanyl acceptor arm of tmRNA. J. Mol. Biol. *314*, 9–21.

Basturea, G.N., Zundel, M.A., and Deutscher, M.P. (2011). Degradation of ribosomal RNA during starvation: comparison to quality control during steady-state growth and a role for RNase PH. RNA N. Y. N *17*, 338–345.

Basu, A., and Yap, M.-N.F. (2016). Ribosome hibernation factor promotes Staphylococcal survival and differentially represses translation. Nucleic Acids Res. *44*, 4881–4893.

Becker, T., Armache, J.-P., Jarasch, A., Anger, A.M., Villa, E., Sieber, H., Motaal, B.A., Mielke, T., Berninghausen, O., and Beckmann, R. (2011). Structure of the no-go mRNA decay complex Dom34–Hbs1 bound to a stalled 80S ribosome. Nat. Struct. Mol. Biol. *18*, 715–720.

Blanchard, S.C., Gonzalez, R.L., Kim, H.D., Chu, S., and Puglisi, J.D. (2004). tRNA selection and kinetic proofreading in translation. Nat. Struct. Mol. Biol. *11*, 1008–1014.

Boël, G., Smith, P.C., Ning, W., Englander, M.T., Chen, B., Hashem, Y., Testa, A.J., Fischer, J.J., Wieden, H.-J., Frank, J., et al. (2014). The ABC-F protein EttA gates ribosome entry into the translation elongation cycle. Nat. Struct. Mol. Biol. *21*, 143–151.

Brandman, O., and Hegde, R.S. (2016). Ribosome-associated protein quality control. Nat. Struct. Mol. Biol. *23*, 7–15.

Brandman, O., Stewart-Ornstein, J., Wong, D., Larson, A., Williams, C.C., Li, G.-W., Zhou, S., King, D., Shen, P.S., Weibezahn, J., et al. (2012). A ribosome-bound quality control complex triggers degradation of nascent peptides and signals translation stress. Cell *151*, 1042–1054.

Brown, A., Shao, S., Murray, J., Hegde, R.S., and Ramakrishnan, V. (2015). Structural basis for stop codon recognition in eukaryotes. Nature *524*, 493–496.

Brown, A., Fernández, I.S., Gordiyenko, Y., and Ramakrishnan, V. (2016). Ribosome-dependent activation of stringent control. Nature *534*, 277–280.

Brown, V., Jin, P., Ceman, S., Darnell, J.C., O'Donnell, W.T., Tenenbaum, S.A., Jin, X., Feng, Y., Wilkinson, K.D., Keene, J.D., et al. (2001). Microarray identification of FMRP-associated brain mRNAs and altered mRNA translational profiles in fragile X syndrome. Cell *107*, 477–487.

Buskirk, A.R., and Green, R. (2017). Ribosome pausing, arrest and rescue in bacteria and eukaryotes. Philos. Trans. R. Soc. Lond. B. Biol. Sci. *372*.

Chaker-Margot, M., Hunziker, M., Barandun, J., Dill, B.D., and Klinge, S. (2015). Stage-specific assembly events of the 6-MDa small-subunit processome initiate eukaryotic ribosome biogenesis. Nat. Struct. Mol. Biol.

Chen, B., Boël, G., Hashem, Y., Ning, W., Fei, J., Wang, C., Gonzalez, R.L., Hunt, J.F., and Frank, J. (2014). EttA regulates translation by binding the ribosomal E site and restricting ribosome-tRNA dynamics. Nat. Struct. Mol. Biol. *21*, 152–159.

Chen, L., Muhlrad, D., Hauryliuk, V., Cheng, Z., Lim, M.K., Shyp, V., Parker, R., and Song, H. (2010). Structure of the Dom34–Hbs1 complex and implications for no-go decay. Nat. Struct. Mol. Biol. *17*, 1233–1240.

Cole, S.E., LaRiviere, F.J., Merrikh, C.N., and Moore, M.J. (2009). A convergence of rRNA and mRNA quality control pathways revealed by mechanistic analysis of nonfunctional rRNA decay. Mol. Cell *34*, 440–450.

Corbin, F., Bouillon, M., Fortin, A., Morin, S., Rousseau, F., and Khandjian, E.W. (1997). The fragile X mental retardation protein is associated with poly(A)+ mRNA in actively translating polyribosomes. Hum. Mol. Genet. *6*, 1465–1472.

Cornish, P.V., Ermolenko, D.N., Noller, H.F., and Ha, T. (2008). Spontaneous intersubunit rotation in single ribosomes. Mol. Cell *30*, 578–588.

Darnell, J.C., Jensen, K.B., Jin, P., Brown, V., Warren, S.T., and Darnell, R.B. (2001). Fragile X mental retardation protein targets G quartet mRNAs important for neuronal function. Cell *107*, 489–499.

Darnell, J.C., Fraser, C.E., Mostovetsky, O., Stefani, G., Jones, T.A., Eddy, S.R., and Darnell, R.B. (2005). Kissing complex RNAs mediate interaction between the Fragile-X mental retardation protein KH2 domain and brain polyribosomes. Genes Dev. *19*, 903–918.

Darnell, J.C., Van Driesche, S.J., Zhang, C., Hung, K.Y.S., Mele, A., Fraser, C.E., Stone, E.F., Chen, C., Fak, J.J., Chi, S.W., et al. (2011). FMRP stalls ribosomal translocation on mRNAs linked to synaptic function and autism. Cell *146*, 247–261.

Das, S., Ghosh, R., and Maitra, U. (2001). Eukaryotic translation initiation factor 5 functions as a GTPase-activating protein. J. Biol. Chem. *276*, 6720–6726.

Dever, T.E., and Green, R. (2012). The elongation, termination, and recycling phases of translation in eukaryotes. Cold Spring Harb. Perspect. Biol. *4*, a013706.

Dix, D.B., and Thompson, R.C. (1986). Elongation factor Tu.guanosine 3'-diphosphate 5'-diphosphate complex increases the fidelity of proofreading in protein biosynthesis: mechanism

for reducing translational errors introduced by amino acid starvation. Proc. Natl. Acad. Sci. U. S. A. *83*, 2027–2031.

Doma, M.K., and Parker, R. (2006). Endonucleolytic cleavage of eukaryotic mRNAs with stalls in translation elongation. Nature *440*, 561–564.

Dong, J., Qiu, H., Garcia-Barrio, M., Anderson, J., and Hinnebusch, A.G. (2000). Uncharged tRNA Activates GCN2 by Displacing the Protein Kinase Moiety from a Bipartite tRNA-Binding Domain. Mol. Cell *6*, 269–279.

Duval, M., Simonetti, A., Caldelari, I., and Marzi, S. (2015). Multiple ways to regulate translation initiation in bacteria: Mechanisms, regulatory circuits, dynamics. Biochimie *114*, 18–29.

Ermolenko, D.N., and Noller, H.F. (2011). mRNA translocation occurs during the second step of ribosomal intersubunit rotation. Nat. Struct. Mol. Biol. *18*, 457–462.

Fleischer, T.C., Weaver, C.M., McAfee, K.J., Jennings, J.L., and Link, A.J. (2006). Systematic identification and functional screens of uncharacterized proteins associated with eukaryotic ribosomal complexes. Genes Dev. *20*, 1294–1307.

Flynn, J.M., Levchenko, I., Seidel, M., Wickner, S.H., Sauer, R.T., and Baker, T.A. (2001). Overlapping recognition determinants within the ssrA degradation tag allow modulation of proteolysis. Proc. Natl. Acad. Sci. U. S. A. *98*, 10584–10589.

Gasch, A.P., Spellman, P.T., Kao, C.M., Carmel-Harel, O., Eisen, M.B., Storz, G., Botstein, D., and Brown, P.O. (2000). Genomic expression programs in the response of yeast cells to environmental changes. Mol. Biol. Cell *11*, 4241–4257.

Goldman, E., and Jakubowski, H. (1990). Uncharged tRNA, protein synthesis, and the bacterial stringent response. Mol. Microbiol. *4*, 2035–2040.

Graille, M., and Séraphin, B. (2012). Surveillance pathways rescuing eukaryotic ribosomes lost in translation. Nat. Rev. Mol. Cell Biol. *13*, 727–735.

Gromadski, K.B., and Rodnina, M.V. (2004). Kinetic determinants of high-fidelity tRNA discrimination on the ribosome. Mol. Cell *13*, 191–200.

Guydosh, N.R., and Green, R. (2014). Dom34 rescues ribosomes in 3' untranslated regions. Cell *156*, 950–962.

Hauryliuk, V., Atkinson, G.C., Murakami, K.S., Tenson, T., and Gerdes, K. (2015). Recent functional insights into the role of (p)ppGpp in bacterial physiology. Nat. Rev. Microbiol. *13*, 298–309.

He, H., von der Haar, T., Singh, C.R., Ii, M., Li, B., Hinnebusch, A.G., McCarthy, J.E.G., and Asano, K. (2003). The yeast eukaryotic initiation factor 4G (eIF4G) HEAT domain interacts with eIF1 and eIF5 and is involved in stringent AUG selection. Mol. Cell. Biol. *23*, 5431–5445.

Hershey, P.E.C., McWhirter, S.M., Gross, J.D., Wagner, G., Alber, T., and Sachs, A.B. (1999). The Cap-binding Protein eIF4E Promotes Folding of a Functional Domain of Yeast Translation Initiation Factor eIF4G1. J. Biol. Chem. *274*, 21297–21304.

Hilbert, M., Kebbel, F., Gubaev, A., and Klostermeier, D. (2011). eIF4G stimulates the activity of the DEAD box protein eIF4A by a conformational guidance mechanism. Nucleic Acids Res. *39*, 2260–2270.

Hinnebusch, A.G. (2005). Translational regulation of GCN4 and the general amino acid control of yeast. Annu. Rev. Microbiol. *59*, 407–450.

van Hoof, A., Frischmeyer, P.A., Dietz, H.C., and Parker, R. (2002). Exosome-mediated recognition and degradation of mRNAs lacking a termination codon. Science *295*, 2262–2264.

Huang, H.K., Yoon, H., Hannig, E.M., and Donahue, T.F. (1997). GTP hydrolysis controls stringent selection of the AUG start codon during translation initiation in Saccharomyces cerevisiae. Genes Dev. *11*, 2396–2413.

Hussain, T., Llácer, J.L., Fernández, I.S., Munoz, A., Martin-Marcos, P., Savva, C.G., Lorsch, J.R., Hinnebusch, A.G., and Ramakrishnan, V. (2014). Structural changes enable start codon recognition by the eukaryotic translation initiation complex. Cell *159*, 597–607.

Huter, P., Müller, C., Beckert, B., Arenz, S., Berninghausen, O., Beckmann, R., and Wilson, D.N. (2017). Structural basis for ArfA-RF2-mediated translation termination on mRNAs lacking stop codons. Nature *541*, 546–549.

Hwang, J.-Y., and Buskirk, A.R. (2017). A ribosome profiling study of mRNA cleavage by the endonuclease RelE. Nucleic Acids Res. *45*, 327–336.

Ivanova, N., Pavlov, M.Y., and Ehrenberg, M. (2005). tmRNA-induced Release of Messenger RNA from Stalled Ribosomes. J. Mol. Biol. *350*, 897–905.

Janssen, B.D., Garza-Sánchez, F., and Hayes, C.S. (2013). A-Site mRNA Cleavage Is Not Required for tmRNA-Mediated ssrA-Peptide Tagging. PLoS ONE *8*, e81319.

Jin, H., Kelley, A.C., and Ramakrishnan, V. (2011). Crystal structure of the hybrid state of ribosome in complex with the guanosine triphosphatase release factor 3. Proc. Natl. Acad. Sci. U. S. A. *108*, 15798–15803.

Keiler, K.C., Waller, P.R.H., and Sauer, R.T. (1996). Role of a Peptide Tagging System in Degradation of Proteins Synthesized from Damaged Messenger RNA. Science *271*, 990–993.

Kimball, S.R., Fabian, J.R., Pavitt, G.D., Hinnebusch, A.G., and Jefferson, L.S. (1998). Regulation of guanine nucleotide exchange through phosphorylation of eukaryotic initiation factor eIF2alpha. Role of the alpha- and delta-subunits of eiF2b. J. Biol. Chem. *273*, 12841–12845.

Kobayashi, K., Kikuno, I., Kuroha, K., Saito, K., Ito, K., Ishitani, R., Inada, T., and Nureki, O. (2010). Structural basis for mRNA surveillance by archaeal Pelota and GTP-bound EF1α complex. Proc. Natl. Acad. Sci. U. S. A. *107*, 17575–17579.

Koutmou, K.S., McDonald, M.E., Brunelle, J.L., and Green, R. (2014). RF3:GTP promotes rapid dissociation of the class 1 termination factor. RNA *20*, 609–620.

Krishnamoorthy, T., Pavitt, G.D., Zhang, F., Dever, T.E., and Hinnebusch, A.G. (2001). Tight Binding of the Phosphorylated Subunit of Initiation Factor 2 (eIF2) to the Regulatory Subunits of Guanine Nucleotide Exchange Factor eIF2B Is Required for Inhibition of Translation Initiation. Mol. Cell. Biol. *21*, 5018–5030.

LaRiviere, F.J., Cole, S.E., Ferullo, D.J., and Moore, M.J. (2006). A late-acting quality control process for mature eukaryotic rRNAs. Mol. Cell *24*, 619–626.

Laurberg, M., Asahara, H., Korostelev, A., Zhu, J., Trakhanov, S., and Noller, H.F. (2008). Structural basis for translation termination on the 70S ribosome. Nature *454*, 852–857.

Letzring, D.P., Wolf, A.S., Brule, C.E., and Grayhack, E.J. (2013). Translation of CGA codon repeats in yeast involves quality control components and ribosomal protein L1. RNA N. Y. N *19*, 1208–1217.

Ling, C., and Ermolenko, D.N. (2016). Structural insights into ribosome translocation. Wiley Interdiscip. Rev. RNA *7*, 620–636.

Liu, T., Kaplan, A., Alexander, L., Yan, S., Wen, J.-D., Lancaster, L., Wickersham, C.E., Fredrik, K., Noller, H., Tinoco, I., et al. (2014). Direct measurement of the mechanical work during translocation by the ribosome. eLife *3*.

Llácer, J.L., Hussain, T., Marler, L., Aitken, C.E., Thakur, A., Lorsch, J.R., Hinnebusch, A.G., and Ramakrishnan, V. (2015). Conformational Differences between Open and Closed States of the Eukaryotic Translation Initiation Complex. Mol. Cell *59*, 399–412.

Ma, C., Kurita, D., Li, N., Chen, Y., Himeno, H., and Gao, N. (2017). Mechanistic insights into the alternative translation termination by ArfA and RF2. Nature *541*, 550–553.

Martin-Marcos, P., Nanda, J.S., Luna, R.E., Zhang, F., Saini, A.K., Cherkasova, V.A., Wagner, G., Lorsch, J.R., and Hinnebusch, A.G. (2014). Enhanced eIF1 binding to the 40S ribosome impedes conformational rearrangements of the preinitiation complex and elevates initiation accuracy. RNA *20*, 150–167.

Miller, M.R., Liu, Z., Cazier, D.J., Gebhard, G.M., Herron, S.R., Zaher, H.S., Green, R., and Buskirk, A.R. (2011). The role of SmpB and the ribosomal decoding center in licensing tmRNA entry into stalled ribosomes. RNA N. Y. N *17*, 1727–1736.

Mitchell, S.F., Walker, S.E., Algire, M.A., Park, E.-H., Hinnebusch, A.G., and Lorsch, J.R. (2010). The 5′-7-Methylguanosine Cap on Eukaryotic mRNAs Serves Both to Stimulate Canonical Translation Initiation and to Block an Alternative Pathway. Mol. Cell *39*, 950–962.

Miyashiro, K.Y., Beckel-Mitchener, A., Purk, T.P., Becker, K.G., Barret, T., Liu, L., Carbonetto, S., Weiler, I.J., Greenough, W.T., and Eberwine, J. (2003). RNA cargoes associating with FMRP reveal deficits in cellular functioning in Fmr1 null mice. Neuron *37*, 417–431.

Mohammad, M.P., Munzarová Pondělíčková, V., Zeman, J., Gunišová, S., and Valášek, L.S. (2017). *In vivo* evidence that eIF3 stays bound to ribosomes elongating and terminating on short upstream ORFs to promote reinitiation. Nucleic Acids Res. gkx049.

Neubauer, C., Gillet, R., Kelley, A.C., and Ramakrishnan, V. (2012). Decoding in the Absence of a Codon by tmRNA and SmpB in the Ribosome. Science *335*, 1366–1369.

Nissan, T.A., Bassler, J., Petfalski, E., Tollervey, D., and Hurt, E. (2002). 60S pre-ribosome formation viewed from assembly in the nucleolus until export to the cytoplasm. EMBO J. *21*, 5539–5547.

O'Leary, S.E., Petrov, A., Chen, J., and Puglisi, J.D. (2013). Dynamic Recognition of the mRNA Cap by Saccharomyces cerevisiae eIF4E. Structure *21*, 2197–2207.

Pedersen, K., Zavialov, A.V., Pavlov, M.Y., Elf, J., Gerdes, K., and Ehrenberg, M. (2003). The bacterial toxin RelE displays codon-specific cleavage of mRNAs in the ribosomal A site. Cell *112*, 131–140.

Pestova, T.V., Lomakin, I.B., Lee, J.H., Choi, S.K., Dever, T.E., and Hellen, C.U. (2000). The joining of ribosomal subunits in eukaryotes requires eIF5B. Nature *403*, 332–335.

Pingoud, A., Gast, F.U., Block, W., and Peters, F. (1983). The elongation factor Tu from Escherichia coli, aminoacyl-tRNA, and guanosine tetraphosphate form a ternary complex which is bound by programmed ribosomes. J. Biol. Chem. *258*, 14200–14205.

Polikanov, Y.S., Blaha, G.M., and Steitz, T.A. (2012). How hibernation factors RMF, HPF, and YfiA turn off protein synthesis. Science *336*, 915–918.

Polymenis, M., and Schmidt, E.V. (1997). Coupling of cell division to cell growth by translational control of the G1 cyclin CLN3 in yeast. Genes Dev. *11*, 2522–2531.

Preis, A., Heuer, A., Barrio-Garcia, C., Hauser, A., Eyler, D.E., Berninghausen, O., Green, R., Becker, T., and Beckmann, R. (2014). Cryoelectron microscopic structures of eukaryotic translation termination complexes containing eRF1-eRF3 or eRF1-ABCE1. Cell Rep. *8*, 59–65.

Rodnina, M.V., and Wintermeyer, W. (2009). Recent mechanistic insights into eukaryotic ribosomes. Curr. Opin. Cell Biol. *21*, 435–443.

Schmeing, T.M., Voorhees, R.M., Kelley, A.C., Gao, Y.-G., Murphy, F.V., Weir, J.R., and Ramakrishnan, V. (2009). The crystal structure of the ribosome bound to EF-Tu and aminoacyl-tRNA. Science *326*, 688–694.

Schuller, A.P., Wu, C.C.-C., Dever, T.E., Buskirk, A.R., and Green, R. (2017). eIF5A Functions Globally in Translation Elongation and Termination. Mol. Cell.

Schütz, P., Bumann, M., Oberholzer, A.E., Bieniossek, C., Trachsel, H., Altmann, M., and Baumann, U. (2008). Crystal structure of the yeast eIF4A-eIF4G complex: an RNA-helicase controlled by protein-protein interactions. Proc. Natl. Acad. Sci. U. S. A. *105*, 9564–9569.

Selmer, M. (2006). Structure of the 70S Ribosome Complexed with mRNA and tRNA. Science *313*, 1935–1942.

Shao, S., Murray, J., Brown, A., Taunton, J., Ramakrishnan, V., and Hegde, R.S. (2016). Decoding Mammalian Ribosome-mRNA States by Translational GTPase Complexes. Cell *167*, 1229–1240.e15.

Shoemaker, C.J., and Green, R. (2012). Translation drives mRNA quality control. Nat. Struct. Mol. Biol. *19*, 594–601.

Shoemaker, C.J., Eyler, D.E., and Green, R. (2010). Dom34:Hbs1 promotes subunit dissociation and peptidyl-tRNA drop-off to initiate no-go decay. Science *330*, 369–372.

Soe, R., Mosley, R.T., Justice, M., Nielsen-Kahn, J., Shastry, M., Merrill, A.R., and Andersen, G.R. (2007). Sordarin Derivatives Induce a Novel Conformation of the Yeast Ribosome Translocation Factor eEF2. J. Biol. Chem. *282*, 657–666.

Sonenberg, N., and Hinnebusch, A.G. (2009). Regulation of translation initiation in eukaryotes: mechanisms and biological targets. Cell *136*, 731–745.

Song, H., Mugnier, P., Das, A.K., Webb, H.M., Evans, D.R., Tuite, M.F., Hemmings, B.A., and Barford, D. (2000). The Crystal Structure of Human Eukaryotic Release Factor eRF1—Mechanism of Stop Codon Recognition and Peptidyl-tRNA Hydrolysis. Cell *100*, 311–321.

Stark, H., Rodnina, M.V., Wieden, H.-J., Zemlin, F., Wintermeyer, W., and van Heel, M. (2002). Ribosome interactions of aminoacyl-tRNA and elongation factor Tu in the codon-recognition complex. Nat. Struct. Biol.

Starosta, A.L., Lassak, J., Jung, K., and Wilson, D.N. (2014). The bacterial translation stress response. FEMS Microbiol. Rev. *38*, 1172–1201.

Stefani, G., Fraser, C.E., Darnell, J.C., and Darnell, R.B. (2004). Fragile X mental retardation protein is associated with translating polyribosomes in neuronal cells. J. Neurosci. Off. J. Soc. Neurosci. *24*, 7272–7276.

Suhl, J.A., Chopra, P., Anderson, B.R., Bassell, G.J., and Warren, S.T. (2014). Analysis of FMRP mRNA target datasets reveals highly associated mRNAs mediated by G-quadruplex structures formed via clustered WGGA sequences. Hum. Mol. Genet. *23*, 5479–5491.

Thoreen, C.C. (2017). The molecular basis of mTORC1-regulated translation. Biochem. Soc. Trans. *45*, 213–221.

Thoreen, C.C., Chantranupong, L., Keys, H.R., Wang, T., Gray, N.S., and Sabatini, D.M. (2012). A unifying model for mTORC1-mediated regulation of mRNA translation. Nature *485*, 109–113.

Tsuboi, T., Kuroha, K., Kudo, K., Makino, S., Inoue, E., Kashima, I., and Inada, T. (2012). Dom34:hbs1 plays a general role in quality-control systems by dissociation of a stalled ribosome at the 3' end of aberrant mRNA. Mol. Cell *46*, 518–529.

Ueta, M., Wada, C., and Wada, A. (2010). Formation of 100S ribosomes in *Staphylococcus aureus* by the hibernation promoting factor homolog *Sa* HPF. Genes Cells *15*, 43–58.

Vaidyanathan, P.P., Zinshteyn, B., Thompson, M.K., and Gilbert, W.V. (2014). Protein kinase A regulates gene-specific translational adaptation in differentiating yeast. RNA N. Y. N *20*, 912–922.

Valasek, L. (2002). Direct eIF2-eIF3 contact in the multifactor complex is important for translation initiation in vivo. EMBO J. *21*, 5886–5898.

Vila-Sanjurjo, A., Schuwirth, B.-S., Hau, C.W., and Cate, J.H.D. (2004). Structural basis for the control of translation initiation during stress. Nat. Struct. Mol. Biol. *11*, 1054–1059.

Villa, N., Do, A., Hershey, J.W.B., and Fraser, C.S. (2013). Human Eukaryotic Initiation Factor 4G (eIF4G) Protein Binds to eIF3c, -d, and -e to Promote mRNA Recruitment to the Ribosome. J. Biol. Chem. *288*, 32932–32940.

Voorhees, R.M., and Ramakrishnan, V. (2013). Structural Basis of the Translational Elongation Cycle. Annu. Rev. Biochem. *82*, 203–236.

Voorhees, R.M., Schmeing, T.M., Kelley, A.C., and Ramakrishnan, V. (2010). The Mechanism for Activation of GTP Hydrolysis on the Ribosome. Science *330*, 835–838.

Wada, A., Mikkola, R., Kurland, C.G., and Ishihama, A. (2000). Growth phase-coupled changes of the ribosome profile in natural isolates and laboratory strains of Escherichia coli. J. Bacteriol. *182*, 2893–2899.

Warner, J.R. (1999). The economics of ribosome biosynthesis in yeast. Trends Biochem. Sci. *24*, 437–440.

Weixlbaumer, A., Jin, H., Neubauer, C., Voorhees, R.M., Petry, S., Kelley, A.C., and Ramakrishnan, V. (2008). Insights into translational termination from the structure of RF2 bound to the ribosome. Science *322*, 953–956.

Wendrich, T.M., Blaha, G., Wilson, D.N., Marahiel, M.A., and Nierhaus, K.H. (2002). Dissection of the mechanism for the stringent factor RelA. Mol. Cell *10*, 779–788.

Whitford, P.C., Geggier, P., Altman, R.B., Blanchard, S.C., Onuchic, J.N., and Sanbonmatsu, K.Y. (2010). Accommodation of aminoacyl-tRNA into the ribosome involves reversible excursions along multiple pathways. RNA *16*, 1196–1204.

Yamamoto, Y., Singh, C.R., Marintchev, A., Hall, N.S., Hannig, E.M., Wagner, G., Asano, K. (2005). The eukaryotic initiation factor (eIF) 5 HEAT domain mediates multifactor assembly and scanning with distinct interfaces to eIF1, eIF2, eIF3, and eIF4G. Proc. Natl. Acad. Sci. U. S. A. *102*, 16164-16169.

Young, D.J., Guydosh, N.R., Zhang, F., Hinnebusch, A.G., and Green, R. (2015). Rli1/ABCE1 Recycles Terminating Ribosomes and Controls Translation Reinitiation in 3'UTRs In Vivo. Cell *162*, 872–884.

Zhou, J., Lancaster, L., Trakhanov, S., and Noller, H.F. (2012). Crystal structure of release factor RF3 trapped in the GTP state on a rotated conformation of the ribosome. RNA N. Y. N *18*, 230–240.

Chapter II:

Lso2 is a conserved ribosome-bound protein required for translational recovery in yeast

Abstract

The full complement of proteins that interact with ribosomes to affect translation and physiology remains unknown. Using discovery proteomics, we identified an uncharacterized but broadly conserved protein, Lso2, that is exclusively ribosome-bound in yeast. Yeast lacking Lso2 show global defects in translation following a shift from starvation to rich medium, with an accumulation of monosomes that are not translating normally. Crosslinking, immunoprecipitation, and sequencing demonstrate that Lso2 binds 25S ribosomal RNA in the tRNA channel near the A site and interacts with a broad range of tRNAs *in vivo*. Consistent with its binding site, Lso2 stabilizes ribosomal subunit association *in vitro*, and its specific ribosome binding activity is conserved to man. Based on its ribosome binding site, tRNA targets, and translation phenotype, we propose that Lso2 promotes productive translation elongation during starvation recovery. The widespread distribution of Lso2 orthologs is consistent with a significant role in modulating eukaryotic ribosome function.

Introduction

The ribosome is a universally conserved, multi-megadalton machine that carries out protein synthesis in all organisms. Accurate and efficient translation in eukaryotes requires the interaction of nearly thirty translation factors with the ribosome to ensure orderly execution of initiation, elongation, termination, and recycling of ribosomal subunits. Structural and biochemical studies have elucidated the interactions of these factors with the ribosome, and in many cases, their molecular functions in the translation cycle are well understood. Intriguingly, a growing number of ribosome-associated proteins beyond this core class have also been discovered, but their roles and mechanisms are generally less well characterized.

The known functions of ribosome binding proteins underscore the broader connections of protein synthesis to homeostasis in all domains of life. Some examples include factors for quality control of defective mRNAs and nascent peptides (Brandman and Hegde, 2016;

Brandman et al., 2012); regulators of gene-specific translation (Colón-Ramos et al., 2006; Darnell et al., 2011); signaling effectors of nutrient status at the ribosome (Brown et al., 2016; Wendrich et al., 2002); and modulators of ribosome activity in response to nutrient status (Basu and Yap, 2016; Kazo et al., 2016; Polikanov et al., 2012; Vila-Sanjurjo et al., 2004). Detailed functional characterization of these proteins has been illuminating in two ways. First, it has reinforced our understanding of the core translation cycle, for example, by demonstrating structural and mechanistic parallels between premature termination by quality control proteins and normal termination by release factors (Becker et al., 2011; Chen et al., 2010). Second, ribosome-associated proteins have revealed new links between global adaptive responses and their specific effects on the ribosome. This point is particularly well illustrated in bacteria, where stress-induced proteins affect each stage of the translation cycle by direct ribosome binding. For example, initiation is broadly inhibited by the ribosome hibernation factors YfiA, HPF, and RMF, which sterically occlude translation ligands from their subunit binding sites (Agafonov et al., 1999; Polikanov et al., 2012; Vila-Sanjurjo et al., 2004). In addition, the status of elongation is monitored by RelA, which synthesizes the alarmone (p)ppGpp upon interaction with deacylated tRNA in the A site (Brown et al., 2016; Wendrich et al., 2002). Activation of the stringent response by (p)ppGpp then reprograms metabolism and gene expression by causing large changes to the translatome, the available amino acid pools, and the fidelity of translation (Hauryliuk et al., 2015; Parker, 1989), which together promote adaptation to starvation. Finally, toxins that cleave mRNA in the A site of the ribosome elicit premature termination by quality control factors as a form of gene expression regulation during stress (Maehigashi et al., 2015; Neubauer et al., 2009). Unicellular eukaryotes such as *Saccharomyces cerevisiae* experience equally extreme shifts in nutrient status as do bacteria, and all cells need to adapt to acute stresses. Post-translational modifications of core initiation factors and their regulators are the best characterized mechanisms for widespread translational control in eukaryotes (reviewed in Sonenberg and Hinnebusch, 2009), but changing the composition or modification state of

ribosomal complexes may also play a role (Gilbert, 2011). Improvements in mass spectrometry have now expanded our ability to identify proteins in ribosomal complexes and intermediates in ribosome assembly (Chaker-Margot et al., 2015; Davis et al., 2016; Nissan, 2002; Sung et al., 2016). A proteomic analysis of mature ribosomes in rapidly dividing yeast identified dozens of previously uncharacterized Translation Machinery-Associated proteins, some of which are now known to play conserved roles in translation initiation and ribosome-associated quality control (Brandman et al., 2012; Skabkin et al., 2010). However, the compositions of eukaryotic ribosomal complexes in other growth states and cell types remain to be elucidated.

Here we report the discovery and characterization of a novel and conserved ribosome-bound protein, Lso2 (Late-annotated short open reading frame 2). By quantitative proteomics, Lso2 associates with yeast ribosomes in glucose-rich and glucose-starved conditions, with increased polysome association during starvation. *LSO2* null mutants (*lso2*Δ) show bulk translation defects during recovery from stationary phase, with monosomes accumulated to abnormally high levels. To understand the basis of this phenotype, we used transcriptome-wide crosslinking and deep sequencing to determine that Lso2 interacts broadly with tRNAs and with a specific region of the 25S ribosomal RNA (rRNA) near the A site. This inter-subunit ribosome binding site was further validated by a biochemical assay showing that purified Lso2 promotes subunit association *in vitro*. Remarkably, Lso2's ribosome binding site overlaps the universally conserved GTPase activating center of the large subunit. This location, together with its observed interaction with most tRNAs, suggests that Lso2 may play a role in promoting productive elongation under certain conditions. Finally, we show that its site-specific ribosome binding activity is conserved in the human ortholog of Lso2, CCDC124, suggesting that the cellular requirement for Lso2 in yeast reflects a generally important molecular function in modulating the activity of eukaryotic ribosomes.

Results

Quantitative proteomics of ribosomes from two growth states identifies novel protein Lso2

Glucose withdrawal alters the transcription and translation of a majority of genes in budding yeast (Vaidyanathan et al., 2014; Zaman et al., 2008). Given the magnitude and pervasiveness of changes to the translating mRNA pool, we hypothesized that ribosome compositions might also be altered. Therefore, polyribosomes were isolated from starved and glucose-replete conditions and compared by quantitative mass spectrometry (Figure 2-1A, Materials and Methods). To increase the purity of ribosome complexes, polysomal fractions were digested with limited RNase and fractionated on a second gradient to obtain 80S monoribosomes. Peptide digests of equal amounts of purified monosomes were then differentially labeled with non-isobaric amine labeling reagents prior to analysis by tandem mass spectrometry.

261 proteins met the requirements for quantitative comparison between samples, based on identification by 2 or more unique peptides and quantification of 2 or more peptide ratios. Protein abundance changes were reproducible overall between independent biological replicates (R^2 = 0.49; Figure 2-1B; Appendix Table 1). 78 of 79 core ribosomal proteins (RPs) were quantified, including 22 of 38 ribosomal protein paralogs that differ by at least one amino acid. As expected based on 1:1 mixing of total protein from each condition, RPs were equally abundant in starved and replete samples. Initiation factors were mostly absent, which is consistent with their unstable association with ribosomes in the absence of crosslinking (Valášek et al., 2007). Elongation factors eEF1A (*TEF2*), eEF1B γ (*TEF4*), eEF2 (*EFT2*), and eEF3 (*YEF3*) were recovered at lower levels from starved polysomes. 40 ribosome biogenesis factors, which are known to associate with complexes larger than 80S (Nissan, 2002; Strunk et al., 2012), were also quantified. These generally showed reduced abundance in starved

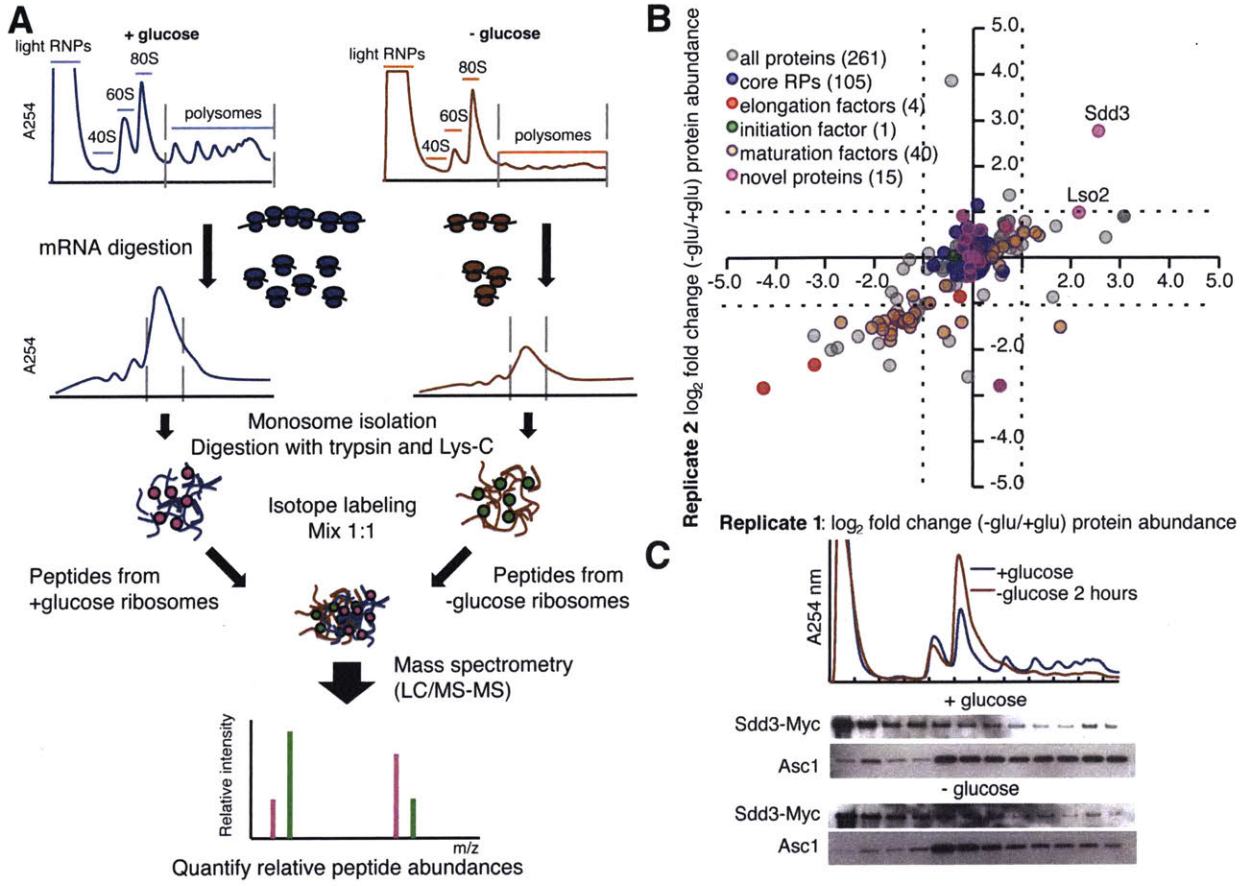

Figure 2-1: Quantitative mass spectrometry identifies reproducible changes in the ribo-proteome during glucose starvation. A) Overview of method for purifying yeast ribosomes from glucose-replete and glucose-starved conditions for analysis by mass spectrometry. **B)** Abundance changes in the ribo-proteome upon glucose starvation. Each axis, which represents one of two biological replicates, shows the $\log_2$ fold change in protein abundance at 2 hours of glucose starvation versus during log phase. The core ribosomal proteins as a cohort are clustered at the origin, which enables quantification of changes in the stoichiometry of other proteins relative to the ribosome. The dashed lines demarcate abundance changes greater than 2-fold. **C)** A minority population of Sdd3 co-migrates with ribosomes. Log phase or glucose-starved cell extract of a myc-tagged *SDD3* strain was fractionated through a sucrose gradient. Each fraction was probed for the myc epitope. Asc1, a core 40S protein, was also probed as a loading control.

samples, consistent with decreased ribosome biogenesis under these conditions (Zaman et al., 2008). Other proteins that were reduced in glucose-starved samples include glycolytic enzymes that are abundant in replete conditions. These are likely contaminants, although we cannot exclude a moonlighting function for these proteins in translation (Beckmann et al., 2015).

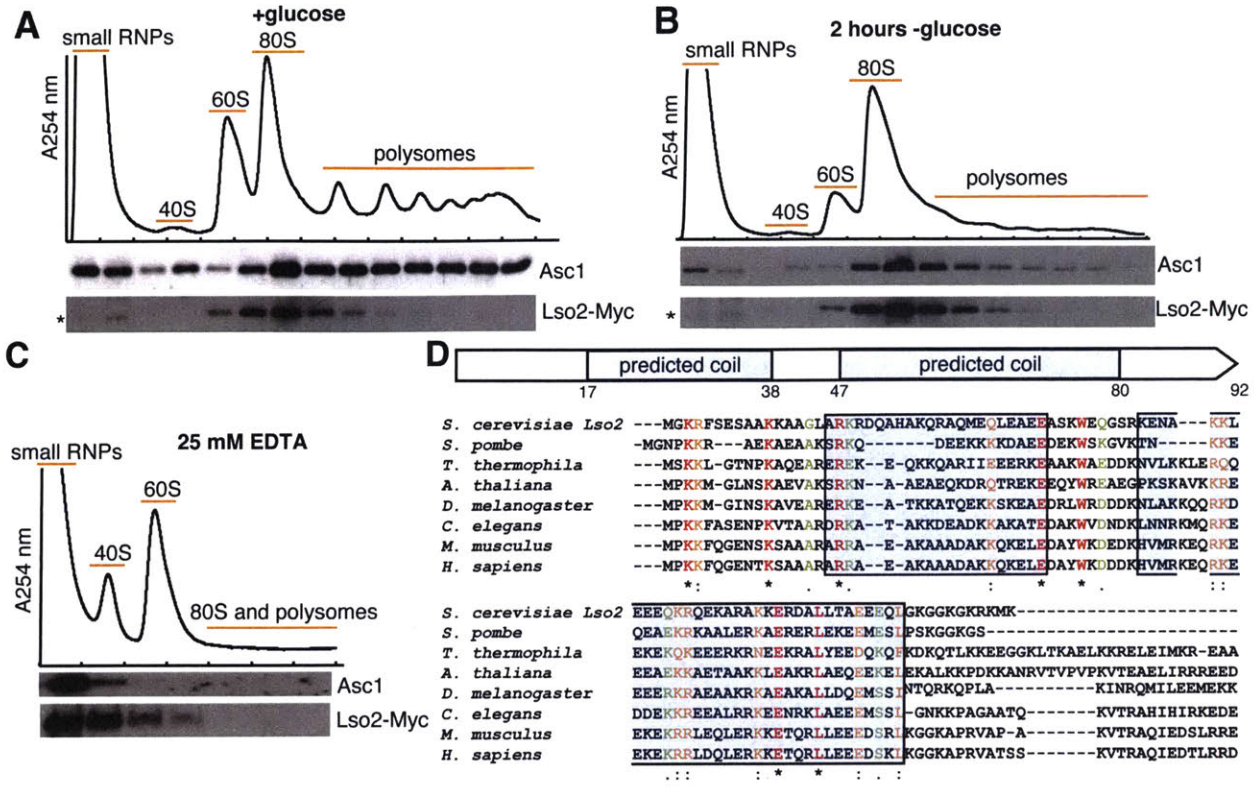

Figure 2-2: Lso2 co-migrates with ribosomes and contains putative orthologs in eukaryotes. A) Log phase cell extract of a myc-tagged *LSO2* strain was fractionated through a sucrose gradient. Each fraction was probed for the myc epitope and for Asc1, respectively. B) A myc-tagged Lso2 strain was grown to log phase in YPAD, then shifted to YPA (lacking glucose) for two hours before harvesting for gradient profiling. C) Log phase extract from a myc-tagged *LSO2* strain was fractionated through a sucrose gradient containing 25 mM EDTA. The indicated fractions were probed for Asc1 and the myc epitope. The anti-myc blots were exposed 5 times longer than those in A). D) Lso2 is predicted to contain a coiled-coil domain, as well as 95 orthologs in other eukaryotes. The boxed regions of the multiple sequence alignment correspond to the predicted coiled-coil in yeast Lso2.

We also identified several previously uncharacterized proteins as novel ribosome binding factors. One such protein is the Late-annotated Short Open Reading Frame 2 (Lso2), a small, basic protein predicted to contain a coiled-coil domain (92 amino acids, 10.5 kDa, pI = 10.78) (Alva et al., 2016; Lupas et al., 1991). Polysome western blots validated the association of Lso2 with ribosomes in both rich medium (Figure 2-2A) and during starvation (Figure 2-2B). Strikingly, the entire cellular population of Lso2 co-migrates with ribosomes and is mostly found in the monosome fractions. Dissociation of polysomes and 80S monosomes with EDTA caused Lso2 to shift to the free pool and to the subunit fractions, as expected for a ribosome-associated

protein (Figure 2-2C). Lso2 is expressed at about one-tenth the level of core ribosomal proteins in rapidly dividing cells based on our ribosome profiling data (Vaidyanathan et al., 2014), which is consistent with the estimated abundance of Lso2 from mass spectrometry-based proteomics (Kulak et al., 2014). Thus, it is plausible that most monosomes, which account for <15% of all ribosomes in growing yeast, contain Lso2 in glucose-grown cultures.

In starved cells, the abundance of Lso2 in small polysomes was increased relative to the core 40S protein Asc1, which is consistent with our mass spec results (Fig 2-1B). Another protein, Suppressor of Degenerative Death 3 (Sdd3), reproducibly showed greater relative enrichment in starved polysome samples (Figure 2-1B); however, unlike Lso2, only a small minority of cellular Sdd3 was observed to co-migrate with ribosomes in rich medium or starvation (Figure 2-1C). We therefore focused on characterizing Lso2. This protein is broadly conserved, with ninety-five predicted orthologs in higher eukaryotes, including humans (Figure 2-2D) (Mi et al., 2016). Thus, we conclude that Lso2 is a novel ribosome-associated protein and likely to be functionally important.

Yeast cells lacking *LSO2* are defective in translational recovery from starvation

LSO2 was omitted from the first annotation of the yeast genome due to its length being less than 100 amino acids, and was therefore excluded from the yeast knockout strain collections that have been used to identify phenotypes for most yeast genes (Hillenmeyer et al., 2008). To test whether Lso2 affects growth or physiology in yeast, we examined *lso2* null mutants (*lso2*Δ) in a variety of conditions. Bulk translation appeared largely normal during exponential growth in rich medium (Figure 2-3A) and at three hours of glucose starvation (Figure 2-3B). Similarly, overall growth was comparable between wild type (WT) and *lso2*Δ at a range of temperatures (16-37°C) and on various carbon sources (data not shown).

In contrast, *lso2*Δ mutants were markedly defective in recovering translation during outgrowth from stationary phase. WT and *lso2*Δ strains were grown to nutrient exhaustion by

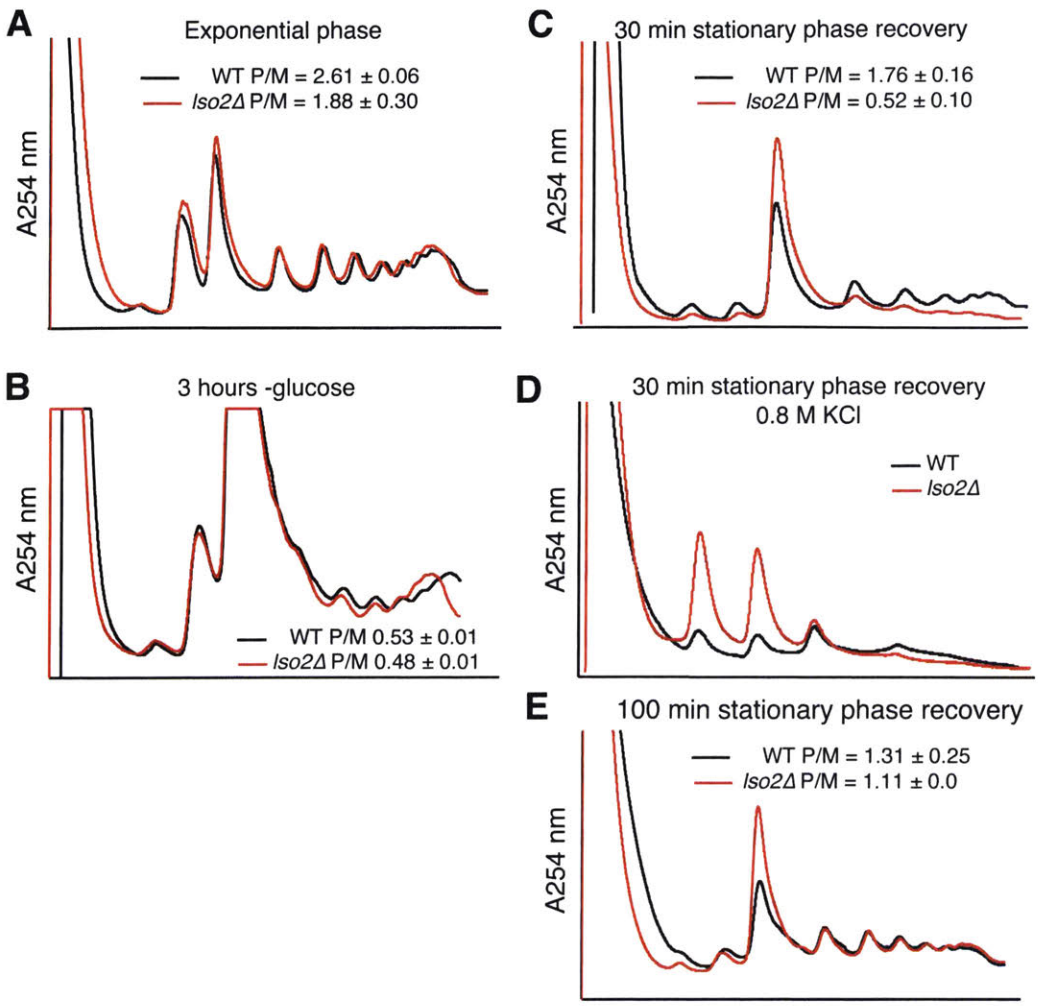

Figure 2-3: *Iso2* nulls are defective in translational recovery from stationary phase. **A)** Gradient profiling of WT and *Iso2* null strains during exponential phase, with quantification of the polysome to monosome ratios. n = 3 biological replicates; mean ± S.D. **B)** As in A), except after three hours of glucose withdrawal. n = 3 biological replicates; mean ± S.D. **C)** WT and *Iso2*Δ were grown in YPAD for four days, then transferred to fresh YPAD for 30 minutes before harvesting for gradient profiling. The polysome to monosome ratios of each strain are quantified. n ≥ 2 biological replicates; mean ± S.D. **D)** Cell extract from the recovery regime in C) was fractionated on a gradient containing 0.8M KCl. n = 2 biological replicates. **E)** As in C), except that WT and *Iso2*Δ were recovered for 100 minutes in YPAD following stationary phase. n = 2 biological replicates; mean ± S.D.

culturing without dilution for four days and then transferred to fresh medium for 30 minutes before gradient profiling. This demanding recovery program, in which a reduced number of cellular ribosomes are actively re-synthesizing the growth-promoting proteome (Martinez et al., 2004; Van Dyke et al., 2013), provides a sensitized assay for potential defects in the translational machinery. *Iso2*Δ accumulated monosomes (M) at the expense of polysomes (P)

compared to WT (P/M ratio decreased 3-fold; Figure 2-3C). Although the 80S fraction can include actively translating ribosomes (Heyer and Moore, 2016), these accumulated monosomes are not elongating normally based on their sensitivity to dissociation by high salt (Figure 2-3D) (Martin and Hartwell, 1970). The *lso2*Δ mutants are delayed but not arrested, as the defect decreased in magnitude by 100 minutes into the recovery (Figure 2-3E). Lso2 is therefore required in yeast for normal recovery of translation following a physiological starvation condition.

Lso2 crosslinks to tRNAs and to 25S rRNA near the A site

As an entrée to understanding the molecular function of Lso2 in translation, we sought to determine its binding site on the ribosome. We used photoactivatable ribonucleoside crosslinking and immunoprecipitation (PAR-CLIP) and an enhanced method of CLIP library preparation for next-generation sequencing (eCLIP-seq) to identify RNAs genome-wide that crosslink to Lso2 in living cells (Materials and Methods) (Beckmann et al., 2015; Van Nostrand et al., 2016). Briefly, yeast strains expressing Myc-tagged Lso2 at endogenous levels (Lso2-Myc) were grown with 4-thiouridine, irradiated at 365 nm, lysed, and digested with limited RNase I before immunoprecipitation of Lso2-Myc and crosslinked RNA. Lso2-RNP complexes from two independent biological replicates were further purified by SDS-PAGE in parallel with a size-matched input (SMI), which was processed identically except for omission of the IP step, and with an anti-Myc IP of a strain lacking the Myc epitope (hereafter called the untagged) (Figure 2-4A). Previous work has shown that comparison to SMI and untagged negative controls eliminates the majority of CLIP peaks as false positives (Conway et al., 2016; Van Nostrand et al., 2016).

We found that Lso2 interacts with a broad range of tRNAs and with a specific region of the 25S rRNA near the A site. Following deep sequencing, reads were collapsed to remove PCR duplicates and mapped to a modified version of the yeast genome containing single copies

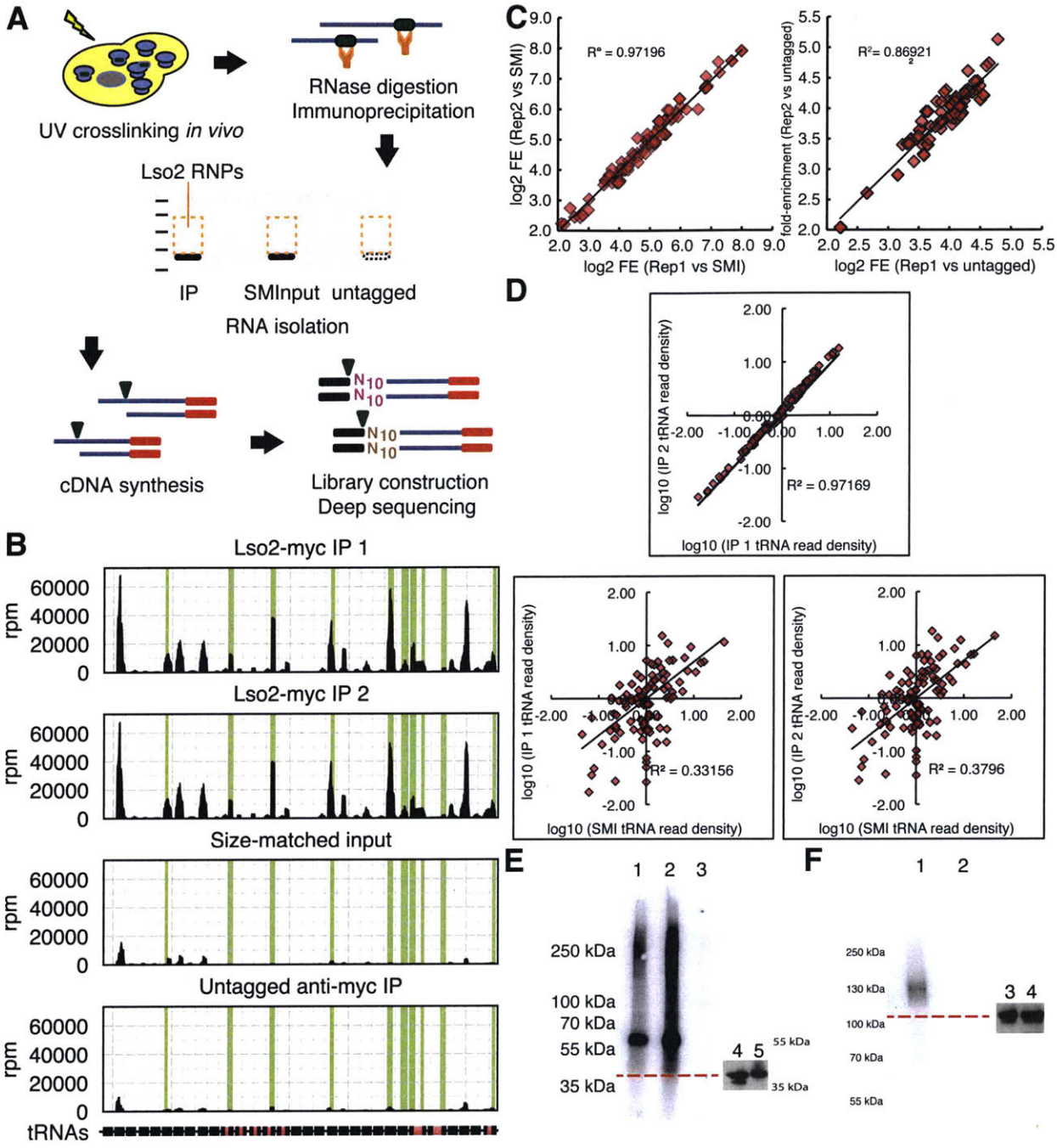

Figure 2-4: Lso2 crosslinks to a broad range of tRNAs. A) Overview of enhanced PAR-CLIP library construction. The libraries in this figure were prepared with a 1:200,000 concentration of RNase I digestion. **B)** Normalized coverage across tRNA loci. The x-axis indicates position along a window of 31 tRNA loci, with black rectangles representing exons and pink boxes introns. The y-axis (rpm) indicates reads per million reads that were mapped and collapsed to remove PCR duplicates. Green bars indicate the regions identified by peak calling that were significantly enriched (fold-enrichment ≥ 4, $p < 10^{-5}$) in both IP replicates relative to the SMI and the untagged libraries. **C)** Reproducibility of tRNA targets identified by peak calling. (Left) Comparison of the fold enrichment of each IP replicate versus the SMI. (Right) Comparison of the fold-enrichment of each IP replicate versus the untagged. **D)** (Top) Correlation of tRNA read densities between the IP replicates. For each tRNA, read density was defined as the number of reads mapping to the feature normalized to the length of the tRNA and the size of the library. Read

densities are centered by the median tRNA read density in that library. (Bottom left) Correlation of median-centered tRNA read densities between the first IP replicate vs the SMI. (Bottom right) Correlation of median-centered tRNA read densities between the second IP replicate vs the SMI. **E)** (Left) Diagnostic electrophoresis membrane of radiolabeled Lso2-RNPs from ePAR-CLIP library construction. Lanes 1 and 2, IP replicates; lane 3, untagged. The region from 35 kDa to 100 kDa was excised for each sample. (Right) Western blot of Lso2-HPM in 2% of the input (lane 4) and in 10% of the IP (lane 5). The red line indicates the position of Lso2-HPM alone (without crosslinked RNAs), based on the positions of western blotting markers. **F)** As for **E)**, except with the tRNA modifying enzyme Pus1-HPM. The membrane was excised from ~120-280 kDa for IP and SMI libraries.

of the rDNA locus and each unique tRNA gene. We used a previously published peak identification algorithm (Lovci et al., 2013) and stringent criteria to identify a subset of high-confidence clusters enriched in both the IP versus SMI and Lso2-Myc versus untagged (Materials and Methods). Unexpectedly, about 90% of all reads in each Lso2-Myc IP replicate mapped to tRNA genes. 34 distinct tRNAs were substantially enriched in the Lso2-Myc eCLIP libraries compared to the corresponding sequences in both the SMI and untagged libraries (≥ 4-fold enrichment, $p<10^{-5}$; Figure 2-4B, Appendix Table 2). These tRNA fold-enrichment values were reproducible between replicates (R^2=0.97 and 0.87 for enrichment versus SMI and untagged, respectively, Figure 2-4C). Given the large fraction of tRNA reads in the IP libraries, and that the length of an entire tRNA gene is approximately the size of sub-features typically identified as peaks, we reasoned that we may also have missed additional enriched tRNAs because they were not identified as peaks. We therefore looked for tRNA genes with 4-fold or greater enrichment of read density in both IPs versus the SMI and untagged (Materials and Methods). 94 of 101 tRNA genes met the minimum read cutoff (64 reads) for this analysis in each of the four libraries. Of these, 71 were enriched 4-fold or more, including 29 that were previously identified by peak calling and 42 additional targets (Appendix Table 3). The read densities across all tRNAs were highly correlated between IP replicates (R^2 = 0.97, Fig 2-4D, top), and the relative abundances in each IP were positively correlated with those in the SMI (R^2 ≥ 0.33, Fig 2-4D, bottom). Furthermore, the prominent ~65 kDa band visible in ^{32}P-labeled Lso2-Myc RNPs was of the expected size for a complex containing Lso2-Myc bound to an intact

tRNA (Figure 2-4E); we verified a 25 kDa shift upon tRNA crosslinking for a well-characterized tRNA modifying enzyme, Pus1 (Figure 2-4F). Together with the fact that Lso2 is undetectable in sub-ribosomal gradient fractions (Figure 2-2A-B), these results suggest that Lso2 associates with a broad range of tRNA-bound ribosome complexes in vivo.

In our initial Lso2 eCLIP experiment, no regions of the rRNA met the stringent enrichment criteria. We reasoned that our RNase digestion conditions may have depleted larger, more labile rRNA fragments from the IP samples. When libraries were made with 10-fold less RNase, we increased rRNA recovery by 2-fold in the Lso2-Myc IP libraries (Figure 2-5A-B). Under these conditions, a single 95 nucleotide cluster in the 25S rRNA – U1188 to G1282 – was the only region of the transcriptome to be reproducibly enriched ≥ 4-fold ($p<10^{-5}$) compared to SMI and untagged (Figure 2-5C). This location on the ribosome overlaps the GTPase activating center, composed of helices 42, 43, and 44 of the 25S rRNA. It is also within 30 Å of the A site tRNA (Figure 2-5D) (Schmidt et al., 2016), which easily positions a protein the size of Lso2 to interact with A site tRNA (Erickson, 2009). Depending on its shape or multimerization status, Lso2 could also conceivably reach to the P site tRNA of a ribosome with an empty A site. Taken together, these eCLIP experiments suggest that Lso2 associates with tRNA-bound ribosomes by binding in the tRNA channel on the A site side of the large ribosomal subunit.

To validate the ribosome binding site of Lso2, we tested whether it is able to stabilize ribosomal subunit association *in vitro*. This biochemical function was previously demonstrated for the bacterial ribosome hibernation factors, a class of ribosome binding proteins with sizes similar to Lso2, and which likewise bind directly in the tRNA channel. For use in a gradient association assay (Holmberg et al., 1994), individual ribosomal subunits were isolated from a yeast *lso2Δ* strain and recombinant His-tagged Lso2 (6XHis-Lso2) was purified from *E. coli* (Figure 2-6A). 40S and 60S subunits were mixed in an equimolar ratio, then mixed either with equimolar Lso2 or the equivalent volume of buffer before fractionation on sucrose gradients to

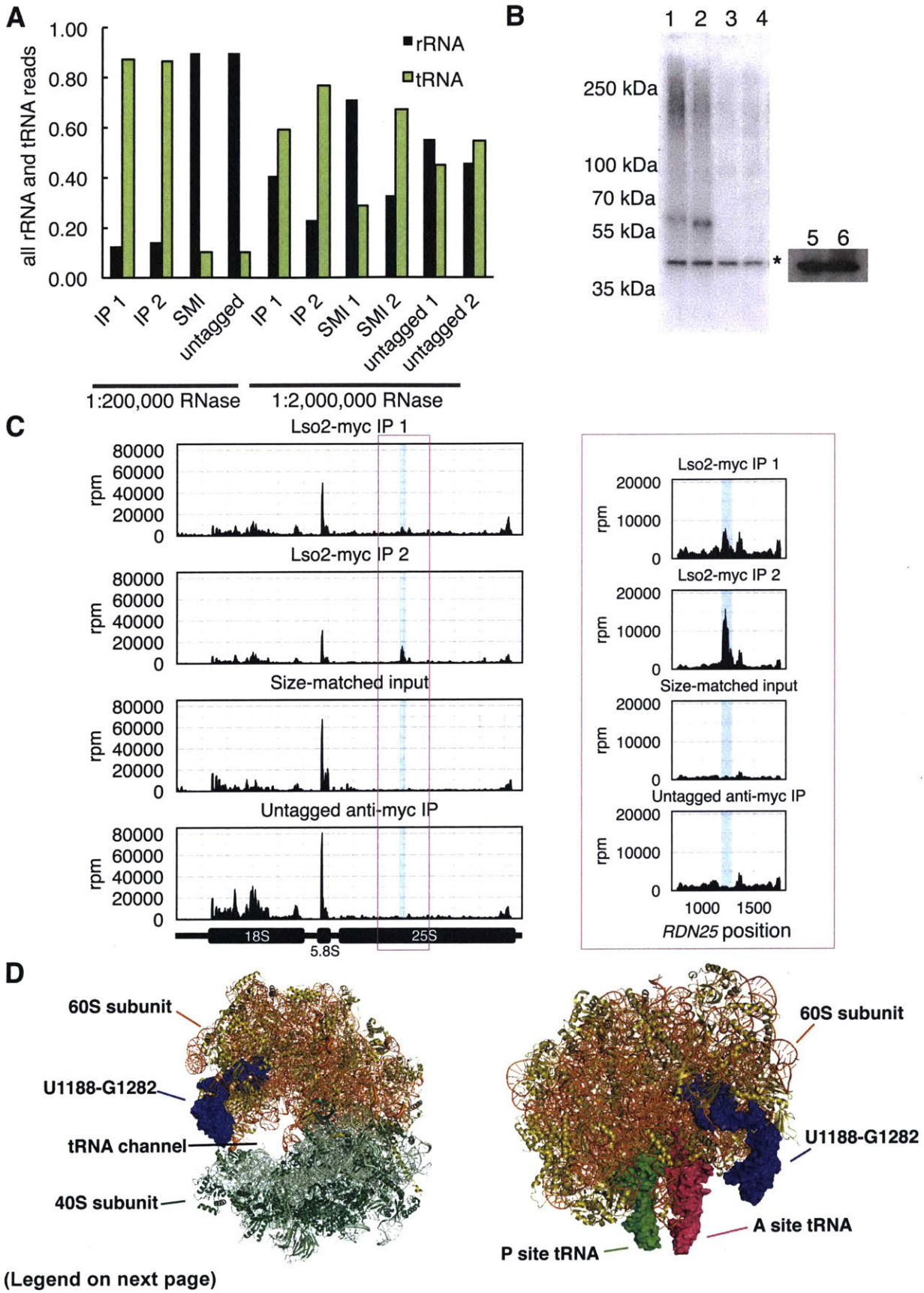

(Legend on next page)

Figure 2-5: Lso2 crosslinks to the 25S rRNA near the A site. A) The effect of RNase I concentration on the distribution of reads between tRNA vs. rRNA features. The libraries in this figure were prepared with a 1:2,000,000 RNase I concentration. **B)** (Left) Diagnostic electrophoresis membrane of radiolabeled Lso2-RNPs from ePAR-CLIP library construction. Lanes 1 and 2, IP replicates; lanes 3 and 4, untagged replicates. The asterisk indicates a non-specific RNA species present in all libraries. (Right) Western blot of Lso2-HPM in 2% of the input (lane 5) and in 10% of the IP (lane 6). The red line indicates the position of Lso2-HPM alone (without crosslinked RNAs), based on the positions of western blotting markers. **C)** (Left) Normalized read coverage across the *RDN37* locus. Two untagged IP libraries and two SMI libraries, each strain-matched to an IP replicate, were the controls in this set. One SMI and one untagged library are shown for clarity. The x-axis indicates position along the *RDN37* locus. The y-axis is as in Figure 2-4B. Blue bars indicate the regions that were significantly enriched (fold-enrichment ≥ 4, $p < 10^{-5}$) in both IP replicates relative to its paired SMI, as well as to the two untagged libraries. (Right) Read coverage from 25S 757-1757. **D)** Lso2 crosslinks to the tRNA channel near the A site. (Upper left) The rRNA crosslink cluster from C) on the crystal structure of the 80S ribosome (Ben-Shem et al., 2011). (Lower right) The identical cluster on a cryo-EM structure of the 60S subunit containing P and A site tRNAs in the post-peptidyl transfer, pre-translocation state (Schmidt et al., 2016).

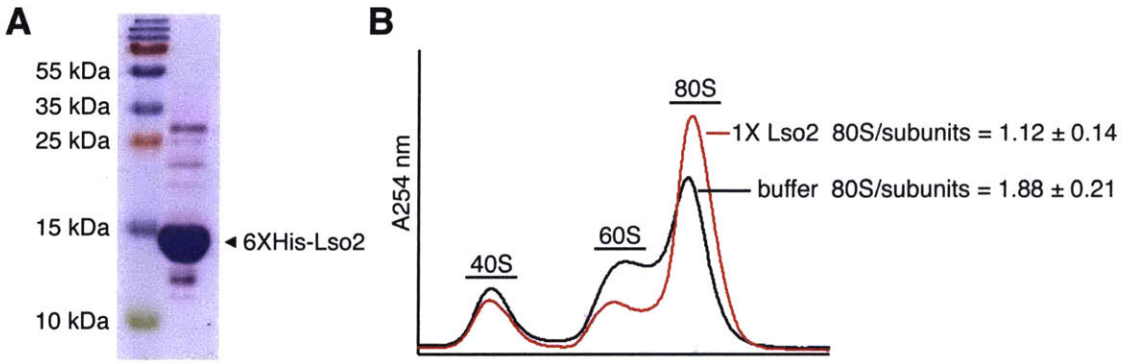

Figure 2-6: Lso2 stabilizes ribosomal subunit association *in vitro*. A) Coomassie staining of recombinant Lso2 purified from *E. coli*. **B)** Lso2 stabilizes ribosomal subunit association *in vitro*. One micromolar each (100 pmol) of purified 40S subunits and 60S subunits were mixed with 1 μM (100 pmol) of purified recombinant Lso2 or with an equivalent volume of buffer. The mixture was incubated at 37°C for 10 minutes before fractionation through a sucrose gradient. The ratio of 80S ribosomes to the sum of 40S and 60S subunits was quantified. n = 3 technical replicates; mean ± S.D.

quantify the distributions of monosomes versus free subunits. At near physiological magnesium concentrations (3 mM), empty ribosome subunits associate only partially to form 80S monosomes. Strikingly, inclusion of equimolar Lso2 increased monosome formation by 2-fold (Figure 2-6B). These data confirm interaction of Lso2 with ribosomes via binding near the tRNA channel, which is sufficient to stabilize association of empty subunits.

Lso2 does not affect ribosome synthesis, storage, or sequestration by Stm1

Having identified tRNA targets and the rRNA binding site of Lso2, we then sought to rationalize the accumulation of monosomes and depletion of polysomes observed in *lso2Δ*

during stationary phase recovery (Figure 2-3C). A decreased polysome to monosome ratio is classically interpreted as a defect in translation initiation. Alternatively, this profile can indicate increased ribosome drop-off during elongation. Finally, the '80S' peak could reflect incompletely or improperly matured ribosomes that are unable to enter the translation cycle. To test this last hypothesis, we examined whether yeast cells produce significant numbers of new ribosomes during the first 30 minutes of recovery from stationary phase. There was no detectable increase in 18S or 25S rRNA during this period in WT or *lso2*Δ (Figure 2-7A), indicating that the translation defect arises entirely from stored ribosomes. Next, we considered that Lso2 may protect rRNA at the subunit interface from cleavage by degradative nucleases, which is a known adaptive response in starved *E. coli* (Basturea et al., 2011). According to this ribosome preservation model, the monosomes that accumulate in recovering *lso2*Δ are defective for translation initiation due to damage acquired during stationary phase. Although we cannot rule out subtler defects, the total rRNA profiles of WT and *lso2*Δ were qualitatively similar in starved cells and at 30 minutes of recovery (Figure 2-7A), and there was no difference in the overall cellular levels of 25S and 18S rRNA immediately prior to recovery (Fig 2-7B). Moreover, comparing rRNA across gradient fractions failed to uncover any differences between ribosome subpopulations in WT versus *lso2*Δ (data not shown).

Given the lack of gross ribosomal abnormalities to explain reduced polysome levels in *lso2*Δ, we then asked whether ribosomes no longer bound to Lso2 could instead be sequestered by Stm1, a yeast ribosome preservation factor. This structurally extended protein lies across the path of the mRNA channel and stabilizes subunits with high affinity, with a binding surface that could potentially clash with Lso2 near the A site (Ben-Shem et al., 2011). Removal of Stm1 and recycling of ribosomes for translation requires the activity of Dom34 (van den Elzen et al., 2014), which is present at reduced levels relative to ribosomes in stationary

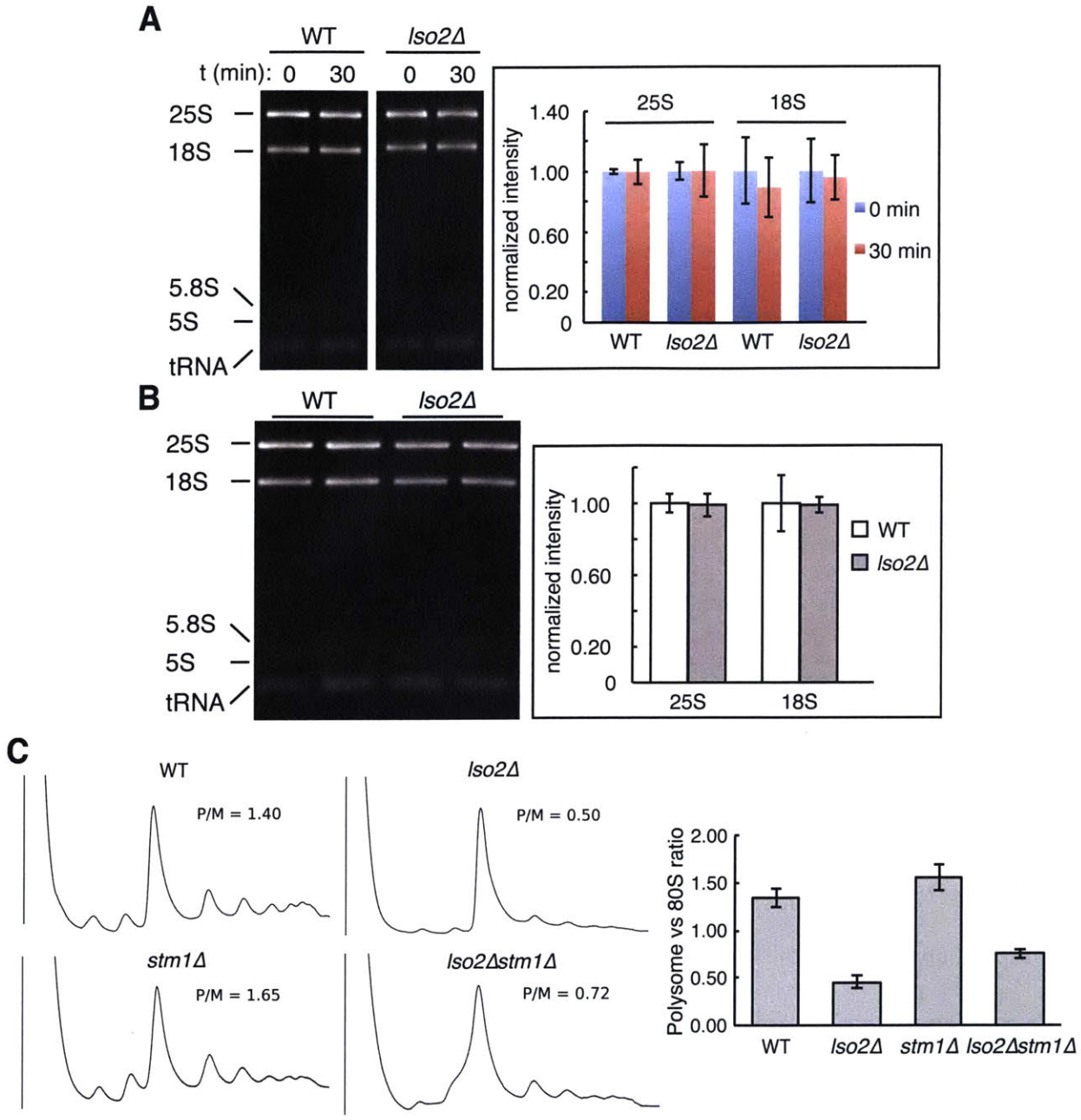

Figure 2-7: Lso2 does not affect ribosome synthesis during recovery, ribosome storage in stationary phase, or sequestration by Stm1 during recovery. A) (Left) Total RNA isolated from WT and *lso2Δ* strains recovering from 4 days in YPAD was separated by synergel-agarose electrophoresis. Time indicates minutes after switch to fresh medium. (Right) Quantification of 25S and 18S rRNA intensities at 0 and 30 minutes of recovery. For each strain, the rRNA intensity at 0 minutes was normalized to 1. n = 2 biological x 2 technical replicates; mean ± S.D. **B)** (Left) Total RNA was isolated from equal culture volumes of WT and *lso2Δ* after 4 days of growth in YPAD. RNA from equivalent culture volumes was loaded in each lane and separated by synergel-agarose electrophoresis. The WT rRNA intensity was normalized to 1.0. Two biological replicates of each strain are shown. (Right) Quantification of 25S and 18S rRNA intensities in WT vs *lso2Δ*. n = 2 biological x 2 technical replicates; mean ± S.D. **C)** Deletion of *STM1* fails to fully rescue the monosome accumulation in *lso2Δ* during starvation recovery. (Left) Each strain was cultured for 4 days in YPAD, then transferred to fresh YPAD for 30 minutes before

harvesting for gradient profiling. (Right) Quantification of polysome to monosome ratios in gradient profiles. n ≥ 2 biological replicates; mean ± S.D.

phase yeast (Davidson et al., 2011). As expected, yeast lacking *STM1* (*stm1*Δ) preserved fewer ribosomes overall during stationary phase (data not shown) (Van Dyke et al., 2013). However, the remaining ribosomes in *stm1*Δ formed polysomes similar to WT during translational recovery. Deletion of *STM1* in the *lso2*Δ background only slightly increased the polysome to monosome ratio, from 0.50 in *lso2*Δ to 0.72 in *lso2*Δ*stm1*Δ compared to 1.40 in WT (Figure 2-7C). Thus, the monosome accumulation in recovering *lso2*Δ is not primarily due to increased ribosome occupancy by Stm1.

Taken together – the lack of obvious perturbations that would prevent accumulated monosomes from initiating, and the crosslinking data indicating that Lso2 associates with tRNA-bound ribosomes – our results suggest that Lso2 targets elongating ribosomes. The accumulated monosomes observed during recovery from stationary phase may arise from premature ribosome drop-off downstream of elongation defects in *lso2*Δ (see Discussion).

The ribosome binding activity of Lso2 is conserved in humans

We identified putative orthologs of yeast Lso2 in many eukaryotes, suggesting a broadly important and conserved function. The human ortholog of Lso2, CCDC124 (Coiled-Coil Domain Containing 124, was independently predicted to contain a coiled-coil domain at its N-terminus (Figure 2-8A) (Alva et al., 2016; Lupas et al., 1991). This poorly characterized human protein was previously shown to localize to the midbody during cytokinesis in HeLa cells (Telkoparan et al., 2013) and to interact with Protein Kinase R during innate immune stimulation of HEK293 cells (Li et al., 2011). Intriguingly, an interactome survey of 1,125 GFP-tagged mammalian proteins expressed in HeLa cells identified interactions between CCDC124 and two 60S ribosomal proteins, RPL10 (human) and Rpl35 (mouse) (Hein et al., 2015). Ccdc124 also crosslinks to poly(A) RNA from Huh7 and HeLa cells (Beckmann et al., 2015). Moreover, it is

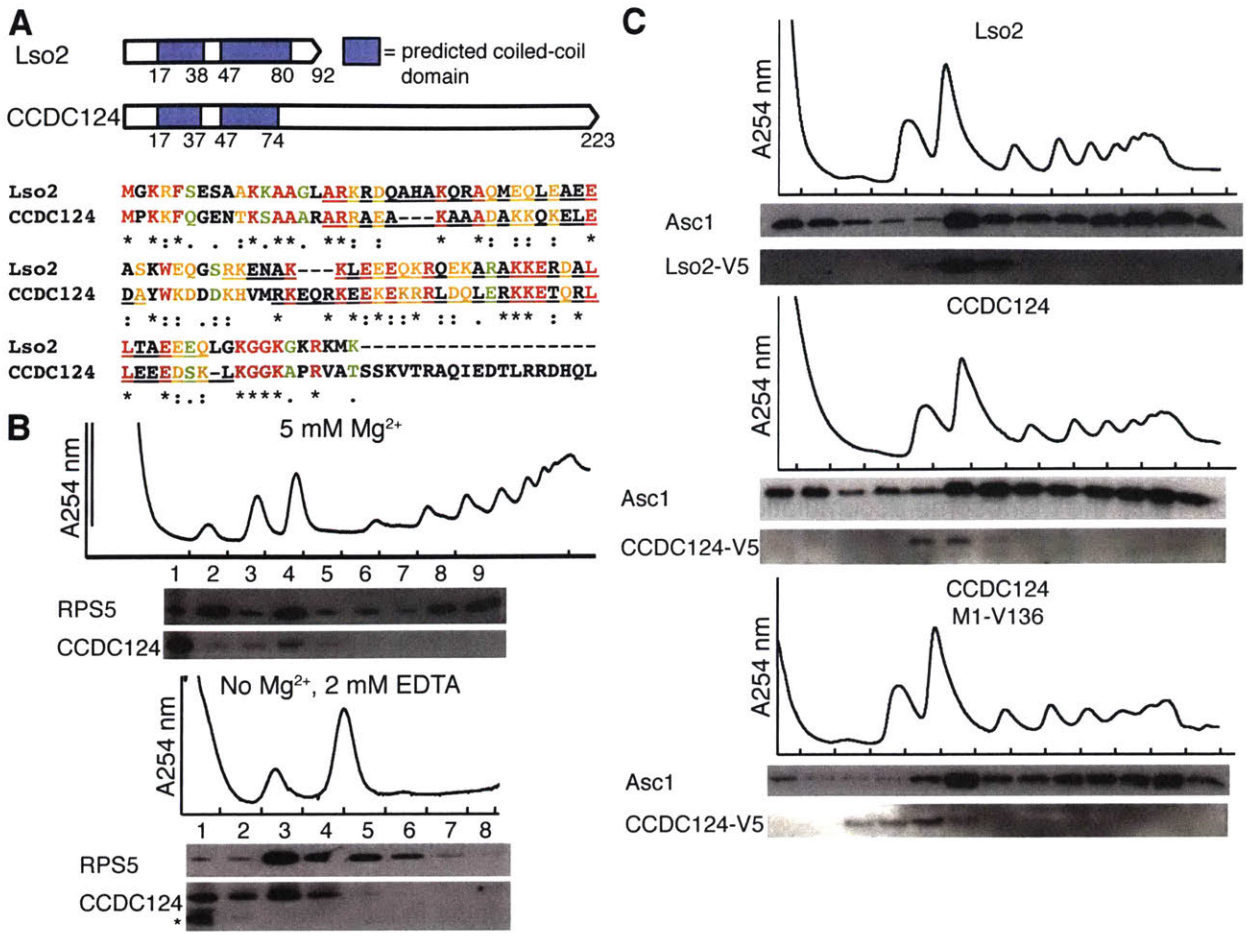

Figure 2-8: The ribosome binding activity of Lso2 is conserved in its human ortholog, CCDC124. **A)** (Top) Schematic of coiled-coil domains in Lso2 and CCDC124. (Bottom) Protein sequence alignment of yeast Lso2 with human CCDC124. **B)** (Top) HeLa cell extract was fractionated through a sucrose gradient containing 5 mM magnesium. Equivalent fraction volumes were TCA precipitated and loaded in each lane. Fractions were probed for Rps5 and for endogenous CCDC124, respectively. (Bottom) HeLa cell extracts were fractionated through a sucrose gradient lacking magnesium and containing 2 mM EDTA. Western blots for CCDC124 were exposed 10 times longer than those in A). The asterisk indicates a likely proteolysis product of CCDC124. **C)** For all three strains, cell extracts were fractionated through a sucrose gradient and the fractions probed for Asc1 and V5, respectively. (Top) The yeast *LSO2* gene was tagged with V5 in a marker-free insertion. (Middle) The yeast *LSO2* gene was swapped with V5-tagged *CCDC124* in a marker-free replacement. (Bottom) As for full-length *CCDC124* above, except that V5 was fused to a putative shorter isoform (Aken et al., 2016) containing the first 136 amino acids of the coding sequence.

ubiquitously expressed in a broad range of human tissues profiled by proteomics (Kim et al., 2014). However, its interaction with ribosomes had never been directly tested.

To determine whether the putative human ortholog of Lso2 also associates with ribosomes in human cells, HeLa extracts were fractionated on a sucrose gradient and the fractions probed for endogenous CCDC124. While the majority of the protein sediments in the free (non-ribosomal) pool, a minority population distinctly co-migrates with monosomes (Figure

2-8B, top). Additionally, this 80S subpopulation shifts entirely to the sub-ribosomal, 40S, and 60S subunit fractions in the presence of EDTA, as expected for a ribosome-associated protein (Figure 2-8B bottom). Given that CCDC124, like *LSO2*, is expressed at levels substoichiometric to core ribosomes (HeLa ribosome profiling data of Guo et al., 2010), total abundance alone fails to explain this difference in its distribution compared to yeast Lso2. We speculate that the human protein, which is 131 amino acids longer than Lso2 (Figure 2-8A), is regulated in a more complex manner vis-à-vis its extraribosomal versus monosome-bound subpopulations. Alternatively, CCDC124 may have additional and independent roles off the ribosome. These observations demonstrate that a subset of CCDC124 is ribosome-bound in human cells and suggest a conserved function in translation.

As further evidence of conservation, CCDC124 expressed in yeast from the *LSO2* locus associated with ribosomes in a manner similar to native Lso2. When yeast *LSO2* was swapped with V5-tagged *CCDC124* in a marker-free chromosomal replacement, the human protein sedimented exclusively with 60S and 80S ribosomes (Figure 2-8C, middle), similar to Lso2. Additionally, a putative shorter isoform of CCDC124 (Aken et al., 2016) that contains a 31 amino acid extension beyond the coiled-coil domain migrates similarly to the longer isoform (Figure 2-8C, bottom). Thus, we conclude that the ribosome binding activity of Lso2 is likely to be conserved from yeast to man.

Discussion

Here we report the discovery and characterization of a novel and conserved ribosome-bound protein that is required in yeast for normal translation during recovery from starvation. Through genome-wide identification of RNA crosslinks, we mapped a specific binding site for Lso2 on the ribosome to the conserved GTPase activating center, located less than 30 angstroms from the A site on the large subunit. Consistent with this location, we demonstrated that Lso2 also interacts with numerous tRNAs (76 of 101) *in vivo* and stabilizes ribosomal

subunit association *in vitro*. The broad interaction of Lso2 with tRNAs, and the lack of a sub-ribosomal pool of Lso2 in the conditions tested thus far, suggest it associates with elongating ribosomes. Additionally, ribosomes stored in starved *lso2Δ* are devoid of obvious abnormalities that would prohibit their entering the translation cycle. Finally, we showed that Lso2's ribosome binding activity is conserved to man. Together, our results suggest that Lso2 and its orthologs play an important role in modulating the activity of tRNA-bound ribosomes.

What molecular function might Lso2 have in translation elongation? Given the location of Lso2 on the ribosome, we envision a role for Lso2 in increasing translational fidelity. Lso2 binding to the GTPase activation center may slow GTP hydrolysis by eEF1A•GTP to further bias selection of cognate tRNAs. Alternatively, Lso2 binding in the tRNA channel could pose an additional barrier to accommodation of A site tRNA, which would again favor correctly paired cognate tRNA. These models are not mutually exclusive. However, despite Lso2's broad conservation and its association with an important functional center of the ribosome, yeast *lso2Δ* strains grow well under standard laboratory conditions. The human ortholog CCDC124 is also not essential in genome-wide screens (Blomen et al., 2015; Hart et al., 2015; Marceau et al., 2016; Shalem et al., 2014; Wang et al., 2015). Thus, any elongation model must include a starvation- or growth change-dependent component.

A number of features of translation during starvation recovery are consistent with increased potential for translation errors leading to premature ribosome drop-off. First, codon demand and charged tRNA supply may be imbalanced. Although some translation is required to maintain viability in stationary phase (Fuge et al., 1994), only ~130 genes are expressed. During the first 35 minutes of nutrient upshift, more than 1000 genes are transcriptionally induced, comprising a gene set that is dominated by ribosomal protein and other growth-promoting mRNAs (Martinez et al., 2004), which have codon usages distinct from the stationary phase mRNAs. Furthermore, stationary phase yeast have a metabolism adapted to slow ATP production (Gray et al., 2004), and a reduced ratio of aminoacyl-tRNA synthetases relative to

the overall pool of tRNAs (Davidson et al., 2011 and our unpublished observations). Thus, it is plausible that nutrient upshift creates a temporary imbalance in the available pool of charged tRNAs versus the transcriptome demands. Under such conditions, increased competition between cognate versus noncognate tRNAs can promote temporary ribosome stalls, which are resolved by the Dom34 quality control pathway (Shoemaker et al., 2010), or lead to miscoding (Kramer and Farabaugh, 2007; Kramer et al., 2010), which can propagate errors in the destabilized decoding center (Weiss and Gallant, 1986; Zaher and Green, 2009) and activate other pathways of premature termination (He and Jacobson, 2015; Zaher and Green, 2009). Although starvation induced ribosome drop-off has not been characterized in eukaryotes, amino acid starvation leads to significant global ribosome drop-off in *E. coli* (Sin et al., 2016; Subramaniam et al., 2014). The role we hypothesize for Lso2 in starvation conditions resembles EF-Tu•ppGpp, which is thought to improve fidelity during the stringent response by slowing peptide bond formation and prolonging kinetic proofreading (Dix and Thompson, 1986; Pingoud et al., 1983). Alternatively, Lso2 could bind in the A site of transiently stalled ribosomes to prevent their irreversible dissociation by Dom34. Ribosomal subunits in stationary phase are at even higher excess to initiation factors than during exponential phase (Davidson et al., 2011), which would explain the accumulation of monosomes in *lso2Δ*.

This model raises the question of why Lso2 co-migrates mostly with monosomes in log phase (Fig 2-2A) and during glucose withdrawal (Fig 2-2B), if its most important function were to promote elongation over stretches of starved codons. We posit that the charged tRNA pool versus codon demand is more balanced in either of these conditions than during recovery from stationary phase, leading to fewer elongating ribosomes that would be targets for Lso2. The gradient association assay also shows that Lso2 not bound to elongating ribosomes has some affinity for empty ribosomes (Fig 2-6B). Finally, it is worth noting that ten-fold overexpression of Lso2 in rich medium leads primarily to its increase in the free pool and to a minor extent on polysomes (our unpublished observations), with no discernable effect on bulk translation. This

suggests that Lso2 can associate with polysomes *in vivo* while not adversely competing with cognate ternary complexes. Future efforts will be directed at determining the complete constituents of Lso2-associated ribosome complexes *in vivo* during log phase and starvation recovery, and elucidating the exact stages of translation during which Lso2 interacts with ribosomes.

More broadly, this study demonstrates the potential for discovery proteomics in diverse growth states to identify novel ribosome-associated proteins that may play critical roles in translation and physiology. The novel protein identified here opens an avenue to explore molecular changes to elongation and their potential effects on the activity of quality control pathways, with implications for the same highly conserved aspects of translation in higher eukaryotes.

Materials and Methods

Yeast strain construction and culture

All experiments except for purification of ribosomal subunits (see below) were conducted in the Sigma1278b strain background (*MATAa ura3-52 his3Δ0 leu2Δ0 trp1Δ0*). Strains were cultured in liquid YPAD (1% yeast extract, 2% peptone, 2% glucose, 0.01% adenine hemisulfate) or on solid YPAD agar (2%). For exponential phase, strains were grown at 30°C with shaking at 200 rpm from an initial OD_{600} of no higher than 0.15 to a final OD_{600} of 1.0. For glucose starvation, exponential cultures at an OD_{600} of 1.0 were spun down and resuspended in pre-warmed YPA (lacking glucose), then grown with shaking at 30°C for the indicated times.

To assay recovery from stationary phase, strains were first grown for 96 hours from OD_{600} 0.05 to OD_{600} ~8, with all strains in this study saturating around 48 hours. Four hundred OD_{600} units of cells (about 50 mL of saturated culture) were then spun down and resuspended in 1.0 L of pre-warmed fresh YPAD for a final concentration of OD_{600} 0.4. Recovery cultures were

grown at 30°C with shaking at 200 rpm. No increases in OD_{600} were detected before 5 hours of recovery.

Single mutants were constructed by transformation of a PCR cassette containing 40 base pairs of homology to either side of the targeted region (Longtine et al., 1998). For *lso2Δ::kan* deletion strains, the kanMX6 cassette in the pFA6a-kanMX6 was amplified with homology to replace the *LSO2* CDS. For *stm1Δ::nat* strains, the nourseothricin resistance cassette in the pFA6a-NatMX6 plasmid was amplified with homology to replace the *STM1* CDS. *lso2Δstm1Δ* strains were constructed by mating of *lso2Δ::kan* with *stm1Δ::nat*, sporulation, and selection for double mutants. All deletion strains were confirmed by PCR genotyping of the target locus.

V5-tagged strains were constructed by 2-step markerless replacement. In the first step, the *LSO2* CDS was replaced by the *URA3* CDS via transformation of a homology-flanked PCR cassette. Transformants were then selected on minimal media lacking uracil. In the second step, the *URA3* CDS was replaced by transformation of a homology-flanked PCR cassette bearing the fusion gene of interest. Ura^- transformants were then selected on 5-fluorootic acid. *LSO2-5XGly-V5* was constructed by PCR amplification of the yeast locus, with additional rounds of PCR to add the linker, epitope tag, and flanking homology using primers (Appendix Table 5). The *CCDC124* CDS was ordered as a synthetic gene from Integrated DNA Technologies with a yeast codon-optimized nucleotide sequence (Appendix Table 5). 5XGly-V5 fusions and flanking homology were added in additional rounds of PCR using primers. Strains were confirmed by sequencing and western blotting for the V5 epitope.

For Myc-tagged *LSO2* strains, the 9xHis-2xPreScission Protease Site-9xMyc-*HIS3* cassette in the pJS-HPM53H plasmid (Graumann et al., 2004) was amplified with homology to replace the *LSO2* stop codon. The same method was used to tag *SDD3* and *PUS1.* Strains were confirmed by sequencing and western blotting for the Myc epitope.

Yeast gradient profiling

Cycloheximide was added to growing culture to a final concentration of 0.1 mg/mL and shaken for 2 minutes. Cultures were quickly poured over ice, spun down, and washed twice with ice-cold Polysome Lysis Buffer (PLB; 20 mM HEPES-KOH pH 7.4, 2 mM MgAc, 0.1 M KAc, 0.1 mg/mL cycloheximide, 1% TritonX-100). For lysis, cells were vortexed with glass beads and PLB supplemented with 1 mM PMSF and 1X EDTA-free protease inhibitors (Roche). Extracts were clarified at 21,000 x *g* for 20 minutes.

For absorbance profiling in 2 mM Mg, 10-25 OD_{260} units were loaded onto 10-50% sucrose PLB gradients, followed by centrifugation at 35,000 rpm in a Beckmann SW41 rotor for 3 hours. For gradient profiling in high salt, 4M KCl was added to cell extract (10 OD_{260} units) immediately prior to centrifugation to raise the final concentration to 0.8M KCl. Extract was then loaded onto 10-40% sucrose PLB gradients containing 0.8M KCl and centrifuged at 35,000 rpm in a Beckmann SW41 rotor for 3 hours. For gradient profiling in EDTA, 60 OD_{260} units of extract made with PLB were loaded onto 10-30% sucrose PLB gradients containing 25 mM EDTA. Gradients were centrifuged at 18,000 rpm in a Beckmann SW28 rotor for 16 hours. All gradients were fractionated from the top down using a Biocomp Gradient Station (Biocomp Instruments), with continual monitoring of absorbance at 254 nm.

For quantification of polysome to monosome ratios, the baseline was first defined as the global minimum excluding the manually selected free RNP peak. The $80S_{start}$ boundary was manually selected from the trough between the 60S peak and 80S peak, and the $80S_{end}$ boundary was manually selected from the trough between the 80S peak and the disome peak. The monosome area was calculated by Riemann summation between the $80S_{start}$ and $80S_{end}$ boundaries, and the polysome area was calculated by Riemann summation between $80S_{end}$ and the final point in the profile. The areas were divided to obtain the ratio.

Mass spectrometry analysis of ribosomal complexes

For analysis of ribosomal complexes in glucose-replete conditions, YWG25 was grown in YPAD to OD_{600} 1.0. For analysis in glucose starvation, YWG25 was grown in YPAD to OD_{600} 1.0, then shifted to YPA for 2 hours. Cultures were harvested and extracts prepared in PLB as described in "Yeast gradient profiling." For the first round of polysome isolation, 200 ODUs of each sample were loaded onto a 10-50% sucrose PLB gradient and centrifuged in a Beckmann SW28 rotor at 28,000 rpm for 4 hours. Gradients were fractionated on a Biocomp gradient station and the polysome region collected manually. Polyribosomes were pelleted through a sucrose cushion (20 mM Hepes KOH pH 7.4, 10 mM Mg Ac, 0.5 M K Ac, 1.0 M sucrose, 2 mM DTT) and the ribosome pellet resuspended in subunit separation buffer lacking DTT (50 mM HEPES-KOH pH 7.4, 5 mM $MgCl_2$, 0.5M KCl) to a final concentration of ~50 A_{260} units per mL. One unit of RNase I per A_{260} unit was added and the mixtures incubated at 24°C for 30 minutes. RNase digest mixtures were immediately loaded onto 10-50% sucrose subunit separation buffer gradients and centrifuged in a Beckmann SW28 rotor at 18,000 rpm for 16 hours. The 40S, 60S, and 80S fractions were pooled, then concentrated and exchanged into 0.1 M ammonium bicarbonate (pH 8.0). Total protein concentrations were determined by the Bradford assay.

Downstream processing for mass spectrometry was as follows. Proteins were digested in parallel reactions using trypsin and lysC, respectively. Prior to trypsin digestion, peptides were partially modified with propionic anhydride to block lysines. Peptide digests were then differentially labeled with mTRAQ non-isobaric amine reagents (mTRAQ Δ 0 and mTRAQ Δ 8). The labels were flipped between biological replicates. Labeled peptides from each condition were mixed 1:1 based on the total protein concentration determined earlier, then fractionated by off-gel electrophoresis to decrease sample complexity prior to analysis by tandem mass spectrometry. All samples were analyzed on an LTQ-Velos Orbitrap instrument.

ePAR-CLIP library preparation

Lso2-Myc and untagged strains were grown in synthetic complete medium with 120 mM uracil to OD_{600} 1.0. 4-thiouracil was added to each culture to a final concentration of 500 uM. Cultures were grown with shaking at 30°C for an additional 3 hours. For UV crosslinking, cultures were poured over ice and pelleted, then resuspended in cold water and transferred to a Petri dish situated on ice. Resuspended cells were crosslinked in a Stratalinker at 365 nm, approximately 5 cm from the UV bulb, for a total of 7.2 J/cm^2 (680 s). UV-treated culture was pelleted. Cells were lysed by vortexing with glass beads in lysis buffer (50 mM Tris-HCl pH 7.4, 100 mM NaCl, 1% NP-40, 0.1% SDS, 0.5% sodium deoxycholate, 1:200 Protease Inhibitor Cocktail III, 11 U/mL SuperaseIN). Extracts were clarified at 10,000 x *g* for 5 minutes.

Downstream library preparation followed the method of Van Nostrand et al., 2016 with the following modifications. 10 μ g of anti-Myc antibody (Sigma M4439) were coupled to 100 μ L of Dynabeads Protein G. For RNase digestion, 26 OD_{600} units were diluted in lysis buffer to a final volume of 1.0 mL in lysis buffer. RNase I was added to a final concentration of either 1:2,000,000 (set 1, Figure 2-5) or 1:20,000,000 (set 2, Figure 2-6) and incubated with extracts for 15 minutes at 22°C and shaking at 1200 rpm. Immunoprecipitation with Myc-coupled beads proceeded for 2.5 hours at 4°C. For 3′ adapter ligation, samples were ligated to the pre-adenylated adapter OJA225 (5′-5Phos/TGGAATTCTCGGGTGCCAAGG/3ddC/) using T4 RNA Ligase 1 (30 U/μ L, NEB M0437M). As a diagnostic of crosslinking efficiency and approximate RNA size distribution, 10% of each IP and 10% of each untagged sample were removed for [γ-^{32}P]ATP labeling, then resolved by SDS-PAGE on a 4-12% Bis-Tris gel. Radiolabeled RNPs were transferred from the gel to a PVDF membrane, which was exposed to a phosphorimager screen to produce the images in Figure 2-4E-F and Figure 2-5B. 2% of the input and 10% of the IP were also separated by SDS-PAGE and analyzed by western blotting for the Myc epitope (Figure 2-4E-F, Figure 2-5B). The remainder of each sample was loaded on a different gel, separated by SDS-PAGE, and transferred to a PVDF membrane. For the first set of libraries

(made with 1:2,000,000 RNase I), the region of the membrane from 35 to 100 kDa was excised. For the second set (made with 1:20,000,000 RNase I), the region of the membrane from 55 to approximately 130 kDa was excised to avoid a non-specific species migrating around 50 kDa in the IP and the untagged libraries. Primer OWG915 (5′-GCCTTGGCACCCGAGAATTCC) was used for first-strand cDNA synthesis. The barcoded adapter OWG920 (5′-/5Phos/N_{10}GATCGTCGGACTGTAGAACTCTGAACGTG/3SpC3/-3′) was used for ligation to the 5′ end of first-strand cDNA. For PCR amplification, OBC (5′-CAAGCAGAAGACGGCATACGAGAT$\underline{N_6}$GTGACTGGAGTTCCTTGGCACCCGAGAATTCCA) was used as the forward primer, in which the N_6 was used to barcode each library on a flow cell, and Illumina RP1 (5′-AATGATACGGCGACCACCGAGATCTACACGTTCAGAGTTCTACAGTCCGA) was used as the reverse primer. Libraries generally required 8-14 cycles of PCR amplification. Paired-end sequencing was performed on an Illumina NextSeq500 instrument.

Libraries of Pus1-HPM IP, SMI, and strain-matched untagged were prepared as above with several differences. RNase I was added to a final concentration of 1:40,000. Immunoprecipitated species from the untagged strain were visualized on a membrane but not used for further library construction. The membrane was excised from ~120-280 kDa for IP and SMI libraries.

ePAR-CLIP sequencing analysis

Analysis of ePAR-CLIP data followed the pipeline of Van Nostrand et al., 2016 with the following modifications. Individual libraries were first demultiplexed by their library-level barcodes. For reverse reads, which contained at the first 10 positions the N_{10} barcode for collapsing PCR duplicates within a library, these 10 positions were removed and appended to the fastq header. Two rounds of adapter removal by Cutadapt were run with previously published parameters except for the adapter sequences, which were modified to remove OBC

from the 5′ side and NNNNNGATCGTCGGACTGTAGAACTCTGAACGTGTAG (embedded in OWG920) from the 3′ side. For mapping, the genome assembly Sigma1278b_MIT_2009_ACVY01000000 and its annotations were downloaded from *Saccharomyces* Genome Database. To consolidate reads and downstream peak calling on multi-copy genes, the genome was modified as follows. All rRNA and tRNA genes containing a 40 base pair window that multi-mapped elsewhere in the genome were first masked from the endogenous genome. Single copies of unique tRNA genes and the *RDN37* locus (only a single copy of *RDN5* was annotated in the original genome) were then placed on a separate artificial chromosome, with each locus separated by a spacer of 25 Ns. Forward and reverse reads were mapped with the published parameters of "STAR genome mapping," except that a multi-map cutoff of 10 and a mismatch rate of 9% were used. PCR duplicates were collapsed, the mapped files were sorted, and the reverse reads were used for peak identification as described. No replicates were merged in any analyses.

Normalization of IP to control libraries, and subsequent identification of reproducibly enriched Lso2 targets, were performed as follows. In the first set of libraries, two Lso2-Myc replicates were used to prepare IP replicates. RNA from one of these replicates was used to prepare a SMI library, and one untagged strain was used to prepare an untagged library. After peak identification, the read fraction in each peak of an IP library was normalized by the read fraction of the corresponding region in the control libraries (SMI and untagged, respectively). Peaks with fold-enrichment ≥ 4.0 and $p \leq 10^{-5}$ relative to both controls, and that overlapped by at least one nucleotide between the two IP replicates, were taken as reproducible targets. For tRNA enrichment analysis based on read density, read density was defined as the number of alignments in a given tRNA, normalized to the length of that tRNA and the total number of usable alignments in that library (with PCR duplicates removed). Secondary alignments of multi-mapping reads were retained and counted both as tRNA-mapping features and as part of the

total library size. We then defined enriched tRNA targets as those with a ≥4-fold ratio of read density in both IPs relative to the SMI and untagged.

In the second set of libraries, two Lso2-Myc replicates were used to prepare IP replicates. RNA from each of these replicates was used to prepare paired SMI libraries, and two untagged strains were used to prepare untagged libraries. IP peaks with fold-enrichment ≥ 4.0 and $p \leq 10^{-5}$ relative to its paired SMI and both untagged libraries, and that overlapped by at least one nucleotide between the two IP replicates, were taken as reproducible targets.

Purification of recombinant Lso2

The yeast *LSO2* coding sequence was cloned into pET-TEV-28a(+) using Gibson assembly. pET-TEV-28a(+) is identical to pET-28a(+) (Novagen) except that the thrombin cleavage site is replaced by a tobacco etch virus (TEV) protease cleavage site. The forward primer 5′-TCTGTATTTTCAGAGCATGGCTAGCATGGGTAAAAGATTTTCAGAATCCG and the reverse primer 5′-GCTTGTCGACGGAGCTCGAATTCTTATTTCATTTTTCTTTTACCCTTGCC were used to amplify the *LSO2* CDS from yeast genomic DNA (YWG25, Appendix Table 4), where the underlined sequences are complementary to the 5′ and 3′ ends of the *LSO2* CDS, respectively. The forward primer 5′-GAATTCGAGCTCCGTCGACAAGCTTGCG and reverse primer 5′-GCTAGCCATGCTCTGAAAATACAGATTTTCGTG were used to linearize pET-TEV-28a(+), where the underlined sequences are the EcoRI and the NheI digest sites, respectively. Gibson assembly was performed according to the manufacturer's instructions (NEB E5510S). Correct cassette insertion was confirmed by sequencing. The resulting Lso2 protein is tagged with 6xHis at its N-terminus followed by the TEV protease cleavage site.

The plasmid was transformed into *E. coli* BL21(DE) for overexpression. Cells were grown in LB kanamycin from OD_{600} 0.1 to 0.6 at 37°C with shaking. Cultures were then transferred to 18°C and shaken for thirty minutes before inducing with 0.5 mM IPTG. Cultures were grown for an additional 22 hours at 18°C before harvesting. Cells were rapidly spun down

and washed once with lysis buffer (20 mM HEPES-KOH pH 7.4, 0.1 M KCl, 10% glycerol, 0.1% TritonX-100, 20 mM imidazole). Cells were lysed by vortexing with glass beads in lysis buffer supplemented with 2X EDTA-free protease inhibitors, 0.1 mM PMSF, and 10 mM β-mercaptoethanol. DNase I was added to extract to a concentration of 10 U per 1 OD_{600} unit of cells, supplemented with 1 M $MgCl_2$ to a final concentration of 2.5 mM Mg^{2+}. Digestions proceeded at 4°C for 2.5 hours before adding 4M KCl to raise the final concentration to 0.5 M. Extracts were clarified at 21,000 x *g* for 20 minutes and passed through a 0.2 µm filter before loading onto a nickel sepharose column (HisTrap HP, GE). The column was washed with 10 volumes of lysis buffer containing 0.5M KCl, then eluted in a single step using nickel elution buffer (20 mM HEPES-KOH pH 7.4, 0.1 M KCl, 10% glycerol, 0.1% TritonX-100, 250 mM imidazole, 10 mM β-mercaptoethanol). Fractions containing Lso2 were pooled and loaded onto a size exclusion column (Superdex 200 prep grade, GE). Lso2 was eluted with one column volume of storage buffer (20 mM HEPES-KOH pH 7.4, 0.1 M KCl, 10% glycerol, 2 mM DTT) and concentrated for storage at -80°C.

Purification of ribosomal subunits from yeast

YWG1346 (*lso2Δ* null in the BY4741 background, Table 2-4) was grown at 30°C with shaking to OD_{600} 1.0. Cells were quickly spun down and lysed by vortexing with glass beads in lysis buffer (20 mM HEPES-KOH pH 7.4, 10 mM Mg Ac, 0.5 M K Ac, 1 mg/mL heparin, 2 mM DTT, 1X EDTA-free protease inhibitors [Roche]). Extracts were clarified at 21,000 x *g* for 20 minutes. The supernatant was then applied to sucrose cushions (20 mM Hepes KOH pH 7.4, 10 mM Mg Ac, 0.5 M K Ac, 1.0 M sucrose, 2 mM DTT) and centrifuged in a Beckmann Type 70 Ti rotor for 106 minutes at 60,000 rpm. The crude ribosomal pellet from this spin was resuspended in subunit separation buffer (50 mM HEPES-KOH pH 7.4, 2 mM $MgCl_2$, 0.5M KCl, 2 mM DTT). Resuspended ribosomes were diluted to a concentration of 200 OD_{260} units per mL in subunit

separation buffer. Puromycin was added to a final concentration of 1 mM. Samples were incubated on ice for 15 minutes, followed by incubation at 37°C for 10 minutes. Two hundred OD_{260} units then were layered onto each of six 5-20% sucrose gradients (50 mM HEPES-KOH pH 7.4, 5 mM $MgCl_2$, 0.5 M KCl, 0.1 mM EDTA, 2 mM DTT) and centrifuged in a Beckmann SW28 rotor for 9 hours at 24,000 rpm. Gradients were fractionated as described in "Yeast gradient profiling." Fractions for each subunit were pooled, then concentrated and exchanged into storage buffer (20 mM HEPES-KOH pH 7.4, 2.5 mM Mg Ac, 0.1 M K Ac, 250 mM sucrose, 2 mM DTT).

Gradient association assay

2.0E7 M^{-1} cm^{-1} and 4.0E7 M^{-1} cm^{-1} were used as the extinction coefficients of the 40S and 60S subunits, respectively (Acker et al., 2007). 5500 M^{-1} cm^{-1} was used as the extinction coefficient of recombinant Lso2 based on the prediction formula of Pace et al., 1995. One micromolar (100 pmol) each of 40S and 60S subunits were mixed in buffer E with 3 mM magnesium (20mM Tris HCl pH7.5, 3 mM Mg Ac, 0.1 M K Ac pH 7.6, 2 mM DTT, 0.25 mM spermidine). One micromolar of Lso2 or the equivalent amount of buffer was then added to the subunit mix, with the final volume of Lso2 storage buffer (which lacks magnesium) not exceeding 0.7%. The mixture was then incubated at 37°C for 10 minutes, snap cooled on ice, and loaded onto 10-30% sucrose PLB gradients with 3 mM Mg Ac. Gradients were centrifuged in a Beckmann SW41 rotor at 18,000 rpm for 16 hours. Fractionation was performed as described in "Yeast gradient profiling."

For quantification of monosome to subunit ratios, the baseline was first defined as the global minimum. The $40S_{start}$, $60S_{end}$, and $80S_{end}$ boundaries were manually selected. The monosome area was calculated by Riemann summation between $60S_{end}$ and $80S_{end}$ boundaries,

while the subunit area was calculated by Riemann summation between $40S_{start}$ and $60S_{end}$. The areas were divided to obtain the ratio.

Quantification of ribosomal RNA in stationary phase and during recovery

For comparisons across strains of ribosomal RNA content during stationary phase, WT and *Iso2*Δ strains were grown for 96 hours in YPAD to a fully saturated OD_{600} of ~8.0. Because saturated OD_{600} values were comparable between strains, we used total RNA in culture as a proxy for cellular abundance of RNA. Two milliliters of each culture was removed and pelleted. Total RNA was then extracted using the hot phenol method, precipitated, and resuspended in TE. 2.5% of each sample was mixed with loading buffer (final concentrations of 50% formamide and 5% glycerol) for electrophoresis on synergel-agarose gels (0.9% synergel [Diversified Biotech SYN100], 0.7% agarose, 1 µg/mL ethidium bromide, 0.5X TBE).

To measure the change in rRNA after 30 minutes of recovery from stationary phase, yeast strains were first grown for 96 hours to saturation, then diluted to OD_{600} 0.4 in fresh YPAD, as described in "Yeast strain construction and culture." Thirty milliliters of culture was immediately removed and rapidly spun down. The cell pellet was flash-frozen. After 30 minutes of shaking at 30°C, another 30 mL of the recovery culture was removed and spun down for flash freezing of the cell pellet. Because the OD_{600} is unchanged during this period, we used total RNA in culture as a proxy for cellular abundance of RNA. Total RNA extraction and analysis was performed as described above for stationary phase samples.

HeLa cell culture and gradient profiling

HeLa cells were cultured in serum-replete conditions as described in Carlile et al., 2014. Cells were syringe-lysed in 2X lysis buffer (20 mM Tris HCl pH 7.5, 10 mM $MgCl_2$, 0.2 M KCl, 1% TritonX-100, 0.2 mg/mL cycloheximide, 4 mM DTT, 2X EDTA-free protease inhibitors) for polysome profiling, or in 2X lysis buffer with 2 mM EDTA and lacking $MgCl_2$ for EDTA

dissociation profiling. Debris and nuclei were pelleted at 1,300 x *g* for 10 minutes. For polysome profiling, ~5 OD_{260} units were loaded onto each 10-50% sucrose gradient (20 mM HEPES-KOH pH 7.4, 5 mM $MgCl_2$, 0.1M KCl, 2mM DTT, 0.1 mg/mL cycloheximide) and centrifuged in an SW41 rotor for 3 hours at 35,000 rpm. For EDTA dissociation profiling, ~10 OD_{260} units were loaded onto each 10-30% sucrose gradient (20 mM HEPES-KOH pH 7.4, 0.1M KCl, 2mM DTT, 0.1 mg/mL cycloheximide, 2 mM EDTA). Gradients were centrifuged in a Beckmann SW41 rotor at 18,000 rpm for 16 hours. Gradients were fractionated as described in "Yeast gradient profiling."

Western blotting

For western blotting as part of eCLIP, samples were mixed with 3X Laemmli buffer and boiled before loading. For western blots of yeast extract gradient fractions, each fraction from a gradient was mixed with 3X Laemmli buffer, boiled, and loaded in equal volume. For western blots of HeLa extract gradient fractions, equal volumes of gradient fractions were first removed and diluted to no more than 15% sucrose, then precipitated in 20% TCA with 0.8 mg/mL sodium deoxycholate as a co-precipitant. Each pellet was resuspended in 1X Laemmli buffer and boiled before loading. Protein samples were separated by SDS-PAGE on Bis/Tris or Tris/glycine gels. Proteins were transferred onto PVDF membranes for eCLIP and nitrocellulose membranes for all other experiments. Membranes were blocked in 5% nonfat milk, then incubated with primary antibody overnight in TBST (10 mM Tris HCl pH 7.5, 0.1% Tween, 0.5 M NaCl). The following primary antibodies and concentrations were used: 1:5K anti-c-Myc (Sigma M4439), 1:10K anti-Asc1 (Coyle et al., 2009), 1:1K anti-Rps5 (Abcam ab168823), and 1:5K anti-Ccdc124 (Abcam ab184771). Membranes were washed and incubated with 1:10K HRP-conjugated goat anti-mouse IgG (Invitrogen 62-6520) or with 1:10K HRP-conjugated goat anti-rabbit IgG (Promega W4011) for one hour at room temperature. Secondary antibodies were detected with enhanced chemiluminescence and exposure to film.

Contributions

This chapter is based on a manuscript to be submitted in May 2017. Professor Wendy Gilbert conceived the project, supervised research, designed research, and performed ePAR-CLIP. Dr. Pavan Vaidyanathan purified yeast ribosomes for proteomics. Dr. Namrata Udeshi performed mass spectrometry in the laboratory of Professor Steven Carr. Dr. Kristen Bartoli cultured HeLa cells. Maria Rojas-Duran assisted with ePAR-CLIP library preparation. I designed research and performed and analyzed all other experiments. Professor Wendy Gilbert and I wrote this chapter.

Acknowledgements

We thank Cassandra Schaening for eCLIP analysis code and advice, Dr. Boris Zinshteyn for assistance with protein and ribosome purification, Jean-Benoît Lalanne for eCLIP analysis advice, and the MIT BioMicroCenter under the direction of Stuart Levine for sequencing. We are grateful to members of the Gilbert and Li labs and Dr. Monica Guo for helpful discussions, and Dr. Erin Borchardt, Dr. Jiří Koubek, Dr. Lydia Herzel, Jean-Benoît Lalanne, and Darren Parker for critical reading of this chapter. This project was supported by NIH R01 GM094303-01A1 to WVG and an NSF Graduate Research Fellowship to YJW.

References

Acker, M.G., Kolitz, S.E., Mitchell, S.F., Nanda, J.S., and Lorsch, J.R. (2007). Reconstitution of Yeast Translation Initiation. In Methods in Enzymology, (Elsevier), pp. 111–145.

Agafonov, D.E., Kolb, V.A., Nazimov, I.V., and Spirin, A.S. (1999). A protein residing at the subunit interface of the bacterial ribosome. Proc. Natl. Acad. Sci. U. S. A. *96*, 12345–12349.

Aken, B.L., Ayling, S., Barrell, D., Clarke, L., Curwen, V., Fairley, S., Fernandez Banet, J., Billis, K., García Girón, C., Hourlier, T., et al. (2016). The Ensembl gene annotation system. Database *2016*, baw093.

Alva, V., Nam, S.-Z., Söding, J., and Lupas, A.N. (2016). The MPI bioinformatics Toolkit as an integrative platform for advanced protein sequence and structure analysis. Nucleic Acids Res. *44*, W410–W415.

Basturea, G.N., Zundel, M.A., and Deutscher, M.P. (2011). Degradation of ribosomal RNA during starvation: comparison to quality control during steady-state growth and a role for RNase PH. RNA N. Y. N *17*, 338–345.

Basu, A., and Yap, M.-N.F. (2016). Ribosome hibernation factor promotes Staphylococcal survival and differentially represses translation. Nucleic Acids Res. *44*, 4881–4893.

Becker, T., Armache, J.-P., Jarasch, A., Anger, A.M., Villa, E., Sieber, H., Motaal, B.A., Mielke, T., Berninghausen, O., and Beckmann, R. (2011). Structure of the no-go mRNA decay complex Dom34–Hbs1 bound to a stalled 80S ribosome. Nat. Struct. Mol. Biol. *18*, 715–720.

Beckmann, B.M., Horos, R., Fischer, B., Castello, A., Eichelbaum, K., Alleaume, A.-M., Schwarzl, T., Curk, T., Foehr, S., Huber, W., et al. (2015). The RNA-binding proteomes from yeast to man harbour conserved enigmRBPs. Nat. Commun. *6*, 10127.

Ben-Shem, A., Garreau de Loubresse, N., Melnikov, S., Jenner, L., Yusupova, G., and Yusupov, M. (2011). The structure of the eukaryotic ribosome at 3.0 Å resolution. Science *334*, 1524–1529.

Blomen, V.A., Májek, P., Jae, L.T., Bigenzahn, J.W., Nieuwenhuis, J., Staring, J., Sacco, R., van Diemen, F.R., Olk, N., Stukalov, A., et al. (2015). Gene essentiality and synthetic lethality in haploid human cells. Science *350*, 1092–1096.

Brandman, O., and Hegde, R.S. (2016). Ribosome-associated protein quality control. Nat. Struct. Mol. Biol. *23*, 7–15.

Brandman, O., Stewart-Ornstein, J., Wong, D., Larson, A., Williams, C.C., Li, G.-W., Zhou, S., King, D., Shen, P.S., Weibezahn, J., et al. (2012). A ribosome-bound quality control complex triggers degradation of nascent peptides and signals translation stress. Cell *151*, 1042–1054.

Brown, A., Fernández, I.S., Gordiyenko, Y., and Ramakrishnan, V. (2016). Ribosome-dependent activation of stringent control. Nature *534*, 277–280.

Carlile, T.M., Rojas-Duran, M.F., Zinshteyn, B., Shin, H., Bartoli, K.M., and Gilbert, W.V. (2014). Pseudouridine profiling reveals regulated mRNA pseudouridylation in yeast and human cells. Nature *515*, 143–146.

Chaker-Margot, M., Hunziker, M., Barandun, J., Dill, B.D., and Klinge, S. (2015). Stage-specific assembly events of the 6-MDa small-subunit processome initiate eukaryotic ribosome biogenesis. Nat. Struct. Mol. Biol.

Chen, L., Muhlrad, D., Hauryliuk, V., Cheng, Z., Lim, M.K., Shyp, V., Parker, R., and Song, H. (2010). Structure of the Dom34–Hbs1 complex and implications for no-go decay. Nat. Struct. Mol. Biol. *17*, 1233–1240.

Colón-Ramos, D.A., Shenvi, C.L., Weitzel, D.H., Gan, E.C., Matts, R., Cate, J., and Kornbluth, S. (2006). Direct ribosomal binding by a cellular inhibitor of translation. Nat. Struct. Mol. Biol. *13*, 103–111.

Conway, A.E., Van Nostrand, E.L., Pratt, G.A., Aigner, S., Wilbert, M.L., Sundararaman, B., Freese, P., Lambert, N.J., Sathe, S., Liang, T.Y., et al. (2016). Enhanced CLIP Uncovers IMP Protein-RNA Targets in Human Pluripotent Stem Cells Important for Cell Adhesion and Survival. Cell Rep. *15*, 666–679.

Coyle, S.M., Gilbert, W.V., and Doudna, J.A. (2009). Direct link between RACK1 function and localization at the ribosome in vivo. Mol. Cell. Biol. *29*, 1626–1634.

Darnell, J.C., Van Driesche, S.J., Zhang, C., Hung, K.Y.S., Mele, A., Fraser, C.E., Stone, E.F., Chen, C., Fak, J.J., Chi, S.W., et al. (2011). FMRP stalls ribosomal translocation on mRNAs linked to synaptic function and autism. Cell *146*, 247–261.

Davidson, G.S., Joe, R.M., Roy, S., Meirelles, O., Allen, C.P., Wilson, M.R., Tapia, P.H., Manzanilla, E.E., Dodson, A.E., Chakraborty, S., et al. (2011). The proteomics of quiescent and nonquiescent cell differentiation in yeast stationary-phase cultures. Mol. Biol. Cell *22*, 988–998.

Davis, J.H., Tan, Y.Z., Carragher, B., Potter, C.S., Lyumkis, D., and Williamson, J.R. (2016). Modular Assembly of the Bacterial Large Ribosomal Subunit. Cell *167*, 1610–1622.e15.

Dix, D.B., and Thompson, R.C. (1986). Elongation factor Tu.guanosine 3'-diphosphate 5'-diphosphate complex increases the fidelity of proofreading in protein biosynthesis: mechanism for reducing translational errors introduced by amino acid starvation. Proc. Natl. Acad. Sci. U. S. A. *83*, 2027–2031.

van den Elzen, A.M.G., Schuller, A., Green, R., and Séraphin, B. (2014). Dom34-Hbs1 mediated dissociation of inactive 80S ribosomes promotes restart of translation after stress. EMBO J. *33*, 265–276.

Erickson, H.P. (2009). Size and Shape of Protein Molecules at the Nanometer Level Determined by Sedimentation, Gel Filtration, and Electron Microscopy. Biol. Proced. Online *11*, 32–51.

Gilbert, W.V. (2011). Functional specialization of ribosomes? Trends Biochem. Sci. *36*, 127–132.

Graumann, J., Dunipace, L.A., Seol, J.H., McDonald, W.H., Yates, J.R., Wold, B.J., and Deshaies, R.J. (2004). Applicability of tandem affinity purification MudPIT to pathway proteomics in yeast. Mol. Cell. Proteomics MCP *3*, 226–237.

Guo, H., Ingolia, N.T., Weissman, J.S., and Bartel, D.P. (2010). Mammalian microRNAs predominantly act to decrease target mRNA levels. Nature *466*, 835–840.

Hart, T., Chandrashekhar, M., Aregger, M., Steinhart, Z., Brown, K.R., MacLeod, G., Mis, M., Zimmermann, M., Fradet-Turcotte, A., Sun, S., et al. (2015). High-Resolution CRISPR Screens Reveal Fitness Genes and Genotype-Specific Cancer Liabilities. Cell *163*, 1515–1526.

Hauryliuk, V., Atkinson, G.C., Murakami, K.S., Tenson, T., and Gerdes, K. (2015). Recent functional insights into the role of (p)ppGpp in bacterial physiology. Nat. Rev. Microbiol. *13*, 298–309.

He, F., and Jacobson, A. (2015). Nonsense-Mediated mRNA Decay: Degradation of Defective Transcripts Is Only Part of the Story. Annu. Rev. Genet. *49*, 339–366.

Hein, M.Y., Hubner, N.C., Poser, I., Cox, J., Nagaraj, N., Toyoda, Y., Gak, I.A., Weisswange, I., Mansfeld, J., Buchholz, F., et al. (2015). A human interactome in three quantitative dimensions organized by stoichiometries and abundances. Cell *163*, 712–723.

Heyer, E.E., and Moore, M.J. (2016). Redefining the Translational Status of 80S Monosomes. Cell *164*, 757–769.

Hillenmeyer, M.E., Fung, E., Wildenhain, J., Pierce, S.E., Hoon, S., Lee, W., Proctor, M., St.Onge, R.P., Tyers, M., Koller, D., et al. (2008). The Chemical Genomic Portrait of Yeast: Uncovering a Phenotype for All Genes. Science *320*, 362–365.

Holmberg, L., Melander, Y., and Nygård, O. (1994). Probing the conformational changes in 5.8S, 18S and 28S rRNA upon association of derived subunits into complete 80S ribosomes. Nucleic Acids Res. *22*, 2776–2783.

Kazo, Y., Hanai, R., Tagami, K., Yano, K., Kawamura, F., Kato-Yamada, Y., Nanamiya, H., Akanuma, G., Hiraoka, H., and Suzuki, S. (2016). Ribosome dimerization is essential for the efficient regrowth of Bacillus subtilis. Microbiology *162*, 448–458.

Kim, M.-S., Pinto, S.M., Getnet, D., Nirujogi, R.S., Manda, S.S., Chaerkady, R., Madugundu, A.K., Kelkar, D.S., Isserlin, R., Jain, S., et al. (2014). A draft map of the human proteome. Nature *509*, 575–581.

Kramer, E.B., and Farabaugh, P.J. (2007). The frequency of translational misreading errors in E. coli is largely determined by tRNA competition. RNA N. Y. N *13*, 87–96.

Kramer, E.B., Vallabhaneni, H., Mayer, L.M., and Farabaugh, P.J. (2010). A comprehensive analysis of translational missense errors in the yeast Saccharomyces cerevisiae. RNA N. Y. N *16*, 1797–1808.

Kulak, N.A., Pichler, G., Paron, I., Nagaraj, N., and Mann, M. (2014). Minimal, encapsulated proteomic-sample processing applied to copy-number estimation in eukaryotic cells. Nat. Methods *11*, 319–324.

Li, S., Wang, L., Berman, M., Kong, Y.-Y., and Dorf, M.E. (2011). Mapping a dynamic innate immunity protein interaction network regulating type I interferon production. Immunity *35*, 426–440.

Longtine, M.S., McKenzie, A., Demarini, D.J., Shah, N.G., Wach, A., Brachat, A., Philippsen, P., and Pringle, J.R. (1998). Additional modules for versatile and economical PCR-based gene deletion and modification in Saccharomyces cerevisiae. Yeast Chichester Engl. *14*, 953–961.

Lovci, M.T., Ghanem, D., Marr, H., Arnold, J., Gee, S., Parra, M., Liang, T.Y., Stark, T.J., Gehman, L.T., Hoon, S., et al. (2013). Rbfox proteins regulate alternative mRNA splicing through evolutionarily conserved RNA bridges. Nat. Struct. Mol. Biol. *20*, 1434–1442.

Lupas, A., Van Dyke, M., and Stock, J. (1991). Predicting coiled coils from protein sequences. Science *252*, 1162–1164.

Maehigashi, T., Ruangprasert, A., Miles, S.J., and Dunham, C.M. (2015). Molecular basis of ribosome recognition and mRNA hydrolysis by the E. coli YafQ toxin. Nucleic Acids Res. *43*, 8002–8012.

Marceau, C.D., Puschnik, A.S., Majzoub, K., Ooi, Y.S., Brewer, S.M., Fuchs, G., Swaminathan, K., Mata, M.A., Elias, J.E., Sarnow, P., et al. (2016). Genetic dissection of Flaviviridae host factors through genome-scale CRISPR screens. Nature *535*, 159–163.

Martin, T.E., and Hartwell, L.H. (1970). Resistance of active yeast ribosomes to dissociation by KCl. J. Biol. Chem. *245*, 1504–1506.

Martinez, M.J., Roy, S., Archuletta, A.B., Wentzell, P.D., Anna-Arriola, S.S., Rodriguez, A.L., Aragon, A.D., Quiñones, G.A., Allen, C., and Werner-Washburne, M. (2004). Genomic analysis of stationary-phase and exit in Saccharomyces cerevisiae: gene expression and identification of novel essential genes. Mol. Biol. Cell *15*, 5295–5305.

Mi, H., Poudel, S., Muruganujan, A., Casagrande, J.T., and Thomas, P.D. (2016). PANTHER version 10: expanded protein families and functions, and analysis tools. Nucleic Acids Res. *44*, D336–D342.

Neubauer, C., Gao, Y.-G., Andersen, K.R., Dunham, C.M., Kelley, A.C., Hentschel, J., Gerdes, K., Ramakrishnan, V., and Brodersen, D.E. (2009). The structural basis for mRNA recognition and cleavage by the ribosome-dependent endonuclease RelE. Cell *139*, 1084–1095.

Nissan, T.A. (2002). 60S pre-ribosome formation viewed from assembly in the nucleolus until export to the cytoplasm. EMBO J. *21*, 5539–5547.

Pace, C.N., Vajdos, F., Fee, L., Grimsley, G., and Gray, T. (1995). How to measure and predict the molar absorption coefficient of a protein. Protein Sci. *4*, 2411–2423.

Parker, J. (1989). Errors and alternatives in reading the universal genetic code. Microbiol. Rev. *53*, 273–298.

Pingoud, A., Gast, F.U., Block, W., and Peters, F. (1983). The elongation factor Tu from Escherichia coli, aminoacyl-tRNA, and guanosine tetraphosphate form a ternary complex which is bound by programmed ribosomes. J. Biol. Chem. *258*, 14200–14205.

Polikanov, Y.S., Blaha, G.M., and Steitz, T.A. (2012). How hibernation factors RMF, HPF, and YfiA turn off protein synthesis. Science *336*, 915–918.

Schmidt, C., Becker, T., Heuer, A., Braunger, K., Shanmuganathan, V., Pech, M., Berninghausen, O., Wilson, D.N., and Beckmann, R. (2016). Structure of the hypusinylated eukaryotic translation factor eIF-5A bound to the ribosome. Nucleic Acids Res. *44*, 1944–1951.

Shalem, O., Sanjana, N.E., Hartenian, E., Shi, X., Scott, D.A., Mikkelsen, T.S., Heckl, D., Ebert, B.L., Root, D.E., Doench, J.G., et al. (2014). Genome-scale CRISPR-Cas9 knockout screening in human cells. Science *343*, 84–87.

Shoemaker, C.J., Eyler, D.E., and Green, R. (2010). Dom34:Hbs1 promotes subunit dissociation and peptidyl-tRNA drop-off to initiate no-go decay. Science *330*, 369–372.

Sin, C., Chiarugi, D., and Valleriani, A. (2016). Quantitative assessment of ribosome drop-off in *E. coli*. Nucleic Acids Res. *44*, 2528–2537.

Skabkin, M.A., Skabkina, O.V., Dhote, V., Komar, A.A., Hellen, C.U.T., and Pestova, T.V. (2010). Activities of Ligatin and MCT-1/DENR in eukaryotic translation initiation and ribosomal recycling. Genes Dev. *24*, 1787–1801.

Sonenberg, N., and Hinnebusch, A.G. (2009). Regulation of translation initiation in eukaryotes: mechanisms and biological targets. Cell *136*, 731–745.

Strunk, B.S., Novak, M.N., Young, C.L., and Karbstein, K. (2012). A Translation-Like Cycle Is a Quality Control Checkpoint for Maturing 40S Ribosome Subunits. Cell *150*, 111–121.

Subramaniam, A.R., Zid, B.M., and O'Shea, E.K. (2014). An integrated approach reveals regulatory controls on bacterial translation elongation. Cell *159*, 1200–1211.

Sung, M.-K., Porras-Yakushi, T.R., Reitsma, J.M., Huber, F.M., Sweredoski, M.J., Hoelz, A., Hess, S., and Deshaies, R.J. (2016). A conserved quality-control pathway that mediates degradation of unassembled ribosomal proteins. eLife *5*.

Telkoparan, P., Erkek, S., Yaman, E., Alotaibi, H., Bayık, D., and Tazebay, U.H. (2013). Coiled-coil domain containing protein 124 is a novel centrosome and midbody protein that interacts with the Ras-guanine nucleotide exchange factor 1B and is involved in cytokinesis. PloS One *8*, e69289.

Vaidyanathan, P.P., Zinshteyn, B., Thompson, M.K., and Gilbert, W.V. (2014). Protein kinase A regulates gene-specific translational adaptation in differentiating yeast. RNA N. Y. N *20*, 912–922.

Valášek, L., Szamecz, B., Hinnebusch, A.G., and Nielsen, K.H. (2007). In Vivo Stabilization of Preinitiation Complexes by Formaldehyde Cross-Linking. In Methods in Enzymology, (Elsevier), pp. 163–183.

Van Dyke, N., Chanchorn, E., and Van Dyke, M.W. (2013). The Saccharomyces cerevisiae protein Stm1p facilitates ribosome preservation during quiescence. Biochem. Biophys. Res. Commun. *430*, 745–750.

Van Nostrand, E.L., Pratt, G.A., Shishkin, A.A., Gelboin-Burkhart, C., Fang, M.Y., Sundararaman, B., Blue, S.M., Nguyen, T.B., Surka, C., Elkins, K., et al. (2016). Robust transcriptome-wide discovery of RNA-binding protein binding sites with enhanced CLIP (eCLIP). Nat. Methods *13*, 508–514.

Vila-Sanjurjo, A., Schuwirth, B.-S., Hau, C.W., and Cate, J.H.D. (2004). Structural basis for the control of translation initiation during stress. Nat. Struct. Mol. Biol. *11*, 1054–1059.

Wang, T., Birsoy, K., Hughes, N.W., Krupczak, K.M., Post, Y., Wei, J.J., Lander, E.S., and Sabatini, D.M. (2015). Identification and characterization of essential genes in the human genome. Science *350*, 1096–1101.

Weiss, R.B., and Gallant, J.A. (1986). Frameshift suppression in aminoacyl-tRNA limited cells. Genetics *112*, 727–739.

Wendrich, T.M., Blaha, G., Wilson, D.N., Marahiel, M.A., and Nierhaus, K.H. (2002). Dissection of the mechanism for the stringent factor RelA. Mol. Cell *10*, 779–788.

Zaher, H.S., and Green, R. (2009). Quality control by the ribosome following peptide bond formation. Nature *457*, 161–166.

Zaman, S., Lippman, S.I., Zhao, X., and Broach, J.R. (2008). How Saccharomyces responds to nutrients. Annu. Rev. Genet. *42*, 27–81.

Chapter III:

Discussion and Future Directions

Overview

In Chapter 2, I presented a translation phenotype of *lso2* nulls recovering from stationary phase, a specific binding site of Lso2 in the tRNA channel of ribosomes, and evidence for its association with a broad range of tRNAs on the ribosome. The upcoming goal is to refine a model that integrates these observations to explain the molecular function of Lso2 in translation. I will consider four possibilities in this chapter. These include promoting general processive elongation, stimulating initiation as a *bona fide* initiation factor, preserving ribosomes as an extension of the classic ribosome hibernation model, or specifically promoting early rounds of elongation. I favor the first - promoting general elongation - as the most comprehensive integration of my data and other published results. However, I will describe the molecular role of Lso2 in each model and how it rationalizes my existing observations. Next, I will address any underlying assumptions, as well as experiments to test them where particularly informative. Finally, I will describe predictions of the model, assays to test those predictions, and my interpretations of their potential outcomes as favorable or negating evidence. These four possibilities are far from exhaustive but serve as an initial framework for future experiments.

A function in general elongation

In the general elongation model, Lso2 promotes processive elongation of ribosomes at potentially any position along an mRNA (Figure 3-1). Its proximity to the A site tRNA (Figure 2-5D, Figure 3-2) and the overlap of its crosslink cluster with the GTPase activating center of the ribosome suggest some plausible mechanisms to this end. First, Lso2 could increase the fidelity of amino acid selection by slowing eEF1A•GTP hydrolysis (Figure 1-2; Figure 3-1A, left). This would increase the kinetic window in which non-cognate as opposed to cognate tRNA preferentially dissociates while in complex with eEF1A•GTP. Second, following GTP hydrolysis,

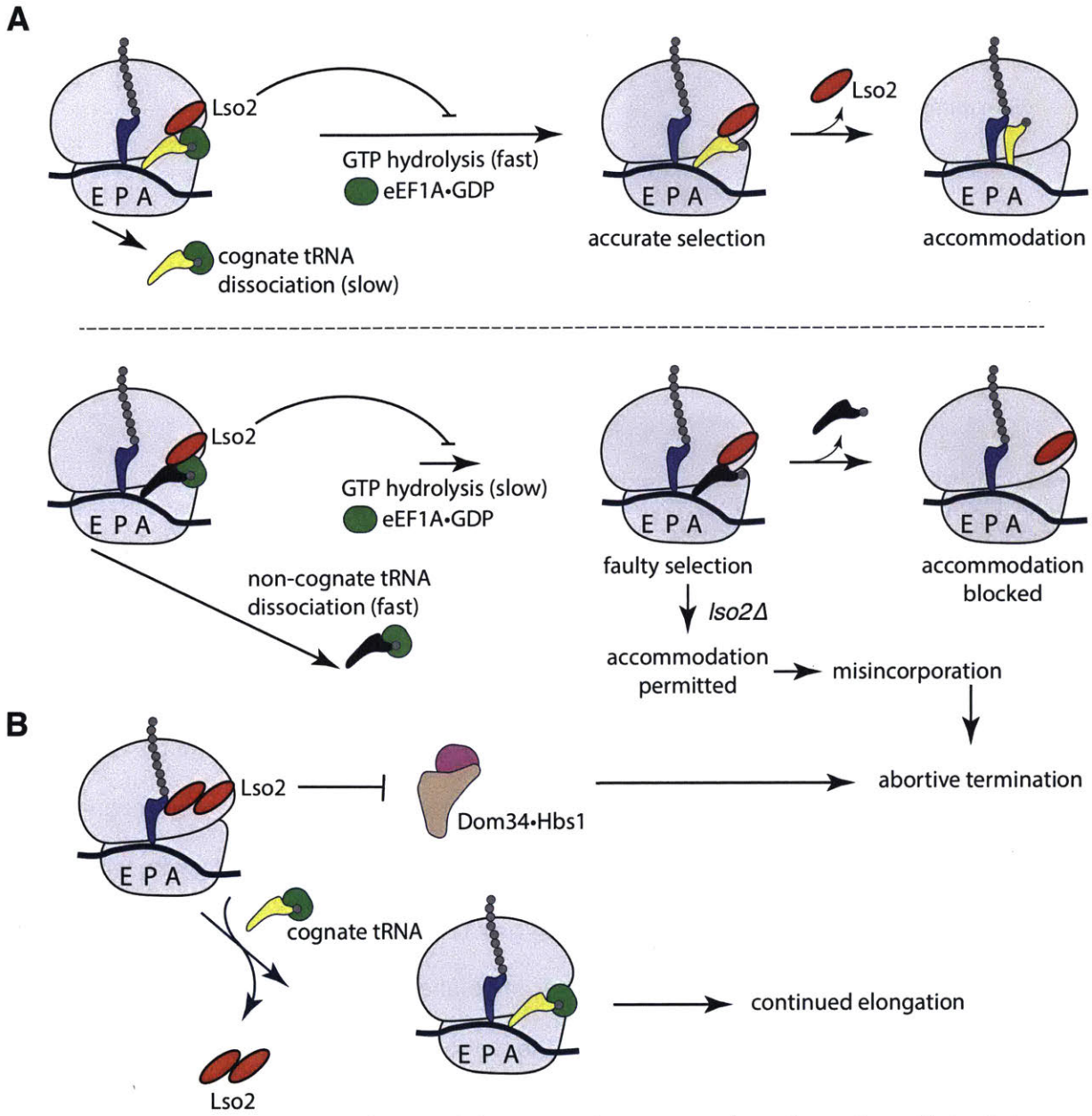

Figure 3-1: Putative functions for Lso2 in promoting processive elongation. A) Lso2 increases fidelity by enhancing selection and/or accommodation of cognate tRNA (top) versus non-cognate tRNA (bottom). (Left) By slowing GTP hydrolysis of eEF1A•GTP, Lso2 prolongs initial selection and increases the time for non-cognate tRNA to dissociate. (Center and right) Lso2 is an additional barrier to accommodation. If cognate tRNA is selected, it is stabilized by correct triplet pairing and displaces Lso2 from the ribosome during accommodation (top). By contrast, non-cognate tRNA lacks stabilizing interactions and dissociates upon sterically clashing with Lso2 (bottom). B) Lso2 binds in the empty A site of transiently stalled ribosomes. This interaction can be outcompeted by the cognate tRNA but inhibits recognition by the quality control complex Dom34•Hbs1. Increased targeting by Dom34 leads to premature termination by mechanisms discussed in Chapter 1. The multimerization of Lso2 in this model is speculative.

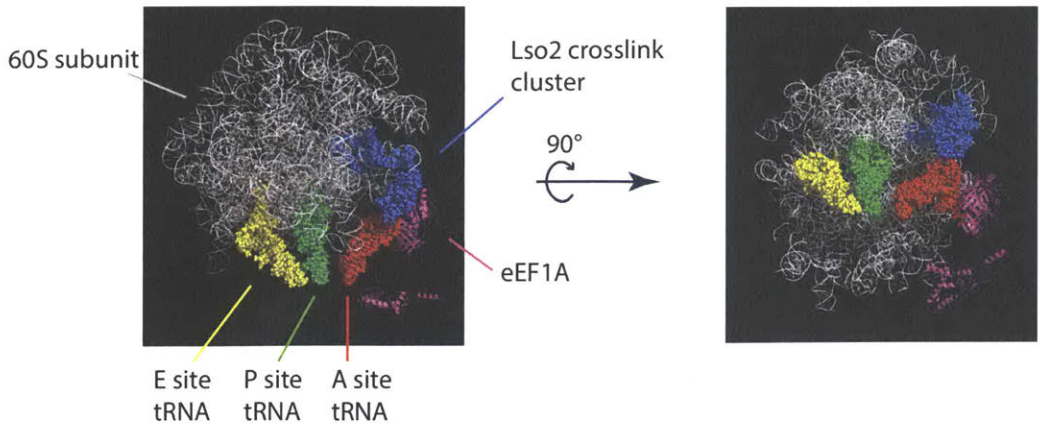

Figure 3-2: The Lso2 crosslink cluster relative to other translation ligands. The cryo-EM structure is of a rabbit ribosome from Shao et al., 2016. (Left) View of the 60S subunit with E and P site tRNAs in the classic state and A site tRNA in the distorted A/T state, bound to eEF1A. The region homologous to the Lso2 crosslink cluster, 28S 1925-2019, is highlighted in blue. (Right) Rotated view of the 60S subunit, looking onto the plane of the subunit interface.

Lso2 bound in the large subunit could present an additional barrier to accommodation (Figure 1-2; Figure 3-1A, center and right). Whereas cognate tRNA is stabilized during rotation by its triplet pairing to mRNA in the decoding center, thus efficiently displacing Lso2, near-cognate tRNA lacks these interactions and would dissociate from the ribosome upon clashing with Lso2. This function is not mutually exclusive with slowing eEF1A•GTP hydrolysis. Finally, Lso2 could bind in the empty A site of temporarily stalled ribosomes and prevent their recognition by Dom34, which ultimately leads to dissociation of the entire translating complex (Figure 3-1B). To explain the monosome accumulation in *lso2Δ* recovering from stationary phase, an increase in miscoding errors and targeting by quality control pathways leads to pervasive premature termination. The accumulated subunits face a limiting pool of initiation factors (Figure 3-3A) and are therefore unable to re-enter the translation cycle.

This model is built on three main assumptions. The first is that miscoding leads to premature termination, when the simplest outcome is uninterrupted translation of the protein product following misincorporation. These mutated protein products were in fact the first readout

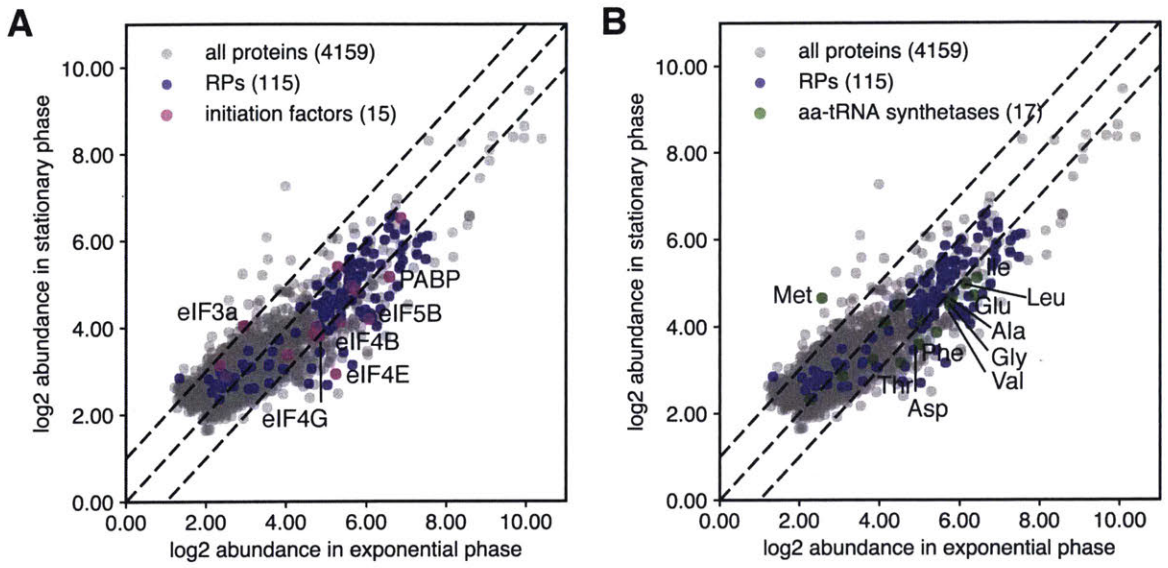

Figure 3-3: Protein abundances of the translational machinery during exponential phase and stationary phase. Data are from Davidson et al., 2011. The yeast GFP collection, wherein each of 4159 strains has a protein fused to a C-terminal GFP tag, was grown either overnight to exponential phase or for 7 days to reach stationary phase. Protein abundance was measured by flow cytometry. Dashed lines indicate abundance changes ≥ 2-fold between stationary vs. exponential phase. A) Abundances of initiation factors and core ribosomal proteins. Note that the ratio of eIF4E and eIF5B to ribosomes is reduced during stationary phase. B) Abundances of aminoacyl-tRNA synthetases and core ribosomal proteins.

of misincorporation rates in *E. coli* (Loftfield and Vanderjagt, 1972; Parker, 1989). However, mispairing between noncognate tRNA and mRNA in the decoding center can also promote premature termination by two characterized pathways. Certain sequence contexts lead to frameshifting during translocation, particularly if the frameshift leads to more stable pairing of the A and P site tRNAs (Barak et al., 1996; Weiss and Gallant, 1986). Translation in the new frame typically leads to decoding of a premature stop codon and activation of nonsense-mediated decay (He and Jacobson, 2015). Additionally, in a recently discovered quality control pathway, a single miscoding error was shown to promote misreading of the subsequent codon. Following translocation, simultaneous codon:anticodon mismatches in the E and P sites elevated canonical termination to a rate comparable to that of tRNA selection (Zaher and Green, 2009). Therefore, these studies offer plausible mechanistic links between miscoding and abortive termination.

The second assumption, broader in scope, is that early nutrient upshift from stationary phase leads to an imbalance in the available charged tRNAs versus codon demand in the transcriptome. This imbalance in turn elevates the potential for miscoding and elongation errors. By contrast, I assume that the tRNA pool is better suited to codon demand during steady-state exponential growth, which would rationalize why *Iso2*Δ has little effect on bulk translation therein (Figure 2-3A) but a more significant impact during stationary phase recovery (Figure 2-3B). Although global tRNA charging status has not been explicitly profiled at 30 minutes of upshift from stationary phase, a synthesis of studies from yeast and bacteria raises the possibility of an imbalance. The most suggestive if indirect evidence is the change in the yeast transcriptome. Whereas only ~130 transcripts are detectable during stationary phase, ~1000 additional genes are expressed and induced 2-fold or more during the first 30 minutes of recovery. Moreover, these stationary phase genes primarily encode enzymes for oxidative phosphorylation (Martinez et al., 2004), which as a category have codon usages distinct from the subset found in ribosome synthesis genes that dominate the recovery transcriptome (Figure 3-4). What does this difference in codon use imply about the state of tRNA charging? In *E. coli*, amino acid starvation leads to differential charging of isoacceptors as a function of their concentrations and their cognate codon abundances in the transcriptome. The isoacceptors that maintain high charging in starvation correlate well with overall codon usage in starvation, suggesting that the charged tRNA pool in stationary phase could be distinct from that of a condition filled with growth-promoting messages (Dittmar et al., 2005; Elf, 2003). The fast rate of aminoacylation in rich medium (Dittmar et al., 2005), however, begs the question of why tRNA charging would continue to be maladapted after thirty minutes of upshift. Here I invoke other aspects of stationary phase physiology. Proteomic data from stationary phase yeast show that the abundances of 9 aminoacyl-tRNA synthetases (of 17 quantified) are reduced by more than 2-fold (Figure 3-3B) relative to exponential phase. Although they maintain their stoichiometry to

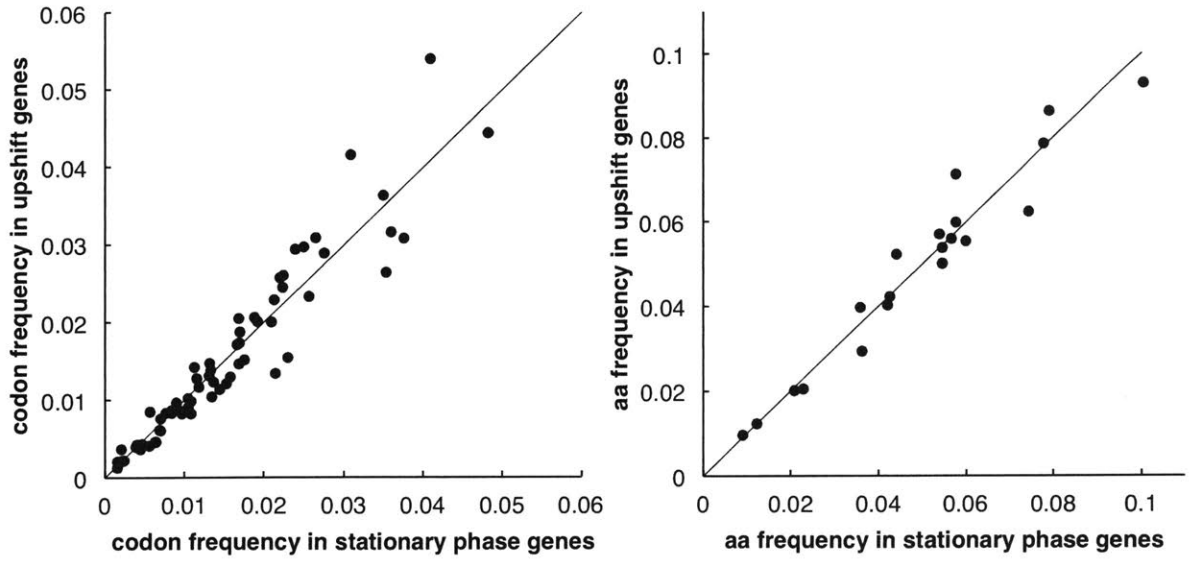

Figure 3-4: Comparison of codon and amino acid frequencies between stationary phase and nutrient upshift. 231 genes annotated as functioning in "aerobic respiration," "TCA cycle," or "oxidative phosphorylation" were analyzed to give the stationary phase (x-axis) values. 374 genes annotated as functioning in "cytoplasmic translation" and "ribosome maturation" were analyzed to give the upshift (y-axis) values. The gene ontology categories for each condition are from (Martinez et al., 2004).

core ribosomes, we have observed that the abundance of bulk tRNAs to ribosomes is increased during stationary phase. Thus, the synthetase to tRNA ratio is likely decreased. Additionally, the energy metabolism of quiescent yeast is adapted for slow oxidation of fatty acids, and the widespread autophagy leading to quiescence (Gray et al., 2004) could also have depleted glycolytic enzymes necessary for generating ATP in the fresh medium. Taken together, these data suggest metabolic and transcriptomic states that could lead to imbalanced tRNA pools immediately after nutrient upshift. Definitive proof, however, will need to come from direct genome-wide measurements of tRNA charging (Dittmar et al., 2005; Schwartz and Pan, 2017; Zaborske et al., 2010) and comparison with the transcriptome codon usage.

As evidence that elongation errors can quantitatively account for the accumulation of empty ribosomes in recovering *Iso2Δ,* ribosome profiling in *E. coli* has yielded hints of significant drop-off during amino acid starvation. The first study compared ribosome occupancy over finely divided bins of ORF length. There was a statistically significant and progressive decrease in occupancy over ORF length during leucine starvation, serine starvation, and acute ethanol

stress (Sin et al., 2016). The second study attempted to rationalize ribosome profiling data from nutrient-stressed *E. coli* through a more comprehensive model, which accounted for rates of initiation, elongation, drop-off, and aminoacylation. Under leucine starvation, ribosome drop-off was evident on two-thirds of all genes. Assuming an aminoacylation rate 100-fold reduced relative to log phase, the model also predicted a drop-off frequency of 0.1 s^{-1} (Subramaniam et al., 2014). Thus, some degree of early termination has been previously inferred from genome-wide measurements during starvation.

The third assumption of the general elongation model is that Lso2 improves fidelity at "slow" ribosomes without adversely affecting the kinetics of cognate ternary complex binding. The fact that 10-fold overexpression of Lso2 has no effect on growth or bulk translation (Figure 3-5) supports the second half of this claim. However, its putative specificity for ribosomes with a shortage of the cognate ternary complex is less clear. In the scenario of Lso2 preferentially recognizing an empty A site, its affinity could be lower than the cognate tRNA's but higher than that of a non-cognate tRNA. In the more complex scenario of Lso2 co-occupying the ribosome with aminoacyl-tRNA•eEF1A•GTP, the stoichiometry of Lso2 to ribosomes during recovery becomes a central question. If Lso2 is still substantially substoichiometric, it may "hop" in the manner of RelA between cellular ribosomes, but its preference for ribosomes with starved A sites is not obvious. Abundance measurements of Lso2 were not included in the yeast stationary phase proteomics study (Davidson et al., 2011) and would need to be generated in-house using quantitative western blots.

Finally, the idea of accessory factors that facilitate chemistry in the ribosome decoding center has a well-characterized precedent. The conserved eIF-5A/EF-P was initially shown to assist in formation of the first peptide bond (Kemper et al., 1976); because of its primary sequence, Met-$tRNA_i$ is slower than its elongator counterpart in moving to the P/E hybrid state that precedes EF-G-catalyzed translocation (Dorner et al., 2006; Studer et al., 2003). By binding

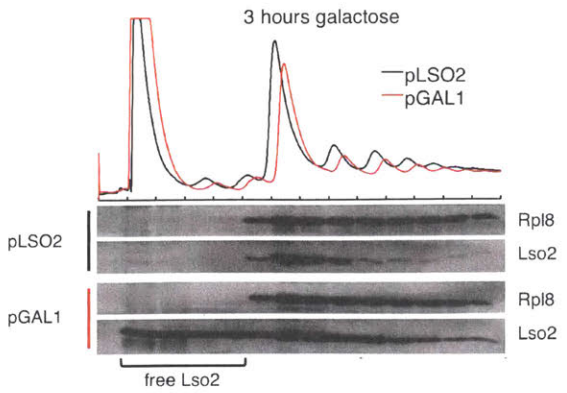

Figure 3-5: Overexpressed Lso2 migrates in the free pool and with polysomes. A strain with endogenous *LSO2* expression (pLSO2) and a strain with 10-fold overexpressed *LSO2* (pGAL1; data not shown) were grown in galactose for 3 hours, then harvested for gradient profiling.

between the P and E sites with contacts to P site tRNA, eIF-5A/EF-P was thought to stabilize the hybrid state of Met-tRNA$_i$. It has since been demonstrated to promote translation through polyproline stretches (Doerfel et al., 2013; Ude et al., 2013; Woolstenhulme et al., 2015), wherein the imino group of proline makes it both a poor peptidyl acceptor and donor, by aligning the P site tRNA for peptidyl transfer (Blaha et al., 2009). Thus, despite the universally conserved steps of elongation, not all of its chemistry is carried out with equal efficiency by the core elongation factors.

Tests of Lso2's molecular functions in general elongation

An open and pressing question is the gradient migration pattern of Lso2 during starvation recovery. The general elongation model predicts a strong skew of Lso2 into heavy polysomes, because they contain more elongating ribosomes overall. Yet the current data show Lso2 co-migrating mainly with 80S monosomes during log phase (Figure 2-2A), with a moderate increase in polysome association during acute glucose withdrawal (Figure 2-2B). What could explain this 80S enrichment? One possibility is that Lso2's translatome targets are restricted to mRNAs translated by a single monosome (Heyer and Moore, 2016); however, the determinant of specificity for such a large class of mRNAs is not obvious. Another possibility is that

transiently stalled ribosomes with starved A sites are uncommon in either rich medium or acute glucose withdrawal, and that the pool of Lso2 not on elongating ribosomes can simply bind empty monosomes in gradients, as the subunit association assay shows (Figure 2-6). Alternatively, Lso2 association with elongating ribosomes could be prevalent but labile during velocity sedimentation, causing Lso2 to bind empty monosomes instead. Formaldehyde crosslinking in extracts may help to preserve these transient interactions (Valášek et al., 2007).

To create a more defined condition of ribosome pausing that should lead to Lso2 association with heavy polysomes, I would treat yeast cultures with 3-amino-triazole (3-AT), an inhibitor of histidine biosynthesis that depletes levels of charged histidyl-tRNA (Guydosh and Green, 2014). A strong correlation between number of elongating ribosomes and Lso2 intensity would be a first step in support of the general elongation model. By contrast, Lso2 that migrates comparably with all polysome fractions would disfavor this model and support a function either in initiation or in early elongation, because all mRNA:polysome complexes contain at most one initiating ribosome or one ribosome between codons 1-6. These models are discussed further in the upcoming sections.

As biochemical evidence of Lso2's *in vivo* target, the general elongation model predicts that Lso2 should bind ribosomes containing mRNA and P site tRNA. Importantly, it should also compete with cognate charged tRNA for A site binding in the large subunit. To test these predictions, I will measure the affinity of Lso2 for ribosomes loaded with different combinations of translation ligands. First, I will qualitatively assess whether purified recombinant Lso2 is able to co-sediment through a sucrose cushion with ribosomes bearing uncharged $tRNA_{Phe}$, which binds in the P site of otherwise empty ribosomes (Stupina et al., 2008). Lso2-V5 will be mixed either with empty ribosomal subunits in an equimolar ratio, or with an equimolar amount of ribosomal subunits pre-incubated with *in vitro* transcribed $tRNA_{Phe}$. Each mixture will be pelleted through a sucrose cushion. The supernatants and pellets from each spin will be probed for V5 to compare the ratios of free vs. ribosome-bound Lso2, and for the core 40S protein Asc1 as a

control for ribosome pelleting. If Lso2 remains substantially ribosome-bound with P site tRNA present, I will quantify its affinity and test whether it competes with cognate tRNA for binding to the A site. I will use fluorescence anisotropy to measure the equilibrium dissociation constant of fluorescently labeled Lso2 for empty ribosomes and ribosomes loaded with both poly(U) and acetyl-$tRNA_{Phe}$, as above. Charged Phe-$tRNA_{Phe}$ will be added as the A site competitor. In an even more specific test of the model, cognate Phe-$tRNA_{Phe}$ should be a more efficient competitor of Lso2 than a noncognate charged tRNA.

What range of Lso2 affinities for these ribosomal complexes is physiologically meaningful? With an estimated total ribosome concentration of 10 μM in log phase (von der Haar and McCarthy, 2002), the ribosome concentration in stationary phase recovery decreases to ~1 μM (my unpublished observations). If 15% are non-translating and 85% are translating in a wild-type yeast cell during stationary phase recovery, then the K_D must be below 1 μM for cellular Lso2 to be substantially bound by either type of ribosome. If the presence of P site tRNA in fact reduces Lso2's interaction with ribosomal subunits, or if Lso2 can co-occupy the A site with tRNA, these results would disfavor the general elongation model. In the upcoming sections I interpret these outcomes in light of other models.

The elongation defects that I conjecture Lso2 to inhibit have also been built into reporter systems. Although they do not prove that such defects are pervasive during stationary phase recovery, they would demonstrate whether Lso2 can mitigate them *in vivo*. For quantifying Lso2's effect on tRNA selection fidelity, rates of misreading at individual codons have been measured by misincorporation events that restore the catalytic activity of firefly luciferase (Kramer et al., 2010). This construct series, wherein a lysine at the catalytic site (encoded by AAA) is systematically mutated to every other codon, measures faulty selection of Lys-$tRNA^{Lys}_{UUU}$. The authors demonstrated that the rare codon AGG (Arg), whose cognate $tRNA^{Arg}_{CCU}$ is also rare, was most prone to miscoding by Lys-$tRNA^{Lys}_{UUU}$. Deletion of the $tRNA^{Arg}_{CCU}$ gene further exacerbated this defect, suggesting that competition between cognate

versus non-cognate tRNA determines the frequency of miscoding. In a WT background, the AGG codon is misread by Lys-tRNA$^{Lys}_{UUU}$ 4 times as frequently as the negative control UUU codon. The *lso2*Δ background should promote further misreading (and an increase in Fluc activity), with larger fold-increases at substituted codons that pair more poorly to Lys-tRNA$^{Lys}_{UUU}$, and that have rarer cognate tRNAs. To rule out that loss of Lso2 indirectly increases Fluc activity (for example, by increasing the expression of its chaperone), I will test whether supplemented expression of the true cognate tRNA can outcompete miscoding by Lys-tRNA$^{Lys}_{UUU}$ and reduce Fluc activity in both WT and *lso2*Δ.

Another path to premature ribosome termination that Lso2 could block is recognition by Dom34•Hbs1, which recognizes empty A sites. A reporter previously shown to trigger this quality control pathway contained tetra-repeats of the rare CGA codon between Renilla luciferase upstream and firefly luciferase downstream (Letzring et al., 2013). Quantification of the Fluc to Rluc activity, as well as their respective protein levels, provided a measure of translation that proceeded to the end of the ORF. If Lso2 association with transiently stalled ribosomes blocks Dom34, then the same reporter should yield a greater bias toward upstream Rluc versus downstream Fluc production in an *lso2*Δ background due to increased ribosome dissociation at the CGA repeats.

Finally, ribosome profiling can provide an *in vivo* snapshot of the stationary phase recovery regime to corroborate the outcomes of these low-throughput assays. However, because indirect effects are also captured at the time of harvest, causality must be inferred with extreme caution. In the simplest extension of the general elongation model, pervasive abortive termination in *lso2*Δ would result in a global ribosome drop-off that increases with ORF length (Sin et al., 2016). One caveat to this interpretation, however, is that the drop-off signature is also consistent with faster elongation rates. That is, ribosomes transit more quickly to the stop codon and terminate normally, but face the same limited pool of initiation factors. True abortive termination may be more evident on a per-gene level: In bacterial *efp*Δ (EF-P) mutants, a subset

of genes show abrupt drops in footprint levels immediately following polyproline motifs (Woolstenhulme et al., 2015). If particular miscoding or termination-prone sequences can be identified - for example, a contiguous stretch of codons that are rare in stationary phase genes, but abundant in recovery ones - it may be possible to look for similar precipices of drop-off in *lso2*Δ. Nevertheless, it is important to note that indirect effects could confound the apparent stage of translation affected. For example, particularly poor elongation of mRNAs encoding initiation factors would depress global initiation. I will therefore interpret ribosome profiling alongside the outcomes of low-throughput assays to mine for gene expression changes that could rationalize apparent contradictions.

A function in canonical initiation

An alternative model is that Lso2 is a canonical initiation factor (Figure 3-6). Based on its crosslink to the 25S rRNA (Figure 2-5C-D) and its ability to stabilize ribosomal subunit association *in vitro*, Lso2 could promote subunit joining of the 60S to the 48S pre-initiation complex (Figure 1-1). One mechanism is by increasing the hydrolysis rate of eIF5B•GTP, the initiation factor already known to carry out this function (Acker et al., 2009; Pestova et al., 2000). Alternatively and not exclusively, Lso2 could directly recruit the 60S subunit to a waiting 48S from which eIF2•GDP has dissociated. According to this model, *lso2*Δ accumulates empty ribosomes downstream of vacant 60S subunits and 48S complexes that have disassembled.

Given that subunit joining is an invariant requirement of proceeding to elongation, why would absence of Lso2 lead to a more dramatic accumulation of non-translating subunits during stationary phase recovery than during log phase? The key assumption is that 60S subunit joining is less efficient during stationary phase recovery. In log phase, 60S subunits are in roughly 2-fold excess to 40S subunits, based on the molar extinction coefficient of the 60S being twice that of the 40S (Acker et al., 2007) (Figure 2-2A). We have previously noted this idiosyncrasy of the Sigma1278b strain (Thompson et al., 2016). During stationary phase

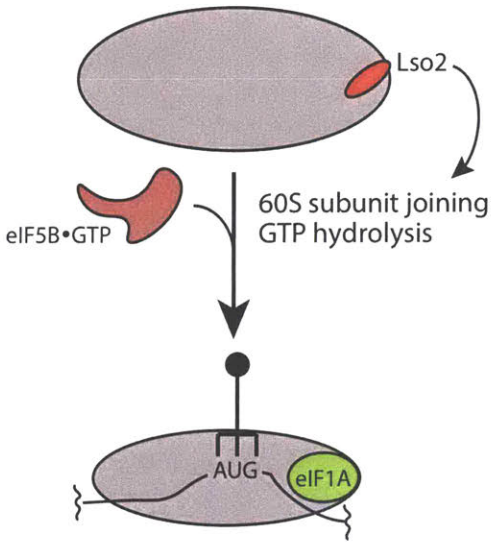

	Log phase	Stationary phase recovery
60S subunits	20	5
Lso2	1	?
eIF5B	1	0.5
40S subunits	10	10

Figure 3-6: Model for effect of Lso2 on stimulating subunit joining. By binding at or near the GTPase activating center, Lso2 stimulates GTP hydrolysis by eIF5B•GTP and increases the rate of subunit joining. During recovery from stationary phase, the mole ratios of 60S subunits and eIF5B to 40S subunits is reduced (our observations and Davidson et al., 2011, respectively).

recovery in the WT strain, however, the 60S to 40S mole ratio is only one-half (Figure 2-3C). Moreover, the ratio of eIF5B to core ribosomes is reduced 2-fold during stationary phase (Figure 3-3A) (Davidson et al., 2011). The other assumption of this model is that empty 40S subunits result from an *in vivo* pathway that disassembles the 48S or from 48S dissociation during sedimentation. While the former question is unknown, 48S initiation intermediates are fairly unstable during sedimentation without crosslinking (Archer et al., 2016; Thompson et al., 2016).

Assaying subunit joining

An assay to directly test whether Lso2 affects 60S subunit joining is to monitor 80S initiation complex formation on an mRNA. The method is to program yeast translation extracts with a radiolabeled, capped, and p(A)-tailed *MFA2* mRNA, which efficiently recruits ribosomes (Balagopal and Parker, 2011). Inclusion of the nonhydrolyzable GTP analog GMPPNP stalls initiation at the 48S pre-initiation complex stage: Because eIF2 cannot hydrolyze GTP upon start codon recognition, 40S subunit-bound initiation factors fail to dissociate and 60S joining is also blocked (Merrick, 1979). The translation extract is then fractionated on a sucrose gradient

with measurement of *MFA2* radioactive counts in each fraction. To trap the 80S initiation complex, cycloheximide is added to extracts to prevent the first round of elongation (Balagopal and Parker, 2011). If Lso2 promotes 60S subunit joining, it should increase the endpoint quantity of *MFA2* stalled in 80S but not in 48S complexes.

In the defined *in vitro* ribosome binding assay described in the previous section ("Tests...general elongation"), purified recombinant Lso2 should have higher affinity for ribosomes containing P site tRNA than for empty ribosomal subunits. The primary weakness of this model is that it predicts strong internal enrichment for $tRNA^{Met}_i$ among the Lso2-myc tRNA crosslinks, whereas its read density is in fact close to the median (data not shown). A possible reconciliation is that Lso2 remains ribosome-associated until arrival of the next elongator tRNA, which could also be detected in the binding assay via A site competition of Lso2 off ribosomes by an elongator tRNA.

Extending the ribosome hibernation hypothesis

The classic phenotype of bacterial ribosome hibernation factors is the loss of mature rRNA during stationary phase (Kazo et al., 2016; Wada et al., 2000). Although *lso2Δ* has no such defect (Figure 2-7B), it could affect the ability of subunits to initiate by protecting the subunit interface from insults that I have not yet assayed. Examples include mutations, chemical lesions, alterations to the rRNA modification state, or loss of ribosomal proteins, each of which might prevent subunit interaction with initiation factors. In particular, the idea of "invisible" chemical insults is corroborated by the fact that mitochondrial respiration generates most of the energy in quiescent yeast, and that mutants of superoxide dismutase lose viability more quickly in stationary phase (Gray et al., 2004). Thus, stationary phase metabolism is conducive to chemical damage of stored macromolecules.

Assaying a ribosome protection function

This model predicts that the isolated ribosomes of *lso2Δ* after 4 days of stationary phase are necessary and sufficient to recapitulate the initiation defect. To test this, I would add purified ribosomal subunits from *lso2Δ* and WT strains to an *in vitro* translation reporter system. Translation extracts containing other necessary proteins would be prepared from *lso2Δ* log phase cytosolic lysate (Rojas-Duran and Gilbert, 2012), with native ribosomes pelleted and removed. The firefly luciferase reporter, fused downstream of the highly active *PRE2* transcript leader (Rojas-Duran and Gilbert, 2012), allows quantification of the difference in initiation activity of ribosomes from the two strains.

Moreover, this model predicts that Lso2 remains abundant and associated with 80S monosomes during stationary phase, and that it is entirely excluded from the polysome region during recovery. These predictions are testable by western blotting of sucrose gradient fractions from both growth conditions. Finally, both P and A site tRNAs should outcompete Lso2 from ribosomal subunits in the *in vitro* binding assay.

The hybrid model: A function in early rounds of elongation

In a model at the interface of initiation and elongation, Lso2 could specifically promote very early rounds of elongation (Figure 3-7). With its footprint of ~28 nucleotides, a ribosome paused at any of codons 2 to 6 in the A site would sterically prevent an upstream scanning ribosome from being able to position the start codon (codon 1) in its P site (Zinshteyn and Gilbert, 2013). If loss of Lso2 led to a severe enough accumulation of early elongating ribosomes, upstream scanning ribosomes could dissociate from the mRNA to yield an increase in non-translating monosomes. Additionally, there would be an accumulation of mRNAs engaged on a single translating ribosome, with both species contributing to the large 80S peak in recovering *lso2Δ*. Some plausible molecular functions for Lso2 in this model are to stabilize A and P site tRNA interaction with the large subunit, to promote translocation by stabilizing their hybrid states, or to promote translocation by stimulating eEF2•GTP hydrolysis.

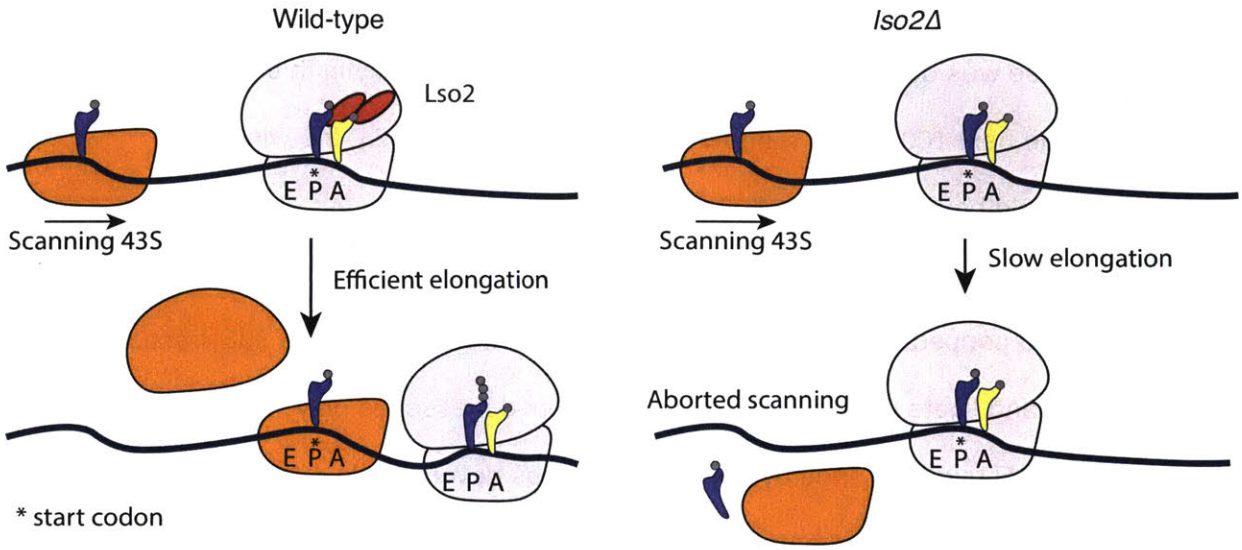

Figure 3-7: A model for Lso2 in promoting early rounds of elongation. (Left) In a wild-type cell, Lso2 efficiently clears early elongating ribosomes, permitting upstream scanning ribosomes to initiate. (Right) In *Iso2Δ*, ribosomes at the first six codons are slow to transit, causing upstream scanning 43S complexes to dissociate. Initiation factors on the scanning 43S have been omitted for clarity, and the multimerization of Lso2 is speculative.

One assumption of this model is that Lso2 specifically recognizes early elongating ribosomes. Aside from chaperones that bind to the nascent chain (Liu et al., 2013), there is currently no such precedent among ribosome-associated proteins, so the specificity determinant of Lso2 for such a translational complex is unclear. Moreover, the unique aspect of early elongation - translocation, as determined using biochemistry and single molecule studies - is independent of A site starvation. While the primary sequence of Met-tRNA$_i$ slows its movement into the hybrid state during the first round, as described above (Dorner et al., 2006; Studer et al., 2003), a short nascent chain was proposed to underlie the longer but progressively diminishing dwell times at the next several codons (Aitken and Puglisi, 2010). Thus, this model is an attractive synthesis of the existing data but difficult to rationalize as starvation-specific.

Assaying the status of early elongation

Genome-wide and positional information from ribosome profiling have previously been successful in revealing early elongation pausing. In heat-stressed human cells, titration of

cytosolic chaperones by misfolded proteins causes a strong elongation pause in the first 50 codons. This pause was quantified by comparison of the read density in this window with the read density in the next 100 codon window (Liu et al., 2013). In *lso2*Δ, the window of accumulation should be limited to the first 6 codons.

Another unique prediction of this model is that many of the accumulated monosomes in *lso2*Δ are bound to capped, intact mRNA. To assay this, I would isolate the 80S fraction from recovering *lso2*Δ and ligate a radiolabeled RNA to capped messages only, whose m^7G can be distinguished from 5′ hydroxyl ends by chemical methods developed in our lab (Arribere and Gilbert, 2013). For comparison, when normalized by the same number of ribosomes, the 80S fraction of an eIF4G depletion mutant, which is genuinely compromised in initiation (Park et al., 2011), should yield less m^7G.

Concluding thoughts on tests of molecular function

The models described here are from the exhaustive list of possibilities. Moreover, while I prefer the model of Lso2 promoting accurate and processive elongation, it is not exclusive of other functions that could contribute to starvation recovery. Indeed, a very recent study of the "accessory" elongation factor eIF-5A in yeast discovered new functions beyond promoting elongation through polyproline motifs (Schuller et al., 2017), including promoting elongation through other dipeptide motifs and stimulating canonical termination by eRF1. These are consistent with the fact that eIF-5A makes no specific contacts to a particular tRNA sequence and with its conserved binding site in the decoding center (Blaha et al., 2009), which has the potential to affect every P site tRNA. Given that Lso2 could affect every translational GTPase by virtue of its interaction with the GTPase activating center, its functional repertoire may be just as diverse.

Molecular and physiological implications of this study

I have demonstrated that a direct ribosome-binding protein in yeast is required for normal translation during the ubiquitous shift from famine to feast. This study underscores the cellular challenges of reconstructing the growth-promoting proteome from intensely downscaled reserves of energy and of the translation machinery. In particular, Lso2 raises the intriguing possibility that certain steps of the translation cycle function differently at the molecular level in such an environment. Given the conservation of its ribosome-binding activity in its human ortholog, insight into Lso2's molecular mechanism will inform how Ccdc124 could intersect with the same conserved stages of the translation cycle in human cells.

References

Acker, M.G., Kolitz, S.E., Mitchell, S.F., Nanda, J.S., and Lorsch, J.R. (2007). Reconstitution of Yeast Translation Initiation. In Methods in Enzymology, (Elsevier), pp. 111–145.

Acker, M.G., Shin, B.-S., Nanda, J.S., Saini, A.K., Dever, T.E., and Lorsch, J.R. (2009). Kinetic Analysis of Late Steps of Eukaryotic Translation Initiation. J. Mol. Biol. *385*, 491–506.

Aitken, C.E., and Puglisi, J.D. (2010). Following the intersubunit conformation of the ribosome during translation in real time. Nat. Struct. Mol. Biol. *17*, 793–800.

Archer, S.K., Shirokikh, N.E., Beilharz, T.H., and Preiss, T. (2016). Dynamics of ribosome scanning and recycling revealed by translation complex profiling. Nature *535*, 570–574.

Arribere, J.A., and Gilbert, W.V. (2013). Roles for transcript leaders in translation and mRNA decay revealed by transcript leader sequencing. Genome Res. *23*, 977–987.

Balagopal, V., and Parker, R. (2011). Stm1 modulates translation after 80S formation in Saccharomyces cerevisiae. RNA *17*, 835–842.

Barak, Z., Lindsley, D., and Gallant, J. (1996). On the mechanism of leftward frameshifting at several hungry codons. J. Mol. Biol. *256*, 676–684.

Blaha, G., Stanley, R.E., and Steitz, T.A. (2009). Formation of the First Peptide Bond: The Structure of EF-P Bound to the 70S Ribosome. Science *325*, 966–970.

Davidson, G.S., Joe, R.M., Roy, S., Meirelles, O., Allen, C.P., Wilson, M.R., Tapia, P.H., Manzanilla, E.E., Dodson, A.E., Chakraborty, S., et al. (2011). The proteomics of quiescent and nonquiescent cell differentiation in yeast stationary-phase cultures. Mol. Biol. Cell *22*, 988–998.

Dittmar, K.A., Sørensen, M.A., Elf, J., Ehrenberg, M., and Pan, T. (2005). Selective charging of tRNA isoacceptors induced by amino-acid starvation. EMBO Rep. *6*, 151–157.

Doerfel, L.K., Wohlgemuth, I., Kothe, C., Peske, F., Urlaub, H., and Rodnina, M.V. (2013). EF-P is essential for rapid synthesis of proteins containing consecutive proline residues. Science *339*, 85–88.

Dorner, S., Brunelle, J.L., Sharma, D., and Green, R. (2006). The hybrid state of tRNA binding is an authentic translation elongation intermediate. Nat. Struct. Mol. Biol. *13*, 234–241.

Elf, J. (2003). Selective Charging of tRNA Isoacceptors Explains Patterns of Codon Usage. Science *300*, 1718–1722.

Gray, J.V., Petsko, G.A., Johnston, G.C., Ringe, D., Singer, R.A., and Werner-Washburne, M. (2004). "Sleeping beauty": quiescence in Saccharomyces cerevisiae. Microbiol. Mol. Biol. Rev. MMBR *68*, 187–206.

Guydosh, N.R., and Green, R. (2014). Dom34 rescues ribosomes in 3' untranslated regions. Cell *156*, 950–962.

von der Haar, T., and McCarthy, J.E.G. (2002). Intracellular translation initiation factor levels in *Saccharomyces cerevisiae* and their role in cap-complex function: Translation initiation factor levels in yeast. Mol. Microbiol. *46*, 531–544.

He, F., and Jacobson, A. (2015). Nonsense-Mediated mRNA Decay: Degradation of Defective Transcripts Is Only Part of the Story. Annu. Rev. Genet. *49*, 339–366.

Heyer, E.E., and Moore, M.J. (2016). Redefining the Translational Status of 80S Monosomes. Cell *164*, 757–769.

Kazo, Y., Hanai, R., Tagami, K., Yano, K., Kawamura, F., Kato-Yamada, Y., Nanamiya, H., Akanuma, G., Hiraoka, H., and Suzuki, S. (2016). Ribosome dimerization is essential for the efficient regrowth of Bacillus subtilis. Microbiology *162*, 448–458.

Kemper, W.M., Berry, K.W., and Merrick, W.C. (1976). Purification and properties of rabbit reticulocyte protein synthesis initiation factors M2Balpha and M2Bbeta. J. Biol. Chem. *251*, 5551–5557.

Kramer, E.B., Vallabhaneni, H., Mayer, L.M., and Farabaugh, P.J. (2010). A comprehensive analysis of translational missense errors in the yeast Saccharomyces cerevisiae. RNA N. Y. N *16*, 1797–1808.

Letzring, D.P., Wolf, A.S., Brule, C.E., and Grayhack, E.J. (2013). Translation of CGA codon repeats in yeast involves quality control components and ribosomal protein L1. RNA N. Y. N *19*, 1208–1217.

Liu, B., Han, Y., and Qian, S.-B. (2013). Cotranslational response to proteotoxic stress by elongation pausing of ribosomes. Mol. Cell *49*, 453–463.

Loftfield, R.B., and Vanderjagt, D. (1972). The frequency of errors in protein biosynthesis. Biochem. J. *128*, 1353–1356.

Martinez, M.J., Roy, S., Archuletta, A.B., Wentzell, P.D., Anna-Arriola, S.S., Rodriguez, A.L., Aragon, A.D., Quiñones, G.A., Allen, C., and Werner-Washburne, M. (2004). Genomic analysis

of stationary-phase and exit in Saccharomyces cerevisiae: gene expression and identification of novel essential genes. Mol. Biol. Cell *15*, 5295–5305.

Merrick, W.C. (1979). Evidence that a single GTP is used in the formation of 80 S initiation complexes. J. Biol. Chem. *254*, 3708–3711.

Park, E.-H., Zhang, F., Warringer, J., Sunnerhagen, P., and Hinnebusch, A.G. (2011). Depletion of eIF4G from yeast cells narrows the range of translational efficiencies genome-wide. BMC Genomics *12*.

Parker, J. (1989). Errors and alternatives in reading the universal genetic code. Microbiol. Rev. *53*, 273–298.

Pestova, T.V., Lomakin, I.B., Lee, J.H., Choi, S.K., Dever, T.E., and Hellen, C.U. (2000). The joining of ribosomal subunits in eukaryotes requires eIF5B. Nature *403*, 332–335.

Rojas-Duran, M.F., and Gilbert, W.V. (2012). Alternative transcription start site selection leads to large differences in translation activity in yeast. RNA N. Y. N *18*, 2299–2305.

Schuller, A.P., Wu, C.C.-C., Dever, T.E., Buskirk, A.R., and Green, R. (2017). eIF5A Functions Globally in Translation Elongation and Termination. Mol. Cell.

Schwartz, M.H., and Pan, T. (2017). Determining the fidelity of tRNA aminoacylation via microarrays. Methods San Diego Calif *113*, 27–33.

Sin, C., Chiarugi, D., and Valleriani, A. (2016). Quantitative assessment of ribosome drop-off in *E. coli*. Nucleic Acids Res. *44*, 2528–2537.

Studer, S.M., Feinberg, J.S., and Joseph, S. (2003). Rapid Kinetic Analysis of EF-G-dependent mRNA Translocation in the Ribosome. J. Mol. Biol. *327*, 369–381.

Stupina, V.A., Meskauskas, A., McCormack, J.C., Yingling, Y.G., Shapiro, B.A., Dinman, J.D., and Simon, A.E. (2008). The 3' proximal translational enhancer of Turnip crinkle virus binds to 60S ribosomal subunits. RNA *14*, 2379–2393.

Subramaniam, A.R., Zid, B.M., and O'Shea, E.K. (2014). An integrated approach reveals regulatory controls on bacterial translation elongation. Cell *159*, 1200–1211.

Thompson, M.K., Rojas-Duran, M.F., Gangaramani, P., and Gilbert, W.V. (2016). The ribosomal protein Asc1/RACK1 is required for efficient translation of short mRNAs. eLife *5*.

Ude, S., Lassak, J., Starosta, A.L., Kraxenberger, T., Wilson, D.N., and Jung, K. (2013). Translation elongation factor EF-P alleviates ribosome stalling at polyproline stretches. Science *339*, 82–85.

Valášek, L., Szamecz, B., Hinnebusch, A.G., and Nielsen, K.H. (2007). In Vivo Stabilization of Preinitiation Complexes by Formaldehyde Cross-Linking. In Methods in Enzymology, (Elsevier), pp. 163–183.

Wada, A., Mikkola, R., Kurland, C.G., and Ishihama, A. (2000). Growth phase-coupled changes of the ribosome profile in natural isolates and laboratory strains of Escherichia coli. J. Bacteriol. *182*, 2893–2899.

Weiss, R.B., and Gallant, J.A. (1986). Frameshift suppression in aminoacyl-tRNA limited cells. Genetics *112*, 727–739.

Woolstenhulme, C.J., Guydosh, N.R., Green, R., and Buskirk, A.R. (2015). High-Precision Analysis of Translational Pausing by Ribosome Profiling in Bacteria Lacking EFP. Cell Rep. *11*, 13–21.

Zaborske, J.M., Wu, X., Wek, R.C., and Pan, T. (2010). Selective control of amino acid metabolism by the GCN2 eIF2 kinase pathway in Saccharomyces cerevisiae. BMC Biochem. *11*, 29.

Zaher, H.S., and Green, R. (2009). Quality control by the ribosome following peptide bond formation. Nature *457*, 161–166.

Zinshteyn, B., and Gilbert, W.V. (2013). Loss of a conserved tRNA anticodon modification perturbs cellular signaling. PLoS Genet. *9*, e1003675.

Appendix

Table 1: Proteins reproducibly identified by quantitative mass spectrometry of ribosomes from glucose-replete and -starved conditions. Only proteins with at least two unique peptides in each of two biological replicates are included. Proteins are color-coded to match Figure 2-1B (core ribosomal proteins, blue; elongation factors, red; initiation factor, green; maturation factors, orange; novel proteins, magenta; all other proteins, black).

Systematic name	Short name	Rep.	Unique peptides	No. ratios	log2 (-glu/+glu)	Rep.	Unique peptides	No. ratios	log2 (-glu/+glu)
YMR116C	ASC1	1	19	259	-0.07	2	15	87	-0.18
YLR075W	RPL10	1	27	360	-0.07	2	25	95	0.21
YGR085C	RPL11B	1	13	268	0.1	2	13	68	0.01
YDR418W	RPL12B	1	18	249	0.13	2	14	121	0.23
YDL082W	RPL13A	1	24	255	-0.09	2	21	62	-0.38
YMR142C	RPL13B	1	25	283	-0.04	2	23	77	-0.12
YHL001W	RPL14B	1	17	189	0.06	2	14	58	0.21
YLR029C	RPL15A	1	16	160	0	2	17	73	0.17
YMR121C	RPL15B	1	15	128	0.01	2	14	60	0.19
YIL133C	RPL16A	1	29	327	0.11	2	24	102	0.07
YNL069C	RPL16B	1	31	341	0.1	2	23	100	0.04
YKL180W	RPL17A	1	17	264	0.22	2	11	103	0.2
YJL177W	RPL17B	1	17	265	0.22	2	11	102	0.2
YNL301C	RPL18B	1	15	193	0.08	2	10	81	0.17
YBL027W	RPL19B	1	28	292	-0.12	2	22	98	0.02
YGL135W	RPL1B	1	21	319	0.04	2	15	136	0.24
YMR242C	RPL20A	1	20	169	0.13	2	13	69	0.04
YBR191W	RPL21A	1	22	272	-0.07	2	18	96	0.18
YPL079W	RPL21B	1	23	270	-0.06	2	19	98	0.18
YLR061W	RPL22A	1	8	72	0.1	2	8	33	0.21
YFL034C-A	RPL22B	1	4	17	0.02	2	3	10	0.08
YBL087C	RPL23A	1	8	122	-0.58	2	9	54	0.1
YGL031C	RPL24A	1	19	210	-0.08	2	13	72	-0.13
YGR148C	RPL24B	1	19	223	-0.1	2	15	76	-0.13
YOL127W	RPL25	1	21	163	-0.04	2	13	65	-0.28

YGR034W	RPL26B	1	24	352	0.03	2	15	84	0.07
YDR471W	RPL27B	1	14	218	-0.17	2	12	70	0.1
YGL103W	RPL28	1	21	254	0.04	2	16	79	0.21
YFR032C-A	RPL29	1	8	15	0.15	2	6	11	-0.3
YFR031C-A	RPL2A	1	28	318	-0.08	2	23	125	0.15
YOR063W	RPL3	1	50	617	-0.13	2	40	279	0.04
YGL030W	RPL30	1	10	69	-0.1	2	7	44	0.4
YDL075W	RPL31A	1	12	219	0.14	2	9	62	0.07
YLR406C	RPL31B	1	11	192	0.12	2	8	56	0.12
YBL092W	RPL32	1	15	270	0.06	2	11	108	0.1
YPL143W	RPL33A	1	12	72	0.12	2	7	25	0.4
YOR234C	RPL33B	1	11	58	0.12	2	7	22	0.48
YER056C-A	RPL34A	1	9	52	0.18	2	4	17	0.42
YIL052C	RPL34B	1	9	60	0.31	2	4	20	0.31
YDL136W	RPL35B	1	19	219	0.04	2	16	76	-0.04
YMR194W	RPL36A	1	14	140	-0.04	2	16	52	-0.04
YPL249C-A	RPL36B	1	18	191	-0.02	2	18	74	-0.02
YLR185W	RPL37A	1	8	144	0.17	2	8	76	-0.1
YDR500C	RPL37B	1	7	74	0.22	2	8	44	-0.16
YLR325C	RPL38	1	8	131	-0.08	2	4	48	0.15
YIL148W	RPL40A	1	12	31	-0.79	2	7	17	-0.17
YHR141C	RPL42B	1	9	115	-0.13	2	7	38	0.08
YJR094W-A	RPL43B	1	11	42	-0.08	2	9	17	0.3
YBR031W	RPL4A	1	26	349	0.12	2	20	117	-0.02
YPL131W	RPL5	1	20	180	0.01	2	14	72	-0.05
YML073C	RPL6A	1	25	313	0.12	2	22	114	0
YLR448W	RPL6B	1	23	286	0.01	2	22	112	0.03
YGL076C	RPL7A	1	19	349	-0.05	2	15	141	0.13
YPL198W	RPL7B	1	20	323	-0.03	2	15	134	0.13
YHL033C	RPL8A	1	30	423	0.11	2	31	235	0.07
YLL045C	RPL8B	1	30	485	0.02	2	30	235	0.07

YGL147C	RPL9A	1	17	326	0.07	2	13	153	0.11
YNL067W	RPL9B	1	16	319	0.06	2	13	149	0.12
YFL036W	RPO41	1	3	6	0.06	2	3	5	0.09
YLR340W	RPP0	1	16	236	-0.06	2	15	117	0.17
YDL081C	RPP1A	1	2	26	0.13	2	2	12	0.17
YDL130W	RPP1B	1	5	63	-0.18	2	4	8	0.21
YOL039W	RPP2A	1	9	150	-0.35	2	8	35	0.56
YDR382W	RPP2B	1	8	60	-0.12	2	7	23	0.67
YGR214W	RPS0A	1	11	96	-0.08	2	11	32	-0.12
YLR048W	RPS0B	1	11	93	-0.13	2	11	35	-0.14
YOR293W	RPS10A	1	12	85	0.11	2	11	32	-0.19
YMR230W	RPS10B	1	13	77	0.13	2	12	34	-0.21
YBR048W	RPS11B	1	16	130	-0.02	2	10	46	-0.18
YOR369C	RPS12	1	11	160	0.07	2	10	47	0.11
YDR064W	RPS13	1	12	124	0.09	2	10	36	-0.11
YJL191W	RPS14B	1	9	138	-0.33	2	11	48	-0.39
YOL040C	RPS15	1	8	132	-0.14	2	8	50	-0.2
YDL083C	RPS16B	1	16	195	-0.03	2	13	102	-0.07
YDR447C	RPS17B	1	17	294	0.17	2	15	95	-0.1
YDR450W	RPS18A	1	16	196	-0.12	2	12	90	-0.18
YOL121C	RPS19A	1	12	155	-0.06	2	13	64	-0.11
YLR441C	RPS1A	1	34	360	-0.2	2	22	173	-0.26
YML063W	RPS1B	1	35	349	-0.15	2	24	157	-0.25
YGL123W	RPS2	1	13	269	-0.08	2	13	131	0.01
YHL015W	RPS20	1	11	227	0.08	2	9	75	-0.2
YKR057W	RPS21A	1	7	94	0.1	2	6	21	0.02
YJL136C	RPS21B	1	6	94	0.08	2	6	21	0.02
YJL190C	RPS22A	1	11	86	0.07	2	7	23	0.04
YGR118W	RPS23A	1	16	169	-0.13	2	9	50	-0.05
YIL069C	RPS24B	1	15	260	-0.05	2	17	99	-0.18
YGR027C	RPS25A	1	13	195	0	2	10	90	-0.16

YLR333C	RPS25B	1	13	184	0	2	10	83	-0.23
YGL189C	RPS26A	1	8	61	-0.2	2	10	49	-0.26
YER131W	RPS26B	1	9	34	-0.14	2	10	20	-0.14
YKL156W	RPS27A	1	2	42	0.39	2	2	14	-0.01
YOR167C	RPS28A	1	6	42	0.09	2	6	17	1.15
YLR388W	RPS29A	1	7	68	0.06	2	6	21	-0.35
YDL061C	RPS29B	1	4	50	-0.39	2	5	16	-0.23
YNL178W	RPS3	1	19	222	0.23	2	18	59	-0.07
YLR287C-A	RPS30A	1	6	76	0.62	2	6	9	-0.3
YLR167W	RPS31	1	17	106	-0.21	2	14	47	-0.24
YHR203C	RPS4B	1	30	320	-0.03	2	28	123	-0.13
YJR123W	RPS5	1	19	265	0.12	2	20	85	-0.21
YBR181C	RPS6B	1	34	421	-0.03	2	23	132	-0.11
YOR096W	RPS7A	1	19	210	-0.06	2	15	98	-0.01
YNL096C	RPS7B	1	22	222	-0.17	2	18	93	-0.03
YBL072C	RPS8A	1	18	131	-0.05	2	11	51	-0.24
YPL081W	RPS9A	1	21	165	-0.07	2	16	73	-0.05
YBR189W	RPS9B	1	21	171	-0.03	2	17	77	-0.05
YBR118W	TEF2	1	8	17	-1.5	2	15	18	-1.39
YKL081W	TEF4	1	3	2	-0.26	2	5	4	-0.86
YDR385W	EFT2	1	10	9	-3.21	2	7	6	-2.32
YLR249W	YEF3	1	13	7	-4.26	2	10	5	-2.82
YAL035W	FUN12	1	8	4	-0.38	2	3	2	0.03
YDR101C	ARX1	1	6	6	0.84	2	14	6	0.34
YPL217C	BMS1	1	12	6	-1.48	2	15	15	-1.29
YLR129W	DIP2	1	14	8	-1.86	2	17	19	-1.48
YKL172W	EBP2	1	7	2	0.51	2	9	8	0.14
YGR145W	ENP2	1	4	2	-2.67	2	7	3	-1.41
YMR049C	ERB1	1	12	9	0.87	2	7	6	0.36
YLR051C	FCF2	1	3	2	-1.41	2	5	6	-1.42
YMR290C	HAS1	1	6	2	0.62	2	6	3	0.24

YNL075W	IMP4	1	3	2	-1.67	2	5	4	-1.8
YNL132W	KRE33	1	11	10	-1.22	2	17	20	-1.3
YCL059C	KRR1	1	3	2	-1.39	2	6	4	-1.39
YAL025C	MAK16	1	4	3	0.2	2	4	3	-0.03
YJR002W	MPP10	1	11	5	-1.66	2	10	5	-1.58
YKL009W	MRT4	1	20	64	0.65	2	14	31	0.68
YOR206W	NOC2	1	6	3	-0.06	2	8	6	0.45
YPL093W	NOG1	1	14	13	0.54	2	20	17	-0.17
YDL014W	NOP1	1	8	7	-1.6	2	9	11	-1.26
YDL148C	NOP14	1	8	6	-1.3	2	7	7	-1.34
YER002W	NOP16	1	4	5	0.41	2	5	3	0.17
YLR197W	NOP56	1	13	11	-1.79	2	17	18	-1.39
YOR310C	NOP58	1	5	4	-1.92	2	9	7	-1.41
YGR103W	NOP7	1	6	4	0.39	2	9	12	0.01
YGL111W	NSA1	1	5	2	1.34	2	10	4	0.48
YER126C	NSA2	1	4	3	0.09	2	5	2	-0.04
YBR267W	REI1	1	3	5	1.03	2	3	5	0.55
YLR009W	RLP24	1	6	6	-0.55	2	2	2	-0.62
YNL002C	RLP7	1	4	3	0.11	2	3	2	0.23
YGL171W	ROK1	1	6	5	-1.66	2	11	5	-1.68
YKR081C	RPF2	1	5	4	-0.87	2	5	4	-0.99
YMR229C	RRP5	1	19	8	-1.27	2	23	14	-1.51
YPR137W	RRP9	1	6	3	-1.24	2	14	15	-1.4
YDL153C	SAS10	1	5	3	-1.82	2	11	10	-1.56
YKL099C	UTP11	1	5	4	-1.21	2	4	3	-0.83
YBL004W	UTP20	1	12	2	-1.18	2	16	14	-1.21
YLR409C	UTP21	1	5	2	1.79	2	9	10	-1.51
YDR449C	UTP6	1	4	2	-0.23	2	7	4	-1.41
YER082C	UTP7	1	6	7	-2.04	2	13	12	-1.53
YGR128C	UTP8	1	7	2	-0.58	2	9	9	-1.63
YHR196W	UTP9	1	3	2	-1.29	2	7	7	-1.34

YOR272W	YTM1	1	3	2	1.27	2	3	4	0.54
YHR052W	CIC1	1	4	4	0.51	2	7	6	0.3
YGR187C	HGH1	1	2	2	-0.16	2	4	4	0.39
YOL015W	IRC10	1	3	3	-0.2	2	2	3	0.2
YBR250W	SPO23	1	2	10	-0.05	2	3	3	-0.4
YLL040C	VPS13	1	10	2	-0.08	2	3	3	0.01
YGL117W	YGL117W	1	2	2	0.13	2	2	2	0.59
YGR169C-A	YGR169C-A	1	4	4	2.15	2	4	5	0.98
YHL014C	YLF2	1	3	2	0.13	2	2	3	-0.1
YLR419W	YLR419W	1	7	2	0.56	2	16	7	-2.79
YML002W	YML002W	1	2	3	-0.1	2	2	2	0.64
YMR114C	YMR114C	1	2	3	-0.09	2	3	2	0.03
YNL010W	YNL010W	1	3	3	0.03	2	2	3	0
YNL054W-B	YNL054W-B	1	23	69	0.71	2	28	49	0.66
YPL009C	YPL009C	1	4	8	-0.07	2	3	5	-0.23
YPL068C	YPL068C	1	2	2	-0.01	2	2	2	0.03
YPR117W	YPR117W	1	4	2	-0.21	2	5	2	0.91
YBR085W	AAC3	1	3	7	0.6	2	3	3	0.49
YLR153C	ACS2	1	4	2	-1.9	2	2	2	-1.87
YOL086C	ADH1	1	7	4	-1.54	2	7	8	-1.17
YMR303C	ADH2	1	4	4	-1.54	2	4	3	-0.91
Q0055	AI2	1	4	5	0.77	2	4	2	0.2
YNR019W	ARE2	1	2	2	-0.15	2	4	3	-0.1
YOR058C	ASE1	1	4	2	-0.01	2	4	2	0.03
YBL099W	ATP1	1	4	3	0.74	2	6	3	1.37
YNL271C	BNI1	1	3	2	-0.21	2	2	2	0.02
YAL038W	CDC19	1	7	3	-0.47	2	6	2	-1.81
YDL126C	CDC48	1	5	6	-0.35	2	4	2	-0.1
YHR164C	DNA2	1	11	5	-0.03	2	4	3	0.07
YPR183W	DPM1	1	3	3	-1.28	2	2	3	-0.05
YHL030W	ECM29	1	6	3	0.17	2	4	3	0.57

YBR078W	ECM33	1	2	3	-0.2	2	4	2	-0.3
YLR186W	EMG1	1	6	6	-1.46	2	6	9	-1.35
YGR254W	ENO1	1	10	2	-2.33	2	6	4	-1.72
YHR174W	ENO2	1	15	6	-2.74	2	12	14	-1.95
YGR175C	ERG1	1	4	6	-0.47	2	8	7	-0.61
YHR007C	ERG11	1	8	4	-1.41	2	7	10	-0.25
YGL001C	ERG26	1	2	2	-0.9	2	4	2	0.09
YLR100W	ERG27	1	3	4	-0.92	2	7	5	-0.25
YML008C	ERG6	1	8	7	-0.42	2	11	10	-0.12
YHR190W	ERG9	1	5	13	-0.05	2	6	9	0.07
YKL182W	FAS1	1	38	45	-0.13	2	40	50	-0.42
YPL231W	FAS2	1	51	74	0.21	2	46	57	-0.23
YKL060C	FBA1	1	4	3	-2.87	2	6	3	-2
YLR342W	FKS1	1	9	5	-0.28	2	12	12	0.27
YMR307W	GAS1	1	3	3	-0.68	2	5	2	-0.15
YGL195W	GCN1	1	9	6	0.58	2	5	4	-0.39
YKL152C	GPM1	1	2	2	-3.22	2	5	3	-1.69
YGR032W	GSC2	1	5	3	-0.05	2	6	5	0.24
YFR015C	GSY1	1	3	3	-0.1	2	5	2	-2.6
YMR186W	HSC82	1	11	12	-1.19	2	8	4	-1.33
YKL101W	HSL1	1	7	2	-0.01	2	5	3	0.07
YPL240C	HSP82	1	8	10	-0.94	2	5	2	-1.01
YJR036C	HUL4	1	3	2	-0.34	2	3	2	-0.59
YNL106C	INP52	1	5	9	-0.05	2	3	5	-0.23
YBR140C	IRA1	1	8	4	-0.37	2	3	3	-0.13
YBR086C	IST2	1	2	8	0.01	2	3	4	0.07
YNL071W	LAT1	1	31	143	0.89	2	30	83	0.18
YGL009C	LEU1	1	5	3	1.63	2	10	2	-0.87
YGL068W	MNP1	1	4	4	1.01	2	3	3	0.56
YDL028C	MPS1	1	5	2	0.13	2	3	2	0.59
YGR220C	MRPL9	1	2	2	0.38	2	3	4	0.12

YOL042W	NGL1	1	2	4	0.1	2	2	4	0.2
YHR077C	NMD2	1	3	10	-0.16	2	4	3	-0.3
YGR179C	OKP1	1	2	4	-0.28	2	2	2	-0.04
YDL019C	OSH2	1	7	5	-0.09	2	5	3	0.07
YER165W	PAB1	1	5	2	0.22	2	4	4	-0.82
YER178W	PDA1	1	14	23	0.56	2	17	41	0.44
YBR221C	PDB1	1	4	8	0.75	2	6	14	0.33
YGR193C	PDX1	1	17	22	1	2	22	35	0.28
YBL030C	PET9	1	8	14	0.75	2	8	11	0.49
YCR012W	PGK1	1	8	3	-1.68	2	5	4	-2.34
YBR106W	PHO88	1	7	4	-0.6	2	8	14	-0.22
YIL045W	PIG2	1	3	5	0.18	2	2	5	0.03
YGL008C	PMA1	1	19	41	-0.6	2	19	41	-0.29
YGR170W	PSD2	1	3	2	-0.21	2	3	3	-0.38
YLR032W	RAD5	1	3	2	-0.01	2	2	2	0.03
YDR028C	REG1	1	2	2	-0.01	2	2	2	0.03
YOR305W	RRG7	1	2	2	0.2	2	2	2	-0.06
YDR233C	RTN1	1	6	13	-0.03	2	4	6	0.11
YDR143C	SAN1	1	2	3	-0.44	2	2	2	3.86
YER047C	SAP1	1	4	2	-0.01	2	7	2	0.03
YDL139C	SCM3	1	2	3	0.17	2	2	2	0.59
YOL098C	SDD3	1	2	3	2.5	2	2	2	2.78
YLR166C	SEC10	1	2	3	2.71	2	3	2	0.45
YLR430W	SEN1	1	10	3	0.2	2	5	3	-0.07
YOR327C	SNC2	1	2	5	-0.08	2	2	4	0.57
YCL054W	SPB1	1	2	2	1.06	2	6	4	0.79
YGL093W	SPC105	1	3	9	0.08	2	4	4	0.07
YLL024C	SSA2	1	17	18	-1.18	2	16	16	-0.97
YDL229W	SSB1	1	30	163	-1.37	2	27	75	-1.43
YNL209W	SSB2	1	30	163	-1.37	2	27	75	-1.43
YBR143C	SUP45	1	12	8	0.54	2	12	10	0.31

YAR042W	SWH1	1	5	3	0.06	2	3	2	0.03
YOR086C	TCB1	1	5	8	0.31	2	4	4	0.23
YJR009C	TDH2	1	4	7	-1.11	2	7	9	-1.17
YGR192C	TDH3	1	5	7	-1.11	2	8	11	-1.17
YKR010C	TOF2	1	4	4	0.23	2	2	4	0.2
YNL121C	TOM70	1	5	3	-0.33	2	9	5	0.25
YHR099W	TRA1	1	8	4	-0.01	2	6	4	0.03
YJL130C	URA2	1	20	13	-1.65	2	13	12	-0.76
YKR001C	VPS1	1	46	133	1.69	2	28	51	0.69
YLR240W	VPS34	1	3	2	-0.01	2	3	2	0.03
YAR009C	YAR009C	1	7	5	-0.09	2	8	5	0
YNL064C	YDJ1	1	5	2	0.26	2	5	5	0.11
YDR098C-A	YDR098C-A	1	18	71	0.73	2	18	53	0.8
YDR210C-D	YDR210C-D	1	24	69	0.63	2	25	58	0.75
YDR210W-B	YDR210W-B	1	12	8	3.08	2	12	22	0.9
YDR261W-B	YDR261W-B	1	11	8	3.08	2	13	22	0.9
YHR214C-C	YHR214C-C	1	17	71	0.73	2	18	52	0.79
YOL103W-B	YOL103W-B	1	24	91	0.64	2	27	59	0.75
YOR192C-B	YOR192C-B	1	11	8	3.08	2	13	22	0.9

Table 2: Lso2 tRNA targets identified after initial peak calling. Note that some tRNAs have multiple sub-regions called as peaks. All fold-enrichment values are associated with p-values < 10^{-5}. The tRNAs highlighted in red were not identified as ≥4-fold enriched on the basis of read density alone (see Table 3).

tRNA	IP 1 (peak start, peak stop)	IP 2 (peak start, peak stop)	Fold enrichment log2(IP1/SMI)	Fold enrichment log2(IP1/untagged)	Fold enrichment log2(IP2/SMI)	Fold enrichment log2(IP2/untagged)
tA(UGC)A	(24, 34)	(24, 33)	4.367	4.184	4.254	4.064
tA(UGC)A	(34, 44)	(33, 44)	4.224	4.235	4.105	4.116
tA(UGC)A	(44, 55)	(44, 56)	3.921	4.365	3.806	4.257
tF(GAA)B	(52, 73)	(69, 73)	5.562	4.261	5.942	4.279
tF(GAA)B	(73, 83)	(73, 83)	5.991	4.105	6.066	4.180

tF(GAA)M	(52, 60)	(52, 60)	5.512	3.511	5.633	3.632
tF(GAA)M	(60, 62)	(60, 62)	5.500	3.517	5.623	3.640
tF(GAA)M	(62, 65)	(62, 65)	5.491	3.517	5.616	3.642
tF(GAA)M	(65, 69)	(65, 69)	5.478	3.517	5.604	3.642
tF(GAA)M	(69, 73)	(69, 73)	5.481	3.518	5.608	3.645
tF(GAA)M	(73, 82)	(73, 82)	5.465	3.514	5.593	3.642
tG(GCC)D1	(28, 45)	(28, 45)	2.400	4.779	2.744	5.122
tI(AAU)B	(14, 25)	(14, 25)	5.683	4.286	5.624	4.227
tI(AAU)B	(25, 30)	(25, 30)	5.745	4.324	5.692	4.271
tI(AAU)B	(30, 40)	(30, 40)	5.320	4.087	5.379	4.146
tI(AAU)B	(40, 46)	(40, 46)	5.286	3.999	5.392	4.104
tI(AAU)D	(28, 39)	(26, 29)	4.072	3.854	4.256	3.931
tI(AAU)D	(39, 45)	(39, 45)	4.940	4.017	4.982	4.060
tI(AAU)D	(45, 51)	(45, 57)	4.923	4.004	4.946	4.042
tI(AAU)D	(51, 57)	(45, 57)	4.944	4.004	4.946	4.042
tI(AAU)D	(57, 72)	(59, 70)	5.864	4.027	5.863	4.033
tI(UAU)D	(2, 9)	(2, 9)	5.506	4.497	5.143	4.134
tI(UAU)D	(9, 12)	(9, 13)	5.511	4.499	5.147	4.140
tI(UAU)D	(12, 16)	(9, 13)	5.450	4.553	5.147	4.202
tI(UAU)D	(16, 29)	(16, 29)	5.171	4.543	4.838	4.210
tI(UAU)D	(29, 35)	(31, 35)	4.581	4.489	4.413	4.359
tI(UAU)D	(95, 109)	(95, 113)	4.471	4.452	4.452	4.443
tI(UAU)L	(101, 108)	(104, 108)	3.900	4.152	3.605	3.873
tI(UAU)L	(108, 111)	(108, 111)	3.907	4.127	3.601	3.821
tI(UAU)L	(111, 115)	(111, 115)	3.934	4.126	3.626	3.818
tI(UAU)L	(115, 132)	(128, 132)	4.151	4.112	4.026	3.803
tK(UUU)D	(78, 81)	(78, 93)	4.072	2.657	4.018	2.606
tK(UUU)D	(81, 93)	(78, 93)	4.029	2.649	4.018	2.606
tL(GAG)G	(25, 29)	(25, 28)	4.868	4.636	4.966	4.732
tL(GAG)G	(35, 44)	(38, 44)	2.108	4.592	2.239	4.691
tL(UAA)B1	(30, 49)	(29, 49)	3.009	4.088	3.047	4.103

tL(UAA)J	(53, 56)	(55, 58)	3.757	3.371	4.023	3.494
tL(UAA)J	(56, 67)	(58, 66)	3.546	3.353	3.656	3.470
tL(UAA)J	(67, 78)	(66, 68)	3.536	3.310	3.639	3.425
tL(UAA)J	(78, 80)	(68, 83)	4.016	3.325	3.642	3.425
tL(UAA)J	(80, 83)	(68, 83)	4.005	3.332	3.642	3.425
tL(UAG)J	(25, 36)	(28, 36)	4.846	4.409	4.775	4.435
tL(UAG)J	(55, 83)	(55, 83)	4.306	4.244	4.301	4.239
tL(UAG)L1	(8, 38)	(8, 38)	2.208	3.692	2.213	3.697
tL(UAG)L1	(71, 84)	(71, 97)	3.707	3.303	3.810	3.412
tL(UAG)L1	(84, 100)	(97, 100)	4.589	3.352	5.033	3.412
tM(CAU)J1	(43, 45)	(43, 45)	4.868	3.544	4.725	3.401
tN(GUU)C	(16, 24)	(17, 24)	7.991	3.835	7.904	3.740
tN(GUU)C	(24, 29)	(24, 29)	7.981	3.857	7.888	3.764
tN(GUU)F	(56, 59)	(56, 59)	7.664	3.854	7.563	3.753
tN(GUU)F	(59, 73)	(59, 73)	7.664	3.853	7.560	3.749
tQ(UUG)D1	(15, 29)	(15, 29)	4.957	3.862	4.886	3.791
tR(ACG)D	(34, 37)	(33, 37)	4.279	3.418	3.985	3.123
tR(ACG)D	(37, 45)	(37, 45)	4.849	3.571	4.523	3.245
tR(ACG)D	(45, 71)	(45, 71)	4.605	3.584	4.245	3.224
tR(ACG)K	(13, 23)	(22, 23)	5.148	3.648	5.193	3.394
tR(ACG)K	(23, 32)	(24, 32)	5.337	3.634	5.107	3.405
tR(ACG)K	(32, 35)	(32, 35)	4.290	3.664	4.110	3.484
tR(CCU)J	(24, 32)	(25, 32)	5.079	4.038	4.768	3.729
tR(CCU)J	(32, 59)	(32, 59)	5.103	4.071	4.860	3.827
tS(UGA)I	(30, 48)	(30, 55)	2.540	3.494	2.446	3.542
tT(AGU)B	(26, 28)	(26, 28)	7.224	4.300	7.532	4.609
tT(AGU)B	(30, 51)	(29, 51)	5.966	3.941	6.318	4.290
tT(AGU)B	(51, 55)	(51, 55)	5.962	3.908	6.312	4.258
tT(AGU)B	(55, 61)	(55, 61)	5.634	3.790	5.951	4.107
tT(AGU)D	(8, 12)	(8, 12)	4.913	3.541	5.155	3.783
tT(AGU)D	(13, 17)	(12, 39)	5.269	3.616	5.586	3.943

tT(AGU)D	(17, 20)	(12, 39)	5.280	3.616	5.586	3.943
tT(AGU)D	(20, 38)	(12, 39)	5.306	3.644	5.586	3.943
tT(AGU)D	(42, 45)	(42, 45)	6.818	3.865	7.049	4.096
tT(CGU)K	(41, 44)	(41, 46)	6.790	4.004	6.665	3.875
tT(CGU)K	(44, 48)	(46, 51)	6.819	4.000	6.735	3.872
tT(CGU)K	(48, 51)	(46, 51)	6.876	3.998	6.735	3.872
tT(CGU)K	(51, 54)	(51, 54)	6.824	3.995	6.696	3.867
tT(CGU)K	(54, 71)	(54, 71)	6.827	4.023	6.682	3.878
tV(CAC)D	(40, 45)	(40, 45)	2.726	4.206	2.438	3.918
tV(CAC)D	(45, 48)	(45, 48)	2.802	4.199	2.507	3.903
tV(CAC)D	(51, 71)	(51, 71)	2.981	4.177	2.683	3.879
tV(UAC)B	(45, 56)	(45, 56)	5.903	4.087	5.720	3.904
tV(UAC)B	(56, 66)	(60, 73)	6.177	4.199	5.971	4.020
tV(UAC)B	(66, 73)	(60, 73)	6.572	4.162	5.971	4.020
tY(GUA)F1	(17, 29)	(17, 29)	7.266	3.766	7.193	3.693
tY(GUA)F2	(58, 65)	(59, 65)	5.063	3.148	4.903	2.897
tY(GUA)F2	(65, 72)	(65, 72)	5.162	3.156	4.909	2.903
tA(UGC)E	(14, 28)	(14, 41)	4.430	4.418	4.534	4.300
tA(UGC)E	(28, 41)	(14, 41)	4.592	4.297	4.534	4.300
tA(UGC)E	(41, 48)	(41, 46)	5.223	4.041	5.200	4.018
tE(CUC)I	(18, 29)	(18, 29)	3.664	3.229	3.834	3.399
tL(CAA)D	(84, 86)	(84, 86)	4.648	4.095	4.466	3.913
tL(CAA)D	(86, 95)	(86, 95)	4.230	4.024	4.039	3.833
tL(CAA)D	(95, 114)	(95, 114)	4.172	3.856	3.976	3.660
tS(GCU)F	(73, 89)	(73, 100)	3.761	2.228	3.573	2.040
tS(GCU)F	(89, 97)	(73, 100)	3.937	2.226	3.573	2.040
tS(GCU)F	(97, 100)	(73, 100)	3.989	2.214	3.573	2.040
tS(UGA)E	(54, 64)	(54, 65)	3.489	3.477	3.509	3.497

Table 3: Lso2 tRNA targets identified by fold-enrichment of read density in IP vs SMI and IP vs untagged. tRNAs highlighted in grey were also identified by peak calling (as listed in Table 2).

	ratio of read densities			
tRNA gene	IP1/SMI	IP2/SMI	IP1/untagged	IP2/untagged
tA(AGC)D	16.39	16.77	8.35	8.54
tA(UGC)A	19.13	17.44	16.40	14.95
tF(GAA)B	16.53	17.62	10.83	11.55
tF(GAA)D	12.62	13.80	7.74	8.47
tF(GAA)F	8.82	9.56	8.18	8.86
tF(GAA)M	32.31	34.76	10.33	11.11
tF(GAA)N	24.27	25.63	10.14	10.71
tG(GCC)B	4.54	5.38	8.36	9.91
tG(GCC)D1	10.36	11.93	12.91	14.88
tG(UCC)G	12.20	12.43	9.47	9.65
tG(UCC)N	4.23	4.44	5.09	5.34
tH(GUG)E1	4.15	4.62	7.97	8.87
tI(AAU)B	44.58	43.68	15.81	15.49
tI(AAU)D	22.96	24.72	13.80	14.86
tI(UAU)D	17.35	14.49	17.93	14.97
tI(UAU)L	5.36	4.55	15.00	12.73
tK(CUU)D1	12.25	13.01	6.67	7.08
tK(CUU)E2	7.00	8.06	7.32	8.43
tK(CUU)I	27.26	29.09	7.44	7.94
tK(UUU)D	11.67	10.66	5.81	5.31
tL(CAA)G1	4.33	4.63	13.01	13.89
tL(CAA)M	4.02	4.28	13.00	13.85
tL(GAG)G	9.53	9.83	18.08	18.64
tL(UAA)B1	6.74	6.71	12.94	12.87
tL(UAA)J	4.26	4.56	9.44	10.11
tL(UAG)J	15.45	15.10	15.78	15.43

tL(UAG)L1	5.77	6.04	10.59	11.09
tM(CAU)D	34.32	32.37	13.61	12.84
tM(CAU)E	37.71	38.51	6.71	6.85
tM(CAU)J1	14.46	14.07	11.46	11.15
tM(CAU)J3	15.56	16.24	7.00	7.31
tN(GUU)C	80.28	75.94	11.98	11.33
tN(GUU)F	57.88	56.84	13.95	13.70
tP(AGG)C	20.62	16.68	9.31	7.53
tP(UGG)A	16.48	12.51	6.93	5.26
tP(UGG)F	17.33	13.18	6.96	5.29
tP(UGG)H	16.09	12.63	6.30	4.95
tP(UGG)L	17.28	13.11	7.07	5.37
tP(UGG)M	17.23	13.36	6.18	4.79
tP(UGG)N1	14.71	11.13	7.10	5.38
tP(UGG)O1	17.00	12.80	7.04	5.30
tP(UGG)O2	17.82	13.42	7.10	5.35
tP(UGG)O3	17.96	13.50	7.09	5.33
tQ(CUG)M	49.85	45.27	10.57	9.60
tQ(UUG)B	15.88	16.85	12.56	13.32
tQ(UUG)C	32.85	31.30	10.95	10.44
tQ(UUG)D1	21.30	22.04	13.53	14.01
tQ(UUG)E2	23.43	22.06	7.24	6.82
tR(ACG)D	13.00	11.06	9.77	8.31
tR(ACG)J	20.14	18.13	11.61	10.45
tR(ACG)K	16.05	15.13	11.40	10.75
tR(CCG)L	8.97	9.05	9.88	9.97
tR(CCU)J	35.50	30.61	17.01	14.67
tR(UCU)B	16.66	18.15	7.85	8.54
tR(UCU)G2	23.11	21.16	7.96	7.29
tR(UCU)J2	41.50	34.87	6.94	5.83
tS(AGA)M	4.98	5.30	10.30	10.97

tS(UGA)I	5.29	5.59	11.39	12.06
tT(AGU)B	73.17	89.29	17.08	20.84
tT(AGU)D	39.49	46.43	11.95	14.06
tT(CGU)K	60.19	56.01	14.37	13.37
tT(UGU)G1	9.07	8.48	8.80	8.23
tT(UGU)H	6.72	7.86	4.30	5.03
tV(AAC)E1	4.28	4.45	7.05	7.33
tV(AAC)G1	4.54	4.28	7.79	7.33
tV(CAC)D	4.93	4.13	14.05	11.75
tV(UAC)B	25.04	23.24	12.27	11.39
tY(GUA)D	68.60	70.10	11.48	11.73
tY(GUA)F1	52.88	53.80	9.87	10.04
tY(GUA)F2	12.91	12.03	8.15	7.60
tY(GUA)J2	16.35	15.18	8.15	7.57

Table 4: Yeast strains used in this study.

Name	Genotype	Source	Description	Experiment
YWG25	*MATAa ura3-52 his3Δ0 leu2Δ0 trp1Δ0*	This study	Sigma1278b isogenic WT	Stationary phase recovery, eCLIP (untagged control)
YWG868	*MATAa ura3-52 his3Δ0 leu2Δ0 trp1Δ0 lso2Δ::LSO2-9XHis-2XPrescission-9XMyc-HIS3*	This study	Lso2-myc	Gradient western; eCLIP
YWG869	*MATAa ura3-52 his3Δ0 leu2Δ0 trp1Δ0 lso2Δ::LSO2-9XHis-2XPrescission-9XMyc-HIS3*	This study	Lso2-myc	eCLIP
YWG1874	*MATAa ura3-52 his3Δ0 leu2Δ0 trp1Δ0 lso2Δ::LSO2-9XHis-2XPrescission-9XMyc-HIS3*	This study	Lso2-myc	eCLIP
YWG1875	*MATAa ura3-52 his3Δ0 leu2Δ0 trp1Δ0 lso2Δ::LSO2-9XHis-2XPrescission-9XMyc-HIS3*	This study	Lso2-myc	Gradient western; eCLIP

YWG1142	*MATAa ura3-52 his3Δ0 leu2Δ0 trp1Δ0 lso2Δ::kan*	This study	*lso2* null	Stationary phase recovery
YWG1144	*MATAa ura3-52 his3Δ0 leu2Δ0 trp1Δ0 lso2Δ::kan*	This study	*lso2* null	Stationary phase recovery
YWG1776	*MATAa ura3-52 his3Δ0 leu2Δ0 trp1Δ0 lso2Δ::kan*	This study	*lso2* null	Stationary phase recovery
YWG1795	*MATAa ura3-52 his3Δ0 leu2Δ0 trp1Δ0 LSO2-5XGly-V5*	This study	Lso2-V5 (markerless)	Gradient western
YWG1800	*MATAa ura3-52 his3Δ0 leu2Δ0 trp1Δ0 lso2Δ::CCDC124-V5*	This study	*LSO2* replaced with full-length *CCDC124-V5* (markerless)	Gradient western
YWG1805	*MATAa ura3-52 his3Δ0 leu2Δ0 trp1Δ0 lso2Δ::CCDC124(M1-V136)-V5*	This study	*LSO2* replaced with M1-V136 of *CCDC124-V5* (markerless)	Gradient western
YWG1866	*MATAa ura3-52 his3Δ0 leu2Δ0 trp1Δ0 stm1Δ::nat*	This study	*stm1* null	Stationary phase recovery
YWG1867	*MATAa ura3-52 his3Δ0 leu2Δ0 trp1Δ0 stm1Δ::nat*	This study	*stm1* null	Stationary phase recovery
YWG1862	*MATAa ura3-52 his3Δ0 leu2Δ0 trp1Δ0 lso2Δ::kan stm1Δ::nat*	This study	*lso2stm1* null	Stationary phase recovery
YWG1864	*MATAa ura3-52 his3Δ0 leu2Δ0 trp1Δ0 lso2Δ::kan stm1Δ::nat*	This study	*lso2stm1* null	Stationary phase recovery
YWG1346	*MATa his3Δ1 leu2Δ0 met15Δ0 ura3Δ0 lso2Δ::kan*	This study	*lso2* null in BY4742	Ribosome purification
YWG11	*MATα his3Δ1 leu2Δ0 lys2Δ0 ura3Δ0*	This study	BY4742 isogenic WT	eCLIP (Pus1-paired untagged)
YWG1357	*MATα his3Δ1 leu2Δ0 lys2Δ0 ura3Δ0 pus1Δ::PUS1-9XHis-2XPrescission-9XMyc-HIS3*	This study	Pus1-HPM	eCLIP

Table 5: Synthetic sequences used in this study.

Construct	Sequence (5′ - 3′)
CCDC124	ATGCCGAAGAAATTTCAAGGTGAGAACACTAAGAGTGCCGCAGCCCGTGCGCGTAGAGCGGAAGCCAAAGCA

M1-V136 (shorter isoform)	GCCGCAGACGCCAAAAAACAGAAAGAGCTTGAAGATGCTTATTGGAAAGATGACGACAAACATGTGATGCGTA AAGAGCAAAGGAAGGAGGAAAAAGAGAAAAGGCGTCTTGATCAACTAGAAAGGAAAAAGGAGACACAGAGGTT ACTGGAGGAAGAGGACTCAAAGCTGAAGGGAGGCAAAGCCCCCCGTGTCGCGACAAGTAGCAAGGTCACGA GGGCACAAATCGAGGACACGCTGCGTCGTGATCACCAGTTGAGGGAGGCTCCGGACACGGCGGAGAAGGCC AAGTCCCACCTGGAAGTTCCGCTAGAGGAAAACGTAAACAGGAGAGTC
CCDC124 M1-K223 (full-length)	ATGCCGAAGAAATTTCAAGGTGAGAACACTAAGAGTGCCGCAGCCCGTGCGCGTAGAGCGGAAGCCAAAGCA GCCGCAGACGCCAAAAAACAGAAAGAGCTTGAAGATGCTTATTGGAAAGATGACGACAAACATGTGATGCGTA AAGAGCAAAGGAAGGAGGAAAAAGAGAAAAGGCGTCTTGATCAACTAGAAAGGAAAAAGGAGACACAGAGGTT ACTGGAGGAAGAGGACTCAAAGCTGAAGGGAGGCAAAGCCCCCCGTGTCGCGACAAGTAGCAAGGTCACGA GGGCACAAATCGAGGACACGCTGCGTCGTGATCACCAGTTGAGGGAGGCTCCGGACACGGCGGAGAAGGCC AAGTCCCACCTGGAAGTTCCGCTAGAGGAAAACGTAAACAGGAGAGTCTTGGAGGAGGGATCAGTGGAGGCA AGGACCATAGAAGACGCAATCGCAGTGCTTAGTGTTGCTGAGGAGGCGGCGGACAGACACCCAGAACGTCGT ATGAGGGCGGCATTTACAGCTTTTGAGGAAGCCCAACTACCCAGGTTGAAACAGGAGAATCCCAACATGAGAC TTAGTCAACTAAAGCAATTATTAAAGAAGGAATGGCTTAGGTCTCCCGATAACCCCATGAATCAAAGGGCAGTT CCATTCAACGCACCGAAG
5XGly-V5 C-terminal tag	GGAGGCGGGGGTGGAAAGCCTATCCCTAACCCTCTCCTCGGTCTCGATTCTACG